

PHENYL RINGS MESOGENIC CORE OF AZO-ESTER
BASED LIQUID CRYSTALS: SYNTHESIS,
MESOMORPHIC AND OPTICAL PROPERTIES

KAMAL, SALWA JAMAL M

FACULTY OF SCIENCE
UNIVERSITI MALAYA
KUALA LUMPUR

2022

**PHENYL RINGS MESOGENIC CORE OF AZO-ESTER
BASED LIQUID CRYSTALS: SYNTHESIS,
MESOMORPHIC AND OPTICAL PROPERTIES**

KAMAL, SALWA JAMAL M

**THESIS SUBMITTED IN FULFILMENT OF THE
REQUIREMENTS FOR THE DEGREE OF
DOCTOR OF PHILOSOPHY**

**DEPARTMENT OF CHEMISTRY
FACULTY OF SCIENCE
UNIVERSITI MALAYA
KUALA LUMPUR**

2022

UNIVERSITI MALAYA
ORIGINAL LITERARY WORK DECLARATION

Name of Candidate: **KAMAL, SALWA JAMAL M**

Matric No: **SVA180010 (17036571/1)**

Name of Degree: **DOCTOR OF PHILOSOPHY**

Title of Thesis (“this Work”):

**PHENYL RINGS MESOGENIC CORE OF AZO-ESTER BASED LIQUID
CRYSTALS: SYNTHESIS, MESOMORPHIC AND OPTICAL PROPERTIES**

Field of Study: **ORGANIC CHEMISTRY**

I do solemnly and sincerely declare that:

- (1) I am the sole author/writer of this Work;
- (2) This Work is original;
- (3) Any use of any work in which copyright exists was done by way of fair dealing and for permitted purposes and any excerpt or extract from, or reference to or reproduction of any copyright work has been disclosed expressly and sufficiently and the title of the Work and its authorship have been acknowledged in this Work;
- (4) I do not have any actual knowledge nor do I ought reasonably to know that the making of this work constitutes an infringement of any copyright work;
- (5) I hereby assign all and every rights in the copyright to this Work to the Universiti Malaya (“UM”), who henceforth shall be owner of the copyright in this Work and that any reproduction or use in any form or by any means whatsoever is prohibited without the written consent of UM having been first had and obtained;
- (6) I am fully aware that if in the course of making this work I have infringed any copyright whether intentionally or otherwise, I may be subject to legal action or any other action as may be determined by UM.

Candidate’s Signature

Date: 20/05/2022

Subscribed and solemnly declared before,

Witness’s Signature

Date: 20/05/2022

Name:

Designation:

**PHENYL RINGS MESOGENIC CORE OF AZO-ESTER BASED LIQUID
CRYSTALS: SYNTHESIS, MESOMORPHIC AND OPTICAL PROPERTIES**

ABSTRACT

Azo-ester compounds containing two and three-benzene-ring in the mesogen bearing varied lateral substituent at the 2-position to the azo linkage including the laterally unsubstituted compounds, i.e. -H, -F and -CH₃ with different terminal groups have been designed and synthesized. The chemical structures of all compounds were confirmed by Fourier transform infrared (FT-IR), ¹H and ¹³C nuclear magnetic resonance (NMR) spectroscopy and elemental analysis. All resulting compounds exhibited good thermal stability (above 319°C), as confirmed by thermogravimetric analysis (TGA). The mesomorphic behaviours of liquid crystal compounds were studied by differential scanning calorimetry (DSC), polarized optical microscopy (POM) and small- and wide-angle X-ray scattering (SWAXS). Mesomorphic studies revealed that all derivatives were liquid crystalline materials except for the two-benzene-ring compounds (**T1**, **T2** and **T3**) and the unsubstituted terminal three-benzene-ring analogues (**S1**, **C1** and **C6**). The introduction of terminal electron-donating groups in the laterally unsubstituted derivatives (**S2** and **S3**) gave nematic phase at 124°C and 135°C with marble and Schlieren textures, respectively. The laterally fluorinated azo-esters with terminal electron-donating groups (**C2** and **C3**) exhibited nematic phase at 95°C and 117°C, respectively. The incorporation of terminal electron-withdrawing bromine atom in the laterally neat compound (**S4**) induced enantiotropic nematic-nematic phase transition, while the laterally fluorinated azo-ester analogue (**C4**) showed nematic-nematic phase transition upon cooling only. The terminal nitro group in both laterally neat and laterally fluorinated derivatives (**S5** and **C5**) displayed nematic phase with clearing temperatures of 168°C and 164°C, respectively. The laterally methyl substituted compound with terminal electron-donating groups (**C7** and **C8**) showed nematic mesophase temperatures

at 105°C and 107°C, respectively, which are lower in values compared to the laterally neat and fluorinated analogues. SWAXS analysis confirmed the mesophase textures observed from POM. The absorption maxima of UV-Vis and photoluminescence spectra were influenced by the lateral and terminal substituents. The laterally methyl compounds showed blue-emission with a relatively higher fluorescence intensity compared to the lateral unsubstituted and fluorinated derivatives.

Keywords: azo-ester; lateral substituent; terminal group; mesomorphic behaviour; optical properties

Universiti Malaysia

TERAS MESOGENIK CINCIN FENIL BERASASKAN HABLUR CECAIR

AZO-ESTER: SINTESIS, CIRI-CIRI MESOMORFIK DAN OPTIK

ABSTRAK

Sebatian azo-ester baru yang mengandungi cincin dua dan tiga-benzena dalam mesogen dengan kumpulan pengganti lateral yang bervariasi pada kedudukan 2 daripada penghubung azo termasuk sebatian tanpa kumpulan pengganti lateral iaitu -H, -F dan -CH₃ dengan kumpulan terminal yang berbeza telah direka dan disintesis. Struktur kimia semua sebatian ditentukan oleh spektroskopi inframerah transformasi Fourier (FT-IR), resonans magnetik nuklear ¹H dan ¹³C (NMR) dan analisis unsur. Semua sebatian yang dihasilkan menunjukkan kestabilan terma yang baik (melebihi 319°C) dengan analisis termogravimetri (TGA). Tingkah laku mesomorfik sebatian hablur cecair dikaji dengan kalorimetri imbasan perbezaan (DSC), mikroskop optik berkutub (POM) dan serakan sinar-X bersudut kecil dan lebar (SWAXS). Kajian mesomorfik menunjukkan bahawa semua terbitan adalah sebatian hablur cecair kecuali sebatian cincin dua-benzena (**T1**, **T2** dan **T3**) dan analog cincin tiga-benzena yang tiada kumpulan penukarganti terminal (**S1**, **C1** dan **C6**). Kehadiran kumpulan penderma elektron terminal dalam terbitan yang tiada kumpulan penukarganti lateral (**S2** dan **S3**) memberikan fasa nematik masing-masing pada 124°C dan 135°C dengan tekstur marmor dan Schlieren. Manakala azo-ester dengan kumpulan penukarganti lateral fluorin dan kumpulan penderma elektron terminal (**C2** dan **C3**) masing-masing mempamerkan fasa nematik pada 95°C dan 117°C. Kehadiran atom bromin sebagai penarik elektron terminal dalam sebatian tanpa kumpulan pengganti lateral (**S4**) menyebabkan peralihan fasa nematik-nematik enantiotropik, manakala analog azo-ester dengan kumpulan penukarganti lateral fluorin (**C4**) menunjukkan peralihan fasa nematik-nematik semasa penyejukan sahaja. Kumpulan nitro terminal dalam kedua-dua terbitan tanpa kumpulan pengganti lateral dan dengan kumpulan pengganti lateral fluorin (**S5** dan **C5**) memaparkan fasa nematik pada suhu isotropik

masing-masing pada 168°C dan 164°C. Manakala sebatian dengan kumpulan pengganti lateral metil dan kumpulan penderma elektron terminal (**C7** dan **C8**) menunjukkan suhu mesofasa nematik masing-masing pada 105°C dan 107°C, yang nilainya lebih rendah berbanding analog tanpa kumpulan pengganti lateral dan dengan kumpulan pengganti lateral fluorin. Analisis SWAXS mengesahkan tekstur mesofasa yang diperhatikan dari POM. Penyerapan maksimum spektrum UV-Vis dan fotoluminesen dipengaruhi oleh pengganti lateral dan terminal. Sebatian lateral metil menunjukkan pancaran biru dengan keamatan pendarfluor yang agak tinggi berbanding dengan terbitan tanpa kumpulan pengganti lateral dan dengan kumpulan pengganti lateral fluorin.

Kata kunci: azo-ester; pengganti lateral; kumpulan terminal; tingkah laku mesomorfik; sifat optik

ACKNOWLEDGEMENTS

First and foremost, all praises to Allah Almighty for the guidance, help and strength to complete the PhD journey. Then, I would like to express my gratitude to my supervisors, Dr. Noordini Mohamad Salleh, Assoc. Prof. Dr. H.N.M. Ekramul Mahmud and Dr. Noor Idayu Mat Zahid for their guidance, patience and encouragement throughout my studies and research.

I also would like to thank Universiti Malaya for providing equipment and facilities for the research. I truly appreciate all the Department of Chemistry staff who helped me in my research work. In addition, my deepest gratefulness to my friends for the strongest supporters throughout my research.

Thank you for the financial support from the Universiti Malaya Research University Grant-Faculty Program (GPF060B-2018). In addition, I would like to thank Imam Abdulrahman Bin Faisal University and the Saudi Arabian Cultural Mission for their sponsorship and support.

Finally, I owe special gratitude to my parents, husband, siblings and children (Talal and Ward), who always support and pray for me. Without their support, I think I might not be able to complete my research.

TABLE OF CONTENTS

ABSTRACT	iii
ABSTRAK	v
ACKNOWLEDGEMENTS	vii
TABLE OF CONTENTS	viii
LIST OF FIGURES	xiii
LIST OF TABLES	xvii
LIST OF SCHEMES	xviii
LIST OF SYMBOLS AND ABBREVIATIONS	xix
LIST OF APPENDICES	xx
CHAPTER 1: INTRODUCTION	1
1.1 Background of the Study	1
1.2 Motivations	4
1.3 Objectives of the Study	6
1.4 Thesis Outline	7
CHAPTER 2: LITERATURE REVIEW	8
2.1 Classification of Liquid Crystals	8
2.2 Calamitic Liquid Crystals	9
2.2.1 Nematic Phase	11
2.2.2 Cholesteric Phase.....	12
2.2.3 Smectic Phase	14
2.3 Racemic and Chiral Centre Based Liquid Crystal	15
2.4 Azo-Ester Based Liquid Crystal	18
2.5 Structure-Mesomorphic Properties Relationship.....	23

2.5.1	Effect of Mesogenic Core on Mesomorphic Properties	23
2.5.2	Effect of Lateral Group on Mesomorphic Properties	27
2.5.3	Effect of Terminal Group on Mesomorphic Properties.....	31
2.6	Application of Azo-Ester Liquid Crystal Compounds	37
CHAPTER 3: METHODOLOGY		40
3.1	Materials	40
3.2	Synthesis of Liquid Crystal Compounds	40
3.2.1	Synthesis of Two-Benzene-Ring Azo-Esters (T1, T2 and T3)	41
3.2.1.1	Ethyl 4-(4-Hydroxyphenylazo) Benzoate (T1-1).....	41
3.2.1.2	(<i>R,S</i>)-Ethyl 4-(4-(2-Methylbutoxy)phenylazo) Benzoate (T1-2)	41
3.2.1.3	(<i>R,S</i>)-4-(4-(2-Methylbutoxy)phenylazo) Benzoic Acid (T1-3) .	42
3.2.1.4	(<i>R,S</i>)-Octyl 4-(4-(2-Methylbutoxy)phenylazo) Benzoate (T1) .	43
3.2.1.5	Ethyl 4-(2-Fluoro-4-Hydroxyphenylazo) Benzoate (T2-1).....	44
3.2.1.6	(<i>R,S</i>)-Ethyl 4-(2-Fluoro-4-(2-Methylbutoxy)phenylazo) Benzoate (T2-2).....	44
3.2.1.7	(<i>R,S</i>)-4-(2-Fluoro-4-(2-Methylbutoxy)phenylazo) Benzoic Acid (T2-3).....	45
3.2.1.8	(<i>R,S</i>)-Octyl 4-(2-Fluoro-4-(2-Methylbutoxy)phenylazo) Benzoate (T2).....	45
3.2.1.9	Ethyl 4-((4-Hydroxy-2-Methylphenylazo) Benzoate (T3-1)	46
3.2.1.10	(<i>R,S</i>)-Ethyl 4-((2-Methyl-4-(2-Methylbutoxy)phenylazo) Benzoate (T3-2).....	47
3.2.1.11	(<i>R,S</i>)-4-((2-Methyl-4-(2-Methylbutoxy)phenylazo) Benzoic Acid (T3-3).....	47

3.2.1.12	(<i>R,S</i>)-Octyl	4-(2-Methyl-4-(2-Methylbutoxy)phenylazo)	
	Benzoate (T3)		48
3.2.2	Synthesis of Three-Benzene-Ring Azo-Esters (S1, S2, S3, S4, S5, C1, C2, C3, C4, C5, C6, C7 and C8)		49
3.2.2.1	(<i>R,S</i>)-Phenyl	4-((4-(2-Methylbutoxy)phenylazo) Benzoate (S1)	49
3.2.2.2	(<i>R,S</i>)-4-Methoxyphenyl	4-(4-(2-Methylbutoxy)phenylazo)	
	Benzoate (S2)		49
3.2.2.3	(<i>R,S</i>)-4-Butoxyphenyl	4-(4-(2-Methylbutoxy)phenylazo)	
	Benzoate (S3)		50
3.2.2.4	(<i>R,S</i>)-4-Bromophenyl	4-(4-(2-Methylbutoxy)phenylazo)	
	Benzoate (S4)		51
3.2.2.5	(<i>R,S</i>)-4-Nitrophenyl	4-(4-(2-Methylbutoxy)phenylazo) Benzoate (S5)	51
3.2.2.6	(<i>R,S</i>)-Phenyl	4-(2-Fluoro-4-(2-Methylbutoxy)phenylazo)	
	Benzoate (C1)		52
3.2.2.7	(<i>R,S</i>)-4-Methoxyphenyl	4-(2-Fluoro-4-2-Methylbutoxyphenylazo)	
	Benzoate (C2)		53
3.2.2.8	(<i>R,S</i>)-4-Butoxyphenyl	4-(2-Fluoro-4-2-Methylbutoxyphenylazo)	
	Benzoate (C3)		53
3.2.2.9	(<i>R,S</i>)-4-Bromophenyl	4-(2-Fluoro-4-(2-Methylbutoxy)phenylazo)	
	Benzoate (C4)		54
3.2.2.10	(<i>R,S</i>)-4-Nitrophenyl	4-(2-Fluoro-4-(2-Methylbutoxy)phenylazo)	
	Benzoate (C5)		55
3.2.2.11	(<i>R,S</i>)-Phenyl	4-((2-Methyl-4-(2-Methylbutoxy)phenylazo)	
	Benzoate (C6)		55

3.2.2.12	(<i>R,S</i>)-4-Methoxyphenyl-4-(2-Methyl-4-(2-Methylbutoxy)phenylazo) Benzoate (C7)	56
3.2.2.13	(<i>R,S</i>)-4-Butoxyphenyl 4-(2-Methyl-4-(2-Methylbutoxy)phenylazo) Benzoate (C8)	57
3.3	Characterisation Methods and Instrumentation	58
3.3.1	Fourier Transform Infrared Spectroscopy (FT-IR)	58
3.3.2	Nuclear Magnetic Resonance Spectroscopy (NMR)	59
3.3.3	Elemental Analysis CHN/O	62
3.3.4	Thermogravimetric Analysis (TGA)	63
3.3.5	Differential Scanning Calorimetry (DSC)	65
3.3.6	Polarized Optical Microscopy (POM)	67
3.3.7	Small- and Wide-Angle X-ray Scattering (SWAXS)	68
3.3.8	Ultraviolet-Visible Spectroscopy (UV-Vis)	70
3.3.9	Photoluminescence Spectroscopy (PL)	71
CHAPTER 4: RESULTS AND DISCUSSION		74
4.1	Synthesis	74
4.1.1	Diazotization Reaction	76
4.1.2	Williamson Etherification	77
4.1.3	Base Hydrolysis of Esters	78
4.1.4	Steglich Esterification Reaction	79
4.2	Structural Determination	81
4.2.1	FT-IR Spectra	81
4.2.2	¹ H NMR Spectra	82
4.2.3	¹³ C NMR Spectra	89
4.3	Physico-Chemical Characterization	95
4.3.1	Thermal Stability	95

4.3.2	Mesomorphic Behaviour	99
4.3.3	Optical Properties	123
CHAPTER 5: CONCLUSION AND FUTURE WORK.....		127
5.1	Conclusion	127
5.2	Future Work.....	128
REFERENCES.....		129
LIST OF PUBLICATIONS AND PAPERS PRESENTED		141
APPENDIX		144

Universiti Malaya

LIST OF FIGURES

Figure 1.1	: The ordering of solid crystal, liquid crystal and liquid molecules. Redrawn from (De Gennes, 1992).....	1
Figure 2.1	: The classification of liquid crystals.....	9
Figure 2.2	: General structure of liquid crystal molecule.....	10
Figure 2.3	: The orientation of the molecules in nematic phase	11
Figure 2.4	: Schlieren texture of the nematic phase under POM. Adopted from (Brostow & Lobland, 2016)	12
Figure 2.5	: (a) Thread-like texture and (b) marble texture, of the nematic phase under POM. Adopted from (Dierking, 2003).....	12
Figure 2.6	: Molecular order of cholesteric phase.....	13
Figure 2.7	: Cholesteryl benzoate that exhibits cholesteric phase.....	14
Figure 2.8	: Molecular order in smectic A and smectic C mesophases.....	15
Figure 2.9	: (a) Focal-conic fan shaped texture of SmA phase and (b) Schlieren texture of SmC phase under POM. Adopted from (Govindaiah, 2016).....	15
Figure 2.10	: A series of chiral monomers with end-capped bornyl group.....	16
Figure 2.11	: Ferroelectric liquid crystalline compounds.....	17
Figure 2.12	: <i>S</i> -4-(2-methylbutoxy) phenyl 4-(octyloxy)-benzoate.....	17
Figure 2.13	: Racemic and chiral liquid crystals branched terminal alkyl chains.....	18
Figure 2.14	: A series of 1,2-phenylene bis[4-(4-alkyloxyphenylazo) benzoates] bent-shaped compound.....	19
Figure 2.15	: Azo-ester liquid crystalline compounds.....	20
Figure 2.16	: H-shaped azo-ester liquid crystalline compounds.....	21
Figure 2.17	: A new series of LC compounds consisting of azobenzene ester....	22
Figure 2.18	: A series of azo-ester compounds.....	22
Figure 2.19	: Series of synthesized monophenyl, biphenyl or phenyl benzoate LCs.....	24

Figure 2.20	: Three ring system compounds.....	25
Figure 2.21	: Three- and four-rings azo-esters analogues.....	26
Figure 2.22	: New azo-phenylbenzothiazole analogues (EB1) and azo-benzothiazole (EB2) analogues.....	27
Figure 2.23	: New series of azo-ester LCs.....	28
Figure 2.24	: Azo-ester homologue compounds.....	29
Figure 2.25	: Liquid crystals substituted with lateral fluorine group.....	30
Figure 2.26	: Liquid crystals compounds with different positions of two laterally fluorine atoms.....	30
Figure 2.27	: Two series of 2 and 3 laterally methyl substituted derivatives.....	31
Figure 2.28	: Two new series of azo-Schiff base and azo-ester liquid crystals..	32
Figure 2.29	: Azo benzothiazole chromophore compounds.....	33
Figure 2.30	: Two series of the non-symmetric dimers.....	34
Figure 2.31	: 5-[2-(4-substituted phenyl)diazenyl]pyridin-2-yl 4'-alkoxybenzoate liquid crystals.....	35
Figure 2.32	: Azo-ester linked mesogen bearing polymerizable acrylate end-group.....	36
Figure 2.33	: Azo-ester derivatives with central naphthalene group.....	37
Figure 3.1	: Schematic diagram of FT-IR spectrometer.....	58
Figure 3.2	: Schematic diagram of NMR spectrometer. Redrawn from (Günther, 2013).....	61
Figure 3.3	: Schematic diagram of CHNS/O Elemental Analyzer. Redrawn from (Thompson, 2008).....	63
Figure 3.4	: Basic setup of TGA analyser. Redrawn from (Haines, 2012).....	64
Figure 3.5	: Schematic diagram of a differential scanning calorimeter and a typical DSC curve. Redrawn from (Höhne et al., 2003).....	66
Figure 3.6	: Basic setup of polarized optical microscope. Redrawn from (Dierking, 2003).....	67
Figure 3.7	: Schematic diagram of SWAXS technique.....	69
Figure 3.8	: Schematic diagram of UV-Vis spectrophotometer. Redrawn from (Hof, 2003).....	71

Figure 3.9	: A typical Jablonski diagram. Redrawn from (Lakowicz, 2013)....	72
Figure 3.10	: Schematic diagram of fluorescence spectrometer. Redrawn from (Lakowicz, 2013).....	73
Figure 4.1	: ^1H NMR spectrum of T1.....	83
Figure 4.2	: ^1H NMR spectrum of S1.....	84
Figure 4.3	: ^1H NMR spectrum of S2.....	85
Figure 4.4	: ^1H NMR spectrum of S3.....	86
Figure 4.5	: ^1H NMR spectrum of S4.....	87
Figure 4.6	: ^1H NMR spectrum of S5.....	87
Figure 4.7	: ^1H NMR spectrum of C1.....	88
Figure 4.8	: ^1H NMR spectrum of C6.....	89
Figure 4.9	: ^{13}C NMR spectrum of T1.....	90
Figure 4.10	: ^{13}C NMR spectrum of S1.....	91
Figure 4.11	: ^{13}C NMR and DEPT-135 NMR spectra of S2.....	92
Figure 4.12	: ^{13}C NMR and APT NMR spectrum of S3.....	93
Figure 4.13	: ^{13}C NMR spectrum of C1.....	94
Figure 4.14	: ^{13}C NMR spectrum of C6.....	95
Figure 4.15	: TGA curve and its corresponding derivative (DTG) of (a) T1 and (b) S1 at heating rate of $20^\circ\text{C min}^{-1}$ under nitrogen atmosphere.....	96
Figure 4.16	: DSC thermograms at the scanning rate of $10^\circ\text{C min}^{-1}$ of compounds T1, T2 and T3 upon heating.....	101
Figure 4.17	: DSC thermograms at the scanning rate of $10^\circ\text{C min}^{-1}$ of compounds S1, S2 and S3.....	103
Figure 4.18	: POM textures of S2 upon cooling from isotropic liquid at (a) 211°C , (b) 206°C , (c) at 200°C and (d) 84°C	103
Figure 4.19	: POM textures of S3 upon cooling from isotropic liquid at (a) 207°C , (b) 203°C and (c) 110°C	104
Figure 4.20	: DSC thermograms at the scanning rate of $10^\circ\text{C min}^{-1}$ of compounds C1, C2 and C3.....	106

Figure 4.21	: POM textures of C2 upon cooling from isotropic liquid at (a) 185°C, (b) 180°C, (c) 41°C and (d) 40°C.....	107
Figure 4.22	: POM textures of C3 upon cooling from isotropic liquid at (a) 182°C, (b) 181°C, (c) 180°C and (d) 71°C.....	108
Figure 4.23	: DSC thermograms at the scanning rate of 10°C min ⁻¹ of compounds S4 and S5.....	111
Figure 4.24	: DSC thermograms at the scanning rate of 10°C min ⁻¹ of compounds C4 and C5.....	111
Figure 4.25	: POM textures of S4 upon cooling from isotropic liquid at (a) 209°C, (b) 202°C and (c) 127°C and S5 at (d) 236°C, (e) 183°C and (f) 145°C.	112
Figure 4.26	: POM textures of C4 upon cooling from isotropic liquid at (a) 166°C, (b) 113°C and (c) 83°C and C5 at (d) 181°C, (e) 172°C and (f) 146°C.....	113
Figure 4.27	: DSC thermograms at the scanning rate of 10°C min ⁻¹ of compounds C6, C7 and C8.....	115
Figure 4.28	: POM textures of C7 upon cooling from isotropic liquid at (a) 158°C, (b) 155°C, (c) 49°C and (d) 48°C.....	116
Figure 4.29	: POM textures of C8 upon cooling from isotropic liquid at (a) 158°C, (b) 157°C, (c) 72°C and (d) 71°C.....	117
Figure 4.30	: SWAXS pattern of S2 at 25, 100, 140 and 160°C (a) upon heating, (b) upon cooling.....	118
Figure 4.31	: SWAXS patterns of S3, C2, C3, C7 and C8 (a) at 25°C, (b) at selected temperatures of nematic phase.....	120
Figure 4.32	: SWAXS pattern of (a) S4 at 25, 180 and 205°C; (b) S5 at 25 and 205°C upon heating.....	121
Figure 4.33	: SWAXS pattern of (a) C4 at 25 and 150°C upon heating. The inset shows scattering pattern at 100°C recorded on cooling; (b) C5 at 25 and 190°C upon heating.....	122
Figure 4.34	: UV-Vis absorption spectra of S2, S3, S4, S5, C2, C3, C4, C5, C7 and C8 in CDCl ₃ solution of 5 x 10 ⁻⁵ M.....	125
Figure 4.35	: PL spectra of S2, S3, S4, S5, C2, C3, C4, C5, C7 and C8 in CDCl ₃ solution of 5 x 10 ⁻⁵ M.....	126

LIST OF TABLES

Table 4.1	: The molecular structure and percentage yield of two and three-benzene-ring molecular core of azo-ester compounds.....	75
Table 4.2	: FT-IR spectral data of the synthesized compounds.....	82
Table 4.3	: TGA data of all azo-esters.....	98
Table 4.4	: Phase transition temperatures and enthalpy changes of the synthesized compounds upon the second heating and cooling runs at a scan rate of 10 °C min ⁻¹ by DSC.....	100
Table 4.5	: UV-Vis absorption and PL emission spectral data of LC compounds.....	123

Universiti Malaysia

LIST OF SCHEMES

Scheme 4.1	: Synthetic route of the three-benzene-ring azo-esters.....	76
Scheme 4.2	: Reaction mechanism of diazotization reaction.....	77
Scheme 4.3	: The general reaction mechanism of Williamson etherification....	78
Scheme 4.4	: Base hydrolysis of esters mechanism.....	79
Scheme 4.5	: Steglich esterification reaction mechanism	80
Scheme 4.6	: The use of DMAP in the esterification reaction.....	80

Universiti Malaya

LIST OF SYMBOLS AND ABBREVIATIONS

CDCl ₃	:	Deuterated chloroform
DCC	:	<i>N,N'</i> -dicyclohexylcarbodiimide
DCM	:	Dichloromethane
DMAP	:	<i>p</i> -dimethylaminopyridine
DMF	:	<i>N,N</i> -dimethylformamide
DMSO	:	Dimethylsulfoxide
DMSO-d ₆	:	Deuterated dimethylsulfoxide
DSC	:	Differential Scanning Calorimetry
FT-IR	:	Fourier Transform Infrared Spectroscopy
LC	:	Liquid crystal
NMR	:	Nuclear Magnetic Resonance Spectroscopy
NOE	:	Nuclear overhauser enhancement
POM	:	Polarised Optical Microscopy
ppm	:	Parts per million
SWAXS	:	Small- and Wide-Angle X-ray Scattering
TGA	:	Thermogravimetric analysis
S _N 2	:	Substitution Nucleophilic bimolecular
DEPT	:	Distortionless enhancement by polarization transfer
APT	:	Attached proton test

LIST OF APPENDICES

APPENDIX A	:	FT-IR Spectra.....	144
APPENDIX B	:	^1H NMR Spectra.....	152
APPENDIX C	:	^{13}C NMR Spectra.....	161
APPENDIX D	:	TGA Thermograms.....	171
APPENDIX E	:	DSC Thermograms.....	178

Universiti Malaya

CHAPTER 1: INTRODUCTION

1.1 Background of the Study

Liquid crystalline phenomena were first observed by Friedrich Reinitzer in 1888 (Reinitzer, 1888). In 1904 Lehmann used the term ‘liquid crystal’, to define a state of matter between the crystalline solid and isotropic liquid phases. Liquid crystals (LCs) possess the intermediate properties between the free flow of liquids and the distinguishing optical, electrical, and magnetic properties of solid crystals (Collings & Hird, 1997). In a crystal state, the positional and orientational order are long-range, while in a liquid state, the positional and orientational order are short-range. Figure 1.1 illustrates the ordering of solid crystal, liquid crystal and liquid molecules.

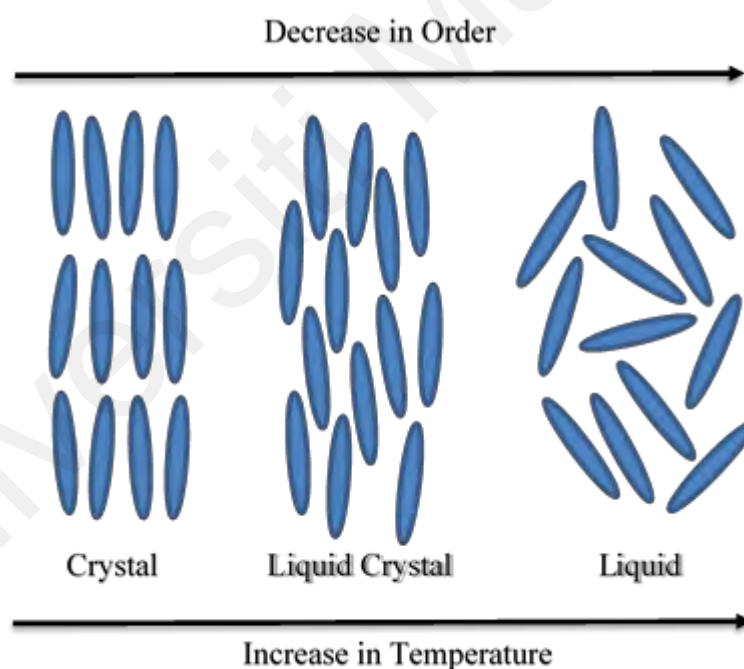


Figure 1.1: The ordering of solid crystal, liquid crystal and liquid molecules. Redrawn from (De Gennes, 1992).

Crystalline state molecules are highly ordered and closely packed, forming a crystal lattice. The physical properties of the solid-state are essentially anisotropic. With an increase in the temperature of matter, the thermal movement of molecules increases intensely, such that the crystal lattice dissolves and becomes more fluidic. At this temperature, the matter becomes unspecified shape liquid. In the liquid state, the molecules are arranged in irregular order, and are tightly attached to each other. On the other hand, in the LC state, the molecules have order between the crystal solid and liquid states. They lose some of the positional order of the crystal while maintaining the liquid orientational order. The molecules incline to rearrange themselves with a degree of order extraordinary than is found in normal liquids and is close to that of solid crystals. Subsequently, even if the molecular positions are ordered randomly, their orientation may be aligned in a regular pattern resulting in the appearance of the liquid ordered structure. LCs flow like liquids, while also having several material and optical properties such as viscosity, refractive index, permittivity, and elasticity, which are anisotropic. LC order can be easily adjusted with corresponding changes in optical properties since it is not fixed as that in a solid. Another term for LC is mesophase or mesomorphic phase, which means an intermediate phase. A compound that exhibits a mesomorphic phase is called a mesogenic compound (Andrienko, 2018; Singh & Dunmur, 2002; Wang & Zhou, 2004).

The development of liquid crystals began over 150 years ago, but their indication was not fully recognized until more than a century later. From 1834 to 1861, some researchers working on biological samples produced from nerve tissue showed that when nerve fibres were placed in water, they created a fluid material which exhibited unknown behaviour under polarised light. They had not perceived the formation of a new phase. Furthermore, in 1877 a German physicist Otto Lehman observed a cloudy liquid phase after a clear liquid when cooling cholesterol derivatives using an optical polarised microscope. However, he also had not correlated it with a new phenomenon. After that in

1888, an Austrian botanical physiologist Friedrich Reinitzer discovered that the colour changes in a cholesteryl benzoate derivative were not the most unusual feature. He observed that cholesteryl benzoate has two melting points, unlike other compounds. At 145.5 °C, the substance melts into a flowy liquid, and upon further heating to 178.5 °C, it becomes clear. Reinitzer was the first to discover this new phase of matter. After that, he wrote to Otto Lehmann asking for help in his discovery. Lehmann and Reinitzer's colleague, von Zepharovich indicated that the intermediate cloudy fluid was crystalline. Finally, Lehmann coined the name “liquid crystal” to the cloudy liquid and described some properties of liquid and crystal. In 1890, Gatterman and Ritschke synthesized the first synthetic *p*-azoxyanisole LC. They reported the LC properties of *p*-methoxycinnamic acid ten years later. After that, Meyer and Dahlem prepared the first smectic mesogen *p*-azoxybenzoate in 1902. In 1992, liquid crystals were divided into three types, namely nematic, smectic and cholesteric phases depending on the level of order possessed by molecules in the bulk materials (Demus et al., 1998).

From the start of the twentieth century until 1935, liquid crystals work was continued and considerably enlarged by the German chemist Daniel Vorländer, who had generated most of the LCs. For about 80 years, liquid crystalline materials have remained uncommon to scientists, making them a pure scientific curiosity (Sluckin et al., 2004).

After World War II, George William Gray restarted work on LCs and investigated the mesomorphic properties of several new synthesized materials in the late 1940s, as well as established a better knowledge of how to construct molecules that exhibit the LC state (Gray, 1962). The first international conference on LCs was organized by Glenn Brown in Kent, Ohio, in 1965 with the presence of many leading LC scientists in the world. This conference marks the commencement of a global effort to continue research

in the LC subject, which has resulted in the creation of various practical applications for these novel materials (Stegemeyer, 1994).

In 1966, the Heilmeyer group at Radio Corporation of America (RCA) developed mixtures of Schiff base nematic compounds for the first LC display device (Heilmeyer et al., 1968). The mixing of nematic compounds technique to obtain a wide range of operating temperature eventually became the industry standard and continues to be used to customize materials to meet specific applications.

In 1969, a nematic phase of N-(4-methoxybenzylidene)-4-butylaniline (MBBA) molecule have been synthesized at room temperature by Hans Kelker, which is one of the most common topics in liquid crystalline research (Kelker & Scheurle, 1969). After that, George Gray prepared varied rod-shaped cyanobiphenyls substances with low melting temperatures to commercialization of liquid-crystal displays (Gray et al., 1973). Later, disc-shaped (Chandrasekhar et al., 1977) and cone or bowl-shaped liquid crystalline materials have been generated (Collyer, 2012). In 1991, French physicist Pierre-Gilles de Gennes awarded the Nobel Prize in Physics for his discoveries on the ordering of LC molecules (De Gennes, 1992). The recent development of LCs science had a major influence by Pierre-Gilles de Gennes work (De Gennes & Prost, 1993). Following these wonderful discoveries, scientists in the relevant fields turn their attention towards a growing number of compounds, which exhibited LC properties. Today, liquid crystalline materials have become part of our daily life in numerous display technologies.

1.2 Motivations

Thermotropic liquid crystalline (LC) materials have been a significant area of research because of their diverse applications in optical organic transistors (Hrozhyk et al., 2010; Yager & Barrett, 2006; Zhang et al., 2012), biomolecules fluorescent probes

(Scott, 2007), liquid crystals display (Thieghi et al., 2003), sensors (Carlton et al., 2013), and signal processing and storage (Åstrand et al., 2000). Thus, various structural modifications and substitutions have been carried out by the researchers to study the effect of mesogenic core, lateral and terminal groups on mesomorphic behaviours (Ahmed et al., 2018; Ahmed et al., 2020; Karim et al., 2019; Naoum et al., 2016; Saad et al., 2019; Sardon et al., 2021; Zaki et al., 2018).

This research work is directed to the synthesis of new LC compounds having two and three-benzene-ring in the mesogen with azo and ester linkage. The synthesis is targeted to produce LC compounds that can be used in various electronic applications, such as electronic displays, data storage and optical computing. The azo linking group was chosen due to its promising optical, thermal and mechanical properties. The combination of the azo linkage with the ester group in the LC core is commonly used to increase the polarizability of the compounds and the stability of mesophase. Additionally, incorporating the lateral substituent in the rigid core of LC compounds interrupts the molecular closed packing and reduces the melting temperature, thereby effectively improving the LC properties of the resulting derivatives. LC properties are also strongly influenced by terminal groups with different polarities which can decrease or increase the mesomorphic properties due to the extremes of the electronic interactions between the substituent and the mesogenic core (Al-Hamdani et al., 2020; Karim et al., 2016; Naoum et al., 2010; Nessim et al., 2004; Salleh et al., 2013; Thaker et al., 2010; Zaki et al., 2018). The study of the effects of the lateral and terminal substituents on the azo-ester liquid crystalline behaviours and their optical properties is the pathway towards this research goal.

According to the literature survey, the synthesis and mesomorphic properties of two and three-benzene-ring with azo and ester linkage groups bearing 2-methylbutoxy

unit in one of the terminals and different polar groups as other side terminal chain with a varied lateral substituent at the 2-position to the azo linkage have not yet been reported.

1.3 Objectives of the Study

This work covers the synthesis and characterization of new nematic liquid crystals. The research objectives are as follows:

1. To synthesize and characterize a series of varied laterally two and three-benzene-ring molecular core of azo-ester compounds bearing 2-methylbutoxy unit as the terminal chain where the opposite terminal side substituent is a polar group that changes between the electron-donating group and electron-withdrawing group.
2. To study the thermal and mesomorphic properties of the synthesized nematic liquid crystals via thermogravimetric analysis (TGA), differential scanning calorimetry (DSC), polarized optical microscopy (POM) and small- and wide-angle X-ray scattering (SWAXS).
3. To study the optical properties via ultraviolet-visible (UV-Vis) and photoluminescence (PL) spectroscopies.

1.4 Thesis Outline

Chapter 1 provides a background of the discovery and development of liquid crystals. Furthermore, the research motivation and objectives on solving this recurring issue are emphasized.

Chapter 2 describes the classification of liquid crystals and calamitic liquid crystals. A recent literature background of racemic, chiral, azo-ester liquid crystalline compounds and structure-mesomorphic properties is provided. In addition, the application which involves the liquid crystal compounds is discussed.

Chapter 3 describes all experimental procedures related to the synthesis of azo-ester compounds. The characterization methods, including common principles and measurements, are elaborated in detail.

Chapter 4 discusses the general outcomes obtained from the synthesis and characterisation techniques applied throughout this study. The synthesized compounds were characterized using ^1H NMR with the spectral assignments supported by ^{13}C NMR and FT-IR spectroscopies and elemental analysis. The thermal behaviour of the compounds was studied using TGA analyzer. Their liquid crystalline properties were studied by POM, DSC and confirmed by SWAXS. Finally, the optical properties were obtained via UV-Vis and PL.

Finally, Chapter 5 outlines the concluding observations of the research output and also contain some recommendations for future works. The appendices provide supplementary data related to the results and discussion of the conducted experimental work.

CHAPTER 2: LITERATURE REVIEW

2.1 Classification of Liquid Crystals

Liquid crystals (LCs) are classified into thermotropic and lyotropic LCs, depending on how the mesophase is produced. Thermotropic LCs display a variety of phases with changes in temperature. Upon heating, LC compounds may form various mesophases, followed by the isotropic phase as the temperature increases. Conversely, the isotropic phase could transform into the mesophases again upon cooling cycle. LC phases are stable for a certain range of temperatures. Melting point, clearing point, monotropic and enantiotropic are the common terms used in describing the thermal properties of LCs. The term melting point refers to the transition temperature from the solid crystal to the mesophase, whereas the clearing point is defined as the transition temperature from the mesophase to isotropic liquid phase. The mesophase obtained during the cooling process only is called a monotropic phase, while the mesophase observed in both heating and cooling processes is called an enantiotropic phase (Kumar, 2011).

Lyotropic LCs are obtained by dissolving specific molecules in the solution. The composition of the mixture at a certain concentration ranges determines the phases of these materials (Liang et al., 2005). As this thesis is mainly focused on thermotropic LC materials, lyotropic LC will not be addressed further.

Thermotropic LC materials can be further divided into two classes: (i) low molecular mass and (ii) high molecular mass. Low molecular mass thermotropic LCs are classified into three main types based on the molecular shape of the constituent molecules, i.e. calamitic LCs containing rod-like, discotic or disc-like and bent-shaped LCs. On the other hand, high molecular mass thermotropic LCs are called liquid crystalline polymers, and can further be categorized into main chain polymers and side chain polymers. In this

thesis, only calamitic LCs will be discussed. Figure 2.1 shows the classification of liquid crystals.

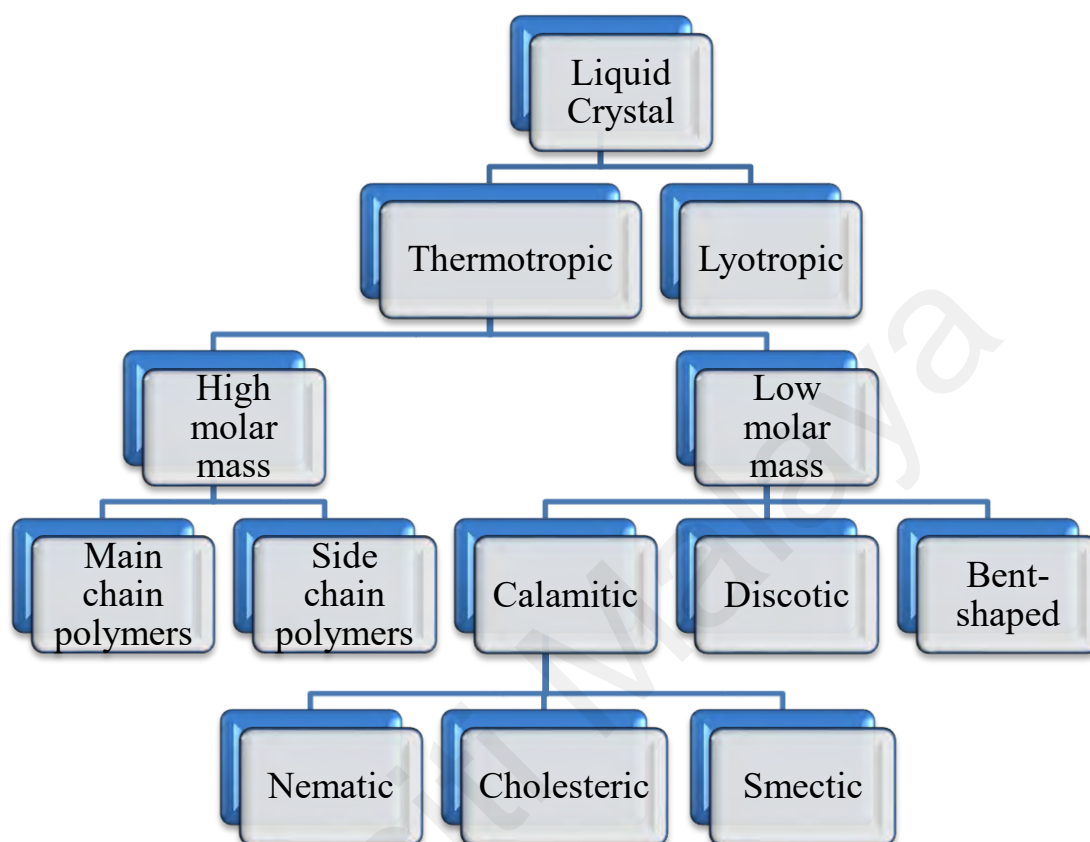


Figure 2.1: The classification of liquid crystals.

2.2 Calamitic Liquid Crystals

Rod-like molecules of calamitic LCs are a common type of low molar mass LC compounds that exhibit a thermotropic mesophase. The molecular length is much larger than the molecular width in these molecules, giving them an elongated shape. Strong attractive forces have been possessed by these elongated molecules with little tendency to collide with each other because the molecules incline to align in the same direction, which helps to stabilize the whole molecular arrangement. Generally, the structure of LC molecules must consist of a rigid core unit called mesogen and a flexible chain known as a spacer unit. The general structure of the liquid crystal molecule is shown in Figure 2.2.

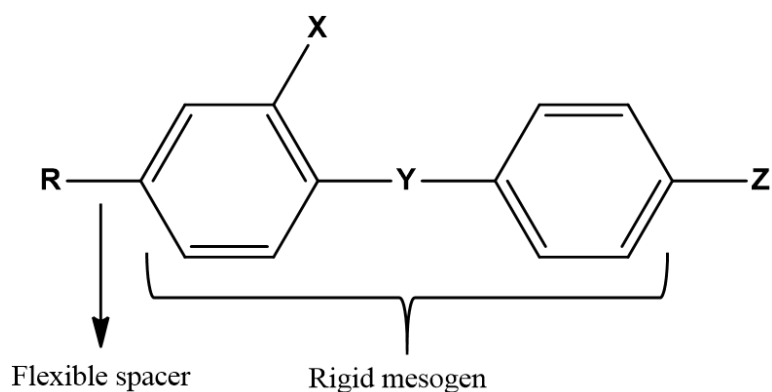


Figure 2.2: General structure of liquid crystal molecule.

Diverse combinations of benzene, naphthalene, biphenyl, triphenyl, saturated cyclohexane and unsaturated phenyl usual formed the mesogen. In addition, benzothiazole, pyridine and pyrimidine heterocyclic compounds are also used as core units. These units are connected to each other by various linking groups such as azo ($-N=N-$), Schiff base ($-CH=N-$), ester ($-COO-$), stilbene ($-CH=CH-$) and acetylene ($-C\equiv C-$). The rigidity of the mesogen is strongly based on the different types of these linking groups. Therefore, the names of LC compounds are usually dependent on the type of linking group e.g. azo-ester LC. The flexible spacer (R) is normally consisting of alkoxy (OC_nH_{2n+1}) or alkyl (C_nH_{2n+1}) groups. When a molecule moves around, its flexibility allows it to easily position itself amongst neighbouring molecules. In order to show LC properties, both flexible and the rigid units must be balanced (Khoo, 2007). Usually, X is a lateral substituent and Z is a terminal substituent consisting of alkoxy or halogen groups at different positions on the rigid mesogen. Liquid crystals thermal properties are highly dependent on the incorporation of these substituents. Three common mesophases exhibited by the calamitic liquid crystalline materials are nematic, cholesteric and smectic phases.

2.2.1 Nematic Phase

The nematic (N) phase, has the simplest structure of all mesophases and the least ordered phase closest to the isotropic liquid phase. The word “nematic” derives from the Greek *nematos*, which means thread-like, originates from the optical texture observed for the phase between crossed polarizers. The nematic phase has a high order of long-range orientation of molecules, and there is no translational order in the phase. The molecules in the nematic phase are oriented with their long axes nearly parallel to each other as shown in Figure 2.3. A uniformly aligned nematic phase has a preferred orientation, often defined by a unit vector known as the director, \hat{n} . This mesophase has a perfect symmetry in the rotation around the director. As the temperature decreases, the phase order is increased and vice versa (Chandrasekhar, 1992).

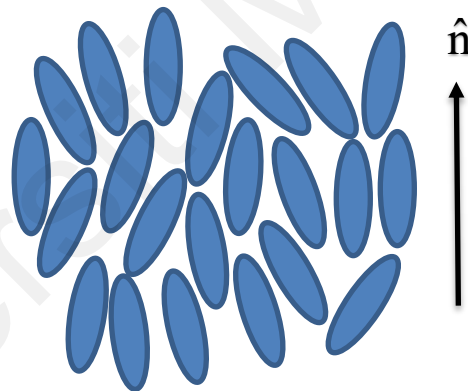


Figure 2.3: The orientation of the molecules in nematic phase.

Nematic LCs are anisotropic due to their microscopic structure. Due to an anisotropy in the distribution of electrical charge, LC molecules may undergo a reorientation. Nematic LCs possess several useful properties such as high refractivity, sensitivity to low-frequency electric fields and structural flexibility. The combination of these properties forms the basis to operate several liquid crystal devices in production. Nematic phases can be determined using polarised optical microscopy (POM) which

displays unique textures with two and four-point defects, known as "Schlieren" texture, as shown in Figure 2.4 (Collings, 2002). In addition, different textures may be exhibited by nematic LCs, such as marble texture and thread-like texture, as shown in Figure 2.5 (Dierking, 2003).

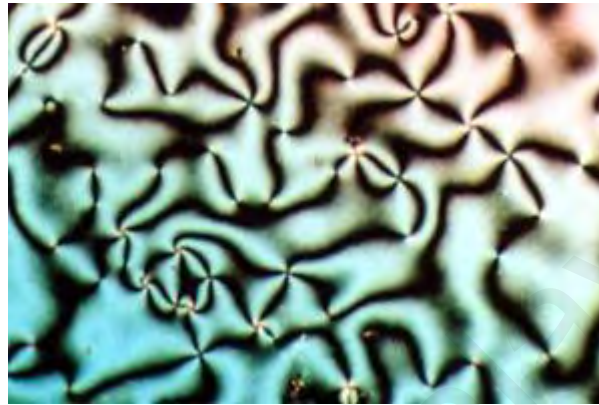


Figure 2.4: Schlieren texture of the nematic phase under POM. Adopted from (Brostow & Lobland, 2016).

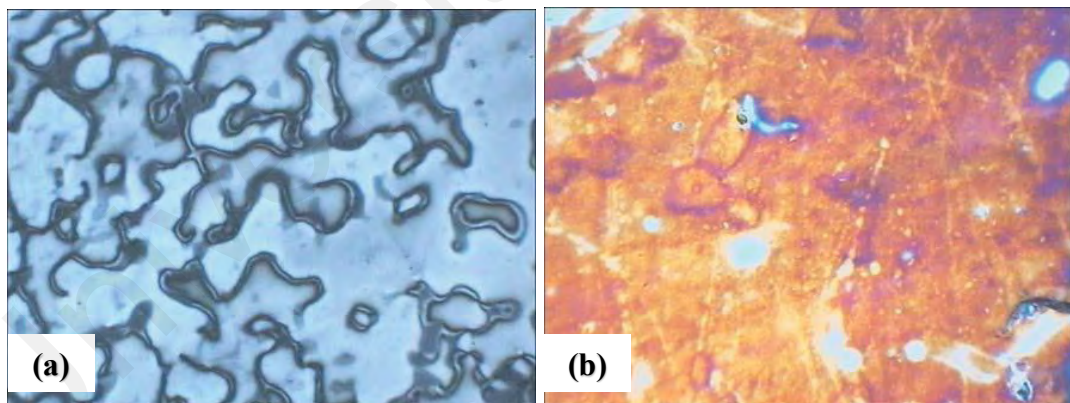


Figure 2.5: (a) Thread-like texture and (b) marble texture, of the nematic phase under POM. Adopted from (Dierking, 2003).

2.2.2 Cholesteric Phase

The cholesteric phase is also known as chiral nematic phase, and is formed when the director, \hat{n} in a nematic mesophase is twisted about an axis perpendicular to the local

director, as illustrated in Figure 2.6. The molecular structures of nematic and cholesteric phases are alike on a local scale, while on a large scale the cholesteric director follows a helical form (Muñoz & Alfaro, 2000). The distance needed to rotate the director by 2π along the helix axis is known as the pitch, P , which usually ranges between 2000 Å and macroscopic values. Cholesterics of low P (below 5000 Å) show the blue phase, which exist over a small temperature range (~ 1 °C) between the cholesteric mesophase and the isotropic phase. In 1888, Friedrich Reinitzer recognized the first cholesteric LC phase and observed a blue phase on cholesteryl benzoate compound. The chemical structure of cholesteryl benzoate is shown in Figure 2.7. Liquid crystalline materials with the cholesteric mesophase have the ability to change colour as a function of temperature, electric fields, mechanical stress or non-chiral solute molecules (Meier et al., 2012). These features make the cholesteric LC materials useful in thermometers as a thermal sensor and in other thermometry technical applications (Winterbottom et al., 2003).

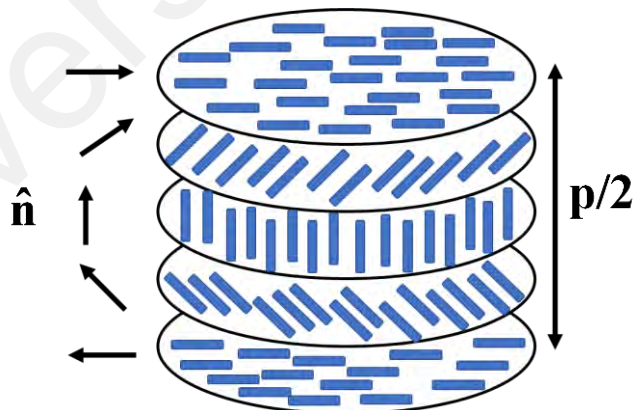


Figure 2.6: Molecular order of cholesteric phase.

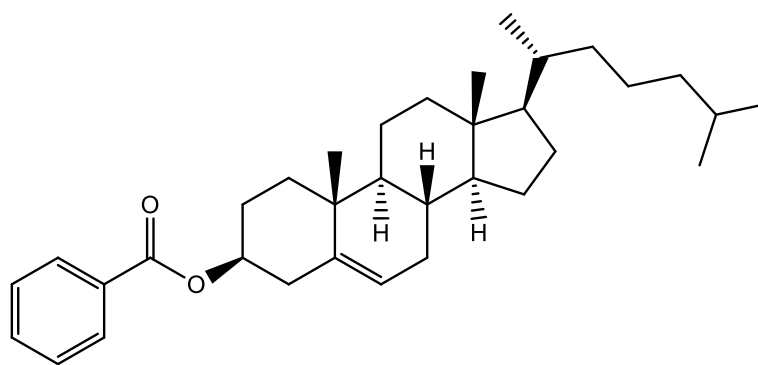


Figure 2.7: Cholesteryl benzoate that exhibits cholesteric phase.

2.2.3 Smectic Phase

The combination of orientational and positional orders form high order LC phase is known as the smectic phase. This phase is recognized by the appearance of the interlayer correlations and the loss of freedom of molecular rotation in some cases. The smectic phase which is usually found at lower temperatures than nematic phase under POM has layered structure that can slide on top of each other in a similar way of soap. The term “smectic” derives from the Latin word *smecticus*, which mean cleaning or possessing soap-like properties (Collings & Hird, 1997).

There are varied number of smectic mesophases, which are positionally arranged along one direction. Smectic LCs are classified based on whether the director is parallel or tilted in relation to the normal layer. The most commonly smectic mesophases observed are Smectic A (SmA) and Smectic C (SmC). In SmA phase, the director, \hat{n} is perpendicular to the normal layer. This mesophase possesses liquid properties but is higher viscosity than the nematic mesophase. The strong interlayer forces and weak attractions between the molecules allow the layers to simply slide over one another, resulting in these features. The molecules of SmC phase are ordered as in the SmA phase, but the director is tilted away from the smectic plane (Chandrasekhar, 1992; De Gennes & Prost, 1993). Figure 2.8 shows the molecular order in SmA and SmC mesophases.

POM shows SmA phase as focal-conic fan texture, whereas SmC appeared as a Schlieren texture (Figure 2.9).

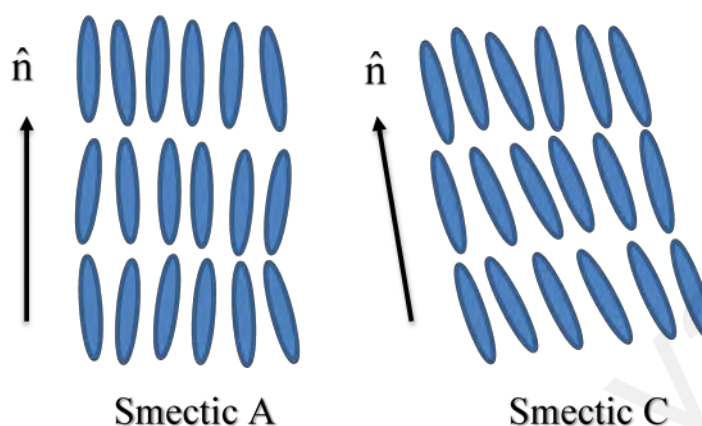


Figure 2.8: Molecular order in smectic A and smectic C mesophases.

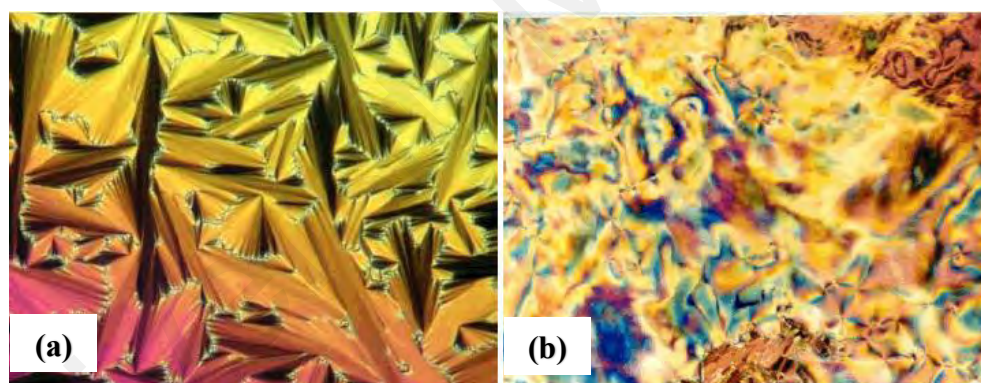


Figure 2.9: (a) Focal-conic fan shaped texture of SmA phase and (b) Schlieren texture of SmC phase under POM. Adopted from (Govindaiah, 2016).

2.3 Racemic and Chiral Centre Based Liquid Crystal

Avast numbers of chiral LC derivatives have been reported (Kašpar et al., 2007; Prasad, 2001). LCs with chiral molecules exhibit various mesophase and physical properties. Liu et al. (Liu et al., 2004) synthesized chiral polyacrylates with end-capped bornyl groups with biphenyl, phenyl benzoate, azobenzene, and benzoyloxy biphenyl

mesogenic moieties as shown in Figure 2.10. High thermal resistance and negative optical rotation were detected for the chiral polymers. Homopolymers of compound 3 have been reported to have two mesophases under DSC thermogram. Oily streak textures of chiral SmA phase were observed during the heating cycle at 125 °C and 150 °C under a polarised optical microscope.

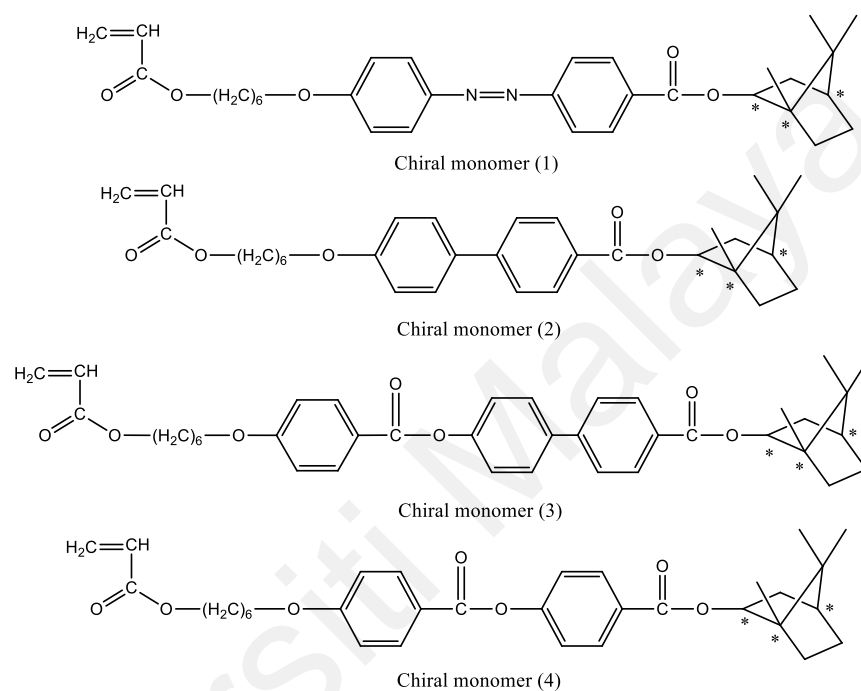


Figure 2.10: A series of chiral monomers with end-capped bornyl groups.

Kašpar et al. studied the ferroelectric mesomorphic properties of liquid crystalline compounds with 2-alkoxypropanoate chiral unit and alkoxy benzoate unit laterally substituted by methoxy (Kašpar et al., 1995), methyl (Kaspar et al., 1997), halogens (Kašpar et al., 2007) as shown in Figure 2.11. All ferroelectric liquid crystalline compounds possess SmC* mesophase on a broad temperature range. The phase transition temperature increased in a sequence of OCH₃ < CH₃ < Br < Cl < F < H, while the spontaneous polarization values increased in a sequence of OCH₃ < H < F < CH₃ < Cl < Br. The lateral substituent mesogenic core, which is far from the chiral centre, lowered

the phase transition temperatures than that of the non-substituted chiral centre compounds.

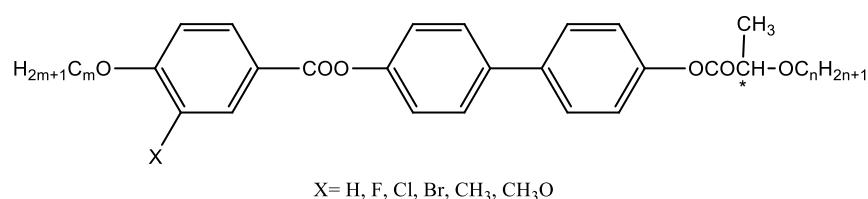


Figure 2.11: Ferroelectric liquid crystalline compounds.

In 2013, Fitas et al. reported the ferroelectric physical properties of (*S*)-4-(2-methylbutoxy) phenyl 4-(octyloxy)-benzoate (Figure 2.12). The compound contains two benzene rings linked by an ester group as a rigid part with an alkoxy group as a flexible part. They observed the appearance of SmA and nematic phases within narrow temperature range, but it was too limited to justify using the material in LCDs on its own. In particular, the nematic phase has never been observed in a stable state. However, as long as the sample remains surface-aligned, the other liquid crystalline phases remain extremely stable (Fitas et al., 2013).

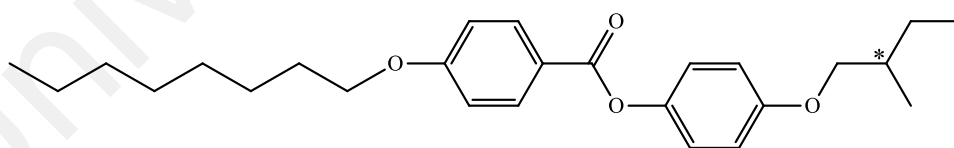


Figure 2.12: *S*-4-(2-methylbutoxy) phenyl 4-(octyloxy)-benzoate.

Racemic and chiral liquid crystalline material containing four phenyl rings connected by Schiff base groups and terminal alkyl chains were synthesised and characterised by Blach and co-workers, as shown in Figure 2.13 (Blatch et al., 1997). The racemic series exhibited both SmA and nematic phases. The transition temperatures of

the chiral series are similar to those of racemic derivatives. A focal-conic fan texture was observed for the chiral analogues which when sheared, exhibited the Grandjean texture of chiral nematic phase. An odd-even number of methylene units in the spacer effect was obtained for the chiral properties of these LC compounds. The heptane and nonane derivatives exhibited blue phase I behaviour, which was not observed in the even membered hexane and octane of the same series (Blatch et al., 1997).

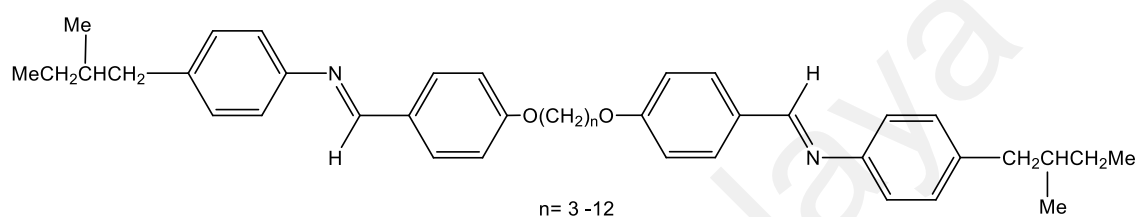


Figure 2.13: Racemic and chiral liquid crystals branched terminal alkyl chains.

2.4 Azo-Ester Based Liquid Crystal

Many researchers have synthesized mesogenic compounds containing azo linking groups due to their promising mechanical, optical and thermal properties (Karim et al., 2014). The efficient and reversible photochemical properties lead them potential in various applications such as liquid crystals display, optical organic transistors, biomolecules fluorescent probes and signal processing and storage (Åstrand et al., 2000; De Sio et al., 2012; Hrozhyk et al., 2010; Li et al., 2012; Sardon et al., 2021; Thieghi et al., 2003; Yager & Barrett, 2006; Yao et al., 2009; Zhang et al., 2012).

In addition, the incorporation of azo central linkage together with ester groups in the LC core is commonly used to increase the polarizability of the compounds and the stability of the mesophase (Singh & Dunmur, 2002). Prasad designed and synthesized a series of 1,2-phenylene bis[4-(4-alkyloxyphenylazo) benzoates] bent-shaped compounds (Figure 2.14) which exhibited nematic and SmA mesophases. The compounds with $n = 4$ gave a maximum nematic mesophase range, which then decreases gradually as n increases

to 8. The low transition temperatures reported for azo compounds make them suitable for physical studies (Prasad, 2001).

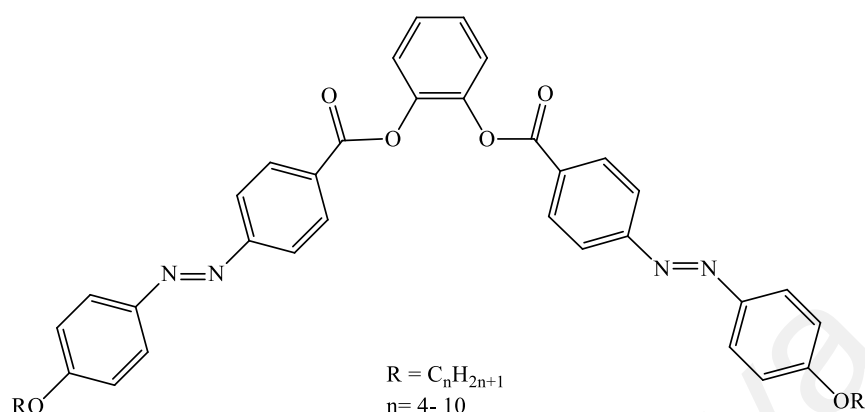
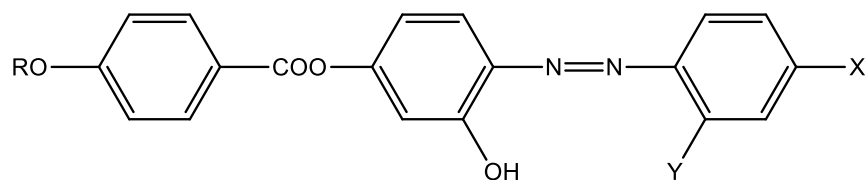


Figure 2.14: A series of 1,2-phenylene bis[4-(4-alkoxyphenylazo) benzoates] bent-shaped compound.

Prajapati et al. (Prajapati & Varia, 2008) prepared and studied two new series of azo-ester liquid crystalline compounds containing three phenyl rings with varied lateral substituents i.e. $-NO_2$, $-Cl$ and $-OH$ groups (Figure 2.15). Enantiotropic nematic and SmA mesophases were observed for all compounds. All compounds of the series I and II showed threaded or marble texture of a nematic mesophase and focal conic texture of a SmA mesophase. Series I and II exhibited higher thermal stabilities due to the existence of polar $-NO_2$ and $-Cl$ substituents. In addition, the compounds with $-OH$ substituent showed higher mesophase length along with thermal stabilities which can be attributed to the strong intramolecular hydrogen bonding compared with corresponding compounds without hydroxy groups.



R = C_nH_{2n+1}, n = 1-8, 10, 12, 14 and 16

Series I: X = NO₂, Y = Cl

Series II: X = Cl, Y = NO₂

Figure 2.15: Azo-ester liquid crystalline compounds.

The synthesis of H-shaped azo-ester twin liquid crystalline compounds containing tetramethylene flexible spacers and methyl or methoxy terminal substituents, as presented in Figure 2.16 was reported by Varia and co-workers (Varia et al., 2012). The Schlieren texture of a SmC mesophase for all compounds was observed under POM. All the H-shaped series II compounds with the methoxy terminal group exhibited higher mesophase transition temperatures as well as high thermal stability compared to series I, compounds with the methyl group, due to the high polarizability and rigidity of the alkoxy group in the former. The introduction of the azo linkage induced photochromism in the H-shaped twin liquid crystalline compounds.

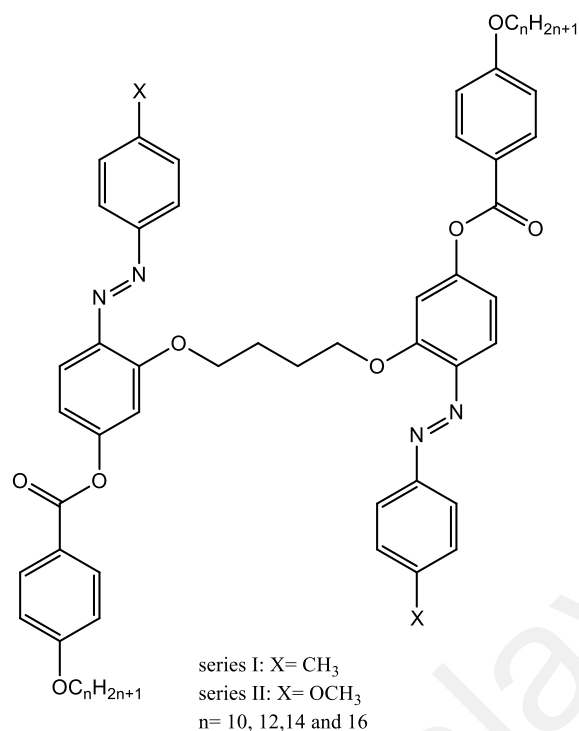


Figure 2.16: H-shaped azo-ester liquid crystalline compounds.

A new series of LC compounds consisting of azobenzene ester varied in the length of the methylene substituted in the rigid core and the side chain (Figure 2.17) were investigated (Xie et al., 2013). The phase transition temperature and the melting point decreased with the increase of methylene units in the rigid core of compounds I and the side chain of compounds II. The monotropic nematic phase changes to the enantiotropic nematic phase with the increase of the main chain of compounds I. The UV spectra of the synthesized LC compounds displayed one absorption band, which is attributed to the π - π^* electronic transition peaks of azo group.

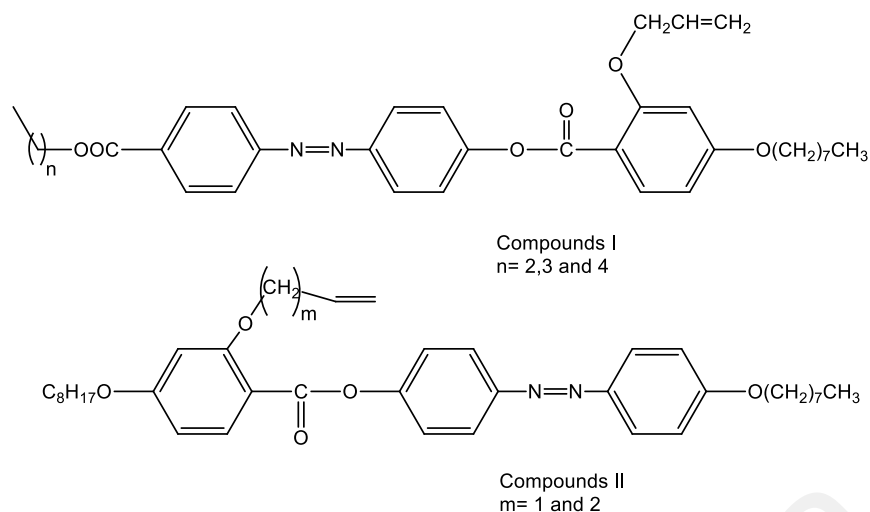


Figure 2.17: A new series of LC compounds consisting of azobenzene ester.

Naoum and co-workers prepared a series of azo-ester compounds with 8, 10, 12, 14 and 16 carbons with varied length alkoxy terminal group and $-\text{CH}_3\text{O}$, $-\text{CH}_3$, $-\text{H}$, $-\text{Br}$, and $-\text{CN}$ polar groups on the other terminal side (Figure 2.18) (Naoum et al., 2015a). The nematic transition temperature for the unsubstituted and electron-donating substituted ($-\text{CH}_3\text{O}$ and $-\text{CH}_3$) compounds decreased fairly, while the electron-withdrawing substituted ($-\text{Br}$ and $-\text{CN}$) decreased sharply with the increase in the length chain alkoxy group. These results are in agreement with those of previously reported works (Gray, 1962; Imrie & Taylor, 1989).

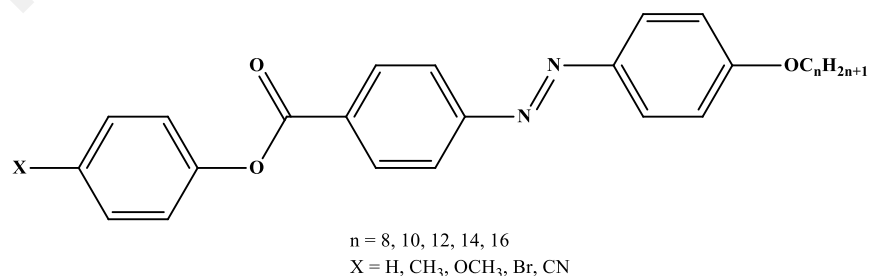


Figure 2.18: A series of azo-ester compounds.

2.5 Structure-Mesomorphic Properties Relationship

It is important to understand the structure-mesomorphic properties relationship of mesogenic units when choosing chemical modification for the synthesis of novel mesogens with eligible LC properties for promising application. The relationship between structure and mesomorphic behaviour was studied to determine: (i) whether the compound showed any mesomorphic behaviours, (ii) which chemical compound constitution have nematic, smectic or cholesteric phases, and (iii) the variation in the phase transition temperatures which occur when the synthetic constitution of a compound is modified (Gray, 1962).

2.5.1 Effect of Mesogenic Core on Mesomorphic Properties

Three series of calamitic LCs consisting of either a monophenyl, biphenyl or phenyl benzoate group were synthesized by Fornasieri et al. (Fornasieri et al., 2003). The mesogenic core was combined with per fluorinated chain by thioester linkage from one side and varying length of a hydrocarbon chain with double bond on the other terminal side (Figure 2.19). The effects of different mesogenic core and hydrocarbon chain length on mesomorphic properties were investigated. The mesomorphic behaviour reduced sharply with the increasing of the length of the hydrocarbon chain. In contrast, the transition temperature increased with the increasing number of phenyl rings in the rigid core, with the widest transition temperature range exhibited by the phenyl benzoate derivatives. Smectogenic enantiotropic phase has been observed near room temperature in monophenyl allyloxy derivatives.

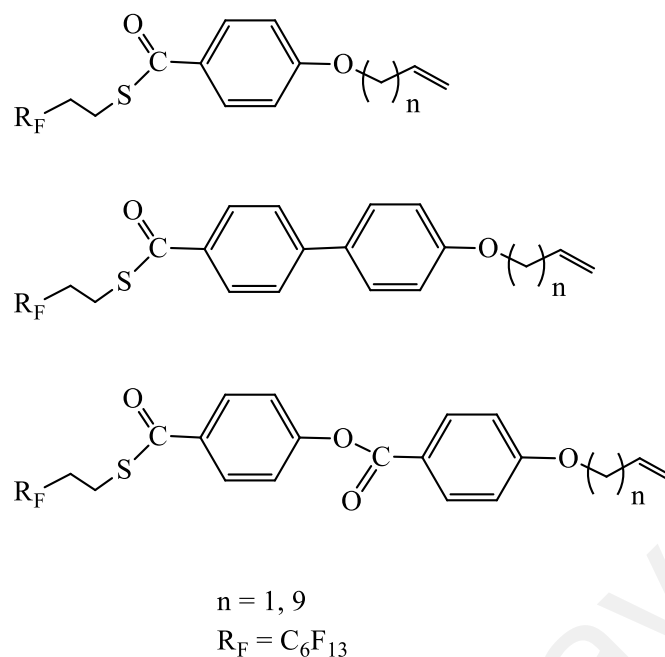


Figure 2.19: Series of synthesized monophenyl, biphenyl or phenyl benzoate LCs.

Mori and co-workers (Mori et al., 2010) prepared three ring systems such as 2,5-dibenzoyloxytropones (1-3), 5-benzoylamino-2-benzoyloxytropones (4-6), and 2,5-dibenzoylamino-2-benzoyloxytropones (7-9) with mono-alkoxy, di-alkoxy, and tri-alkoxy groups on the benzoyl group together with the corresponding benzenoids (10-18) and their mesomorphic properties were studied (Figure 2.20). Two monoalkoxylated benzoyl groups derivatives (1, 4, 7, 10, 13, and 16) exhibited nematic, SmA and SmC phases. The troponoids analogues (1, 4 and 7) showed N phase with lower thermal stability than that of benzenoids analogues (10, 13 and 17), respectively. Hexagonal columnar phases were observed for troponoid tetracatenars with two dialkoxybenzoyl groups, except for the derivative with two ester linking groups. Benzenoids with two dialkoxybenzoyl groups showed non-mesomorphic behaviours. All compounds of troponoid hexacatenars with two trialkoxybenzoyl groups formed hexagonal columnar phases, while all benzenoid hexacatenars formed hexagonal and tetragonal columnar phases, except for the derivatives with two ester-linking groups. The selection of core structure and the linking

groups greatly affect the thermal stability of the mesophases. The polarity of the troponoid core promotes microsegregation and core–core interaction via generating head-to-tail alignments. As a result, the thermal stability of the SmC phases of troponoid derivatives increased more than that of benzenoid derivatives. The replacement of the ester group by the amide-connecting group improves the lateral interaction via intermolecular hydrogen bonding and flattens the core structure by intramolecular hydrogen bonding with the adjacent tropone carbonyl group, consequently enhancing the thermal stability of the mesophases.

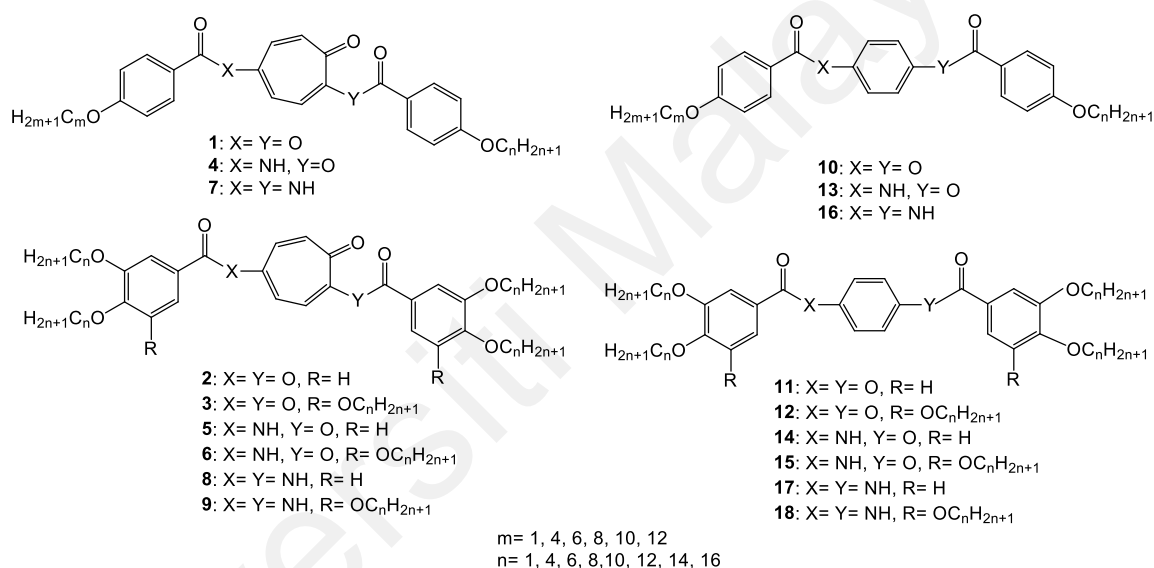


Figure 2.20: Three ring system compounds.

The effect of adding a phenylazo moiety into molecules of three-rings azo-ester analogues (series I) to produce four-ring analogues (series II) was investigated by Saad and co-workers (Saad et al., 2019) (Figure 2.21). The addition of a phenylazo group to each molecule of the three-ring structures has a different effect on the mesomeric interaction between the ester and the alkoxy oxygen group, and therefore on their mesophase behaviour. The melting and clearing temperatures of derivatives II are higher than those of derivatives I for the same terminal substituent (X) and methylene chain (n).

This indicates that the introduction of an additional phenylazo ring can also be regarded as a pronounced improvement of the anisotropic molecular shape.

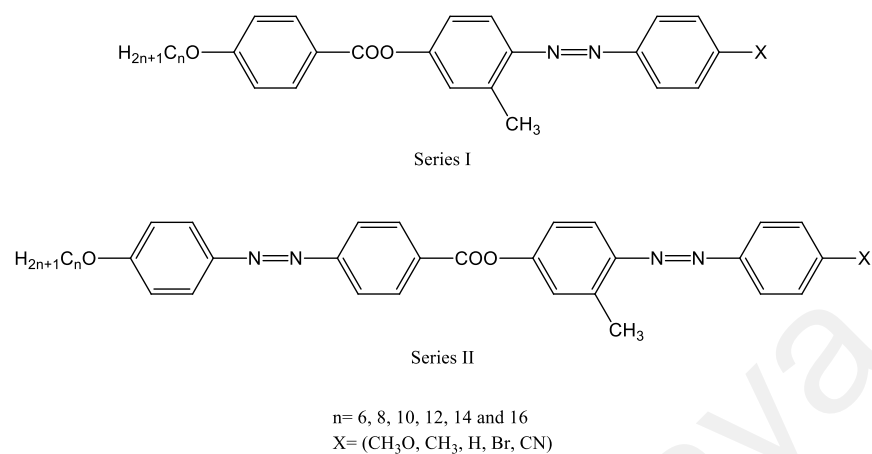


Figure 2.21: Three- and four-rings azo-esters analogues.

The synthesis of new azo-phenylbenzothiazole analogues (EB1) and azo-benzothiazole (EB2) analogues have been reported and their mesomorphic properties compared (Figure 2.22) (Al-Hamdani et al., 2020). All EB1 and EB2 derivatives exhibited an enantiotropic nematic phase only. The thermal stability of EB1 compounds is higher than EB2 due to the incorporation of the phenyl ring between the azo group and the benzothiazole ring. The presence of a phenyl ring increases the polarization of the molecule, which improve the appearance of LC mesophases with a higher temperature range.

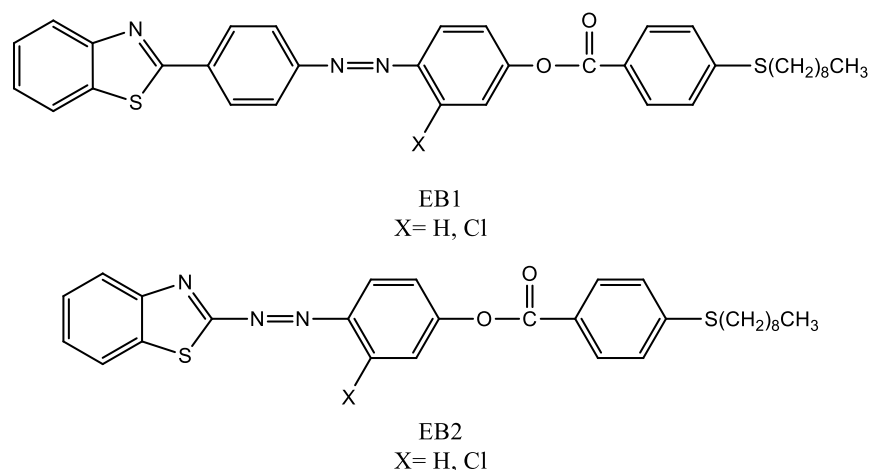


Figure 2.22: New azo-phenylbenzothiazole analogues (EB1) and azo-benzothiazole (EB2) analogues.

2.5.2 Effect of Lateral Group on Mesomorphic Properties

The effects of introducing the lateral methyl group on the mesomorphic properties in two new series of azo-ester LCs possessing lateral methyl group at the central and terminal phenyl rings with varied spacer length chain have been reported (Dave & Bhatt, 2012; Dave et al., 2010). The attachment of lateral methyl substituent to the mesogenic core in the two homologous series (Figure 2.23, Series 1 and 2) decreased the thermal stability of nematic to isotropic mesophase compared to laterally unsubstituted compounds (Figure 2.23, Series 3) synthesized by (Doshi & Ganatra, 1999). In addition, the incorporation of the lateral methyl substituent at the central and terminal phenyl rings (Figure 2.23, Series 2) reduced the thermal stability than those with lateral methyl group only at the central phenyl ring (Figure 2.23, Series 4) (Thaker et al., 2010). The introduction of one more laterally methyl group in the terminal phenyl ring had a great effect in the reduction of nematic to isotropic thermal stability. The inclusion of the lateral methyl group amends the molecular conformation and widens the molecules, by decreasing the melting and clearing temperatures.

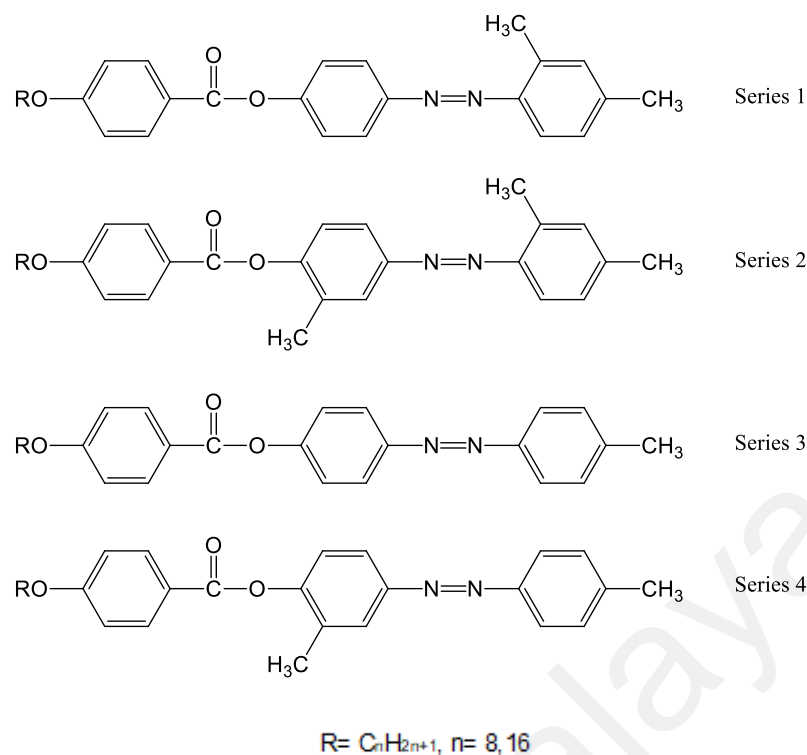


Figure 2.23: New series of azo-ester LCs.

The effect of lateral methyl substitution on the mesophase properties of 4-substituted phenyl 4'-(2'' or 3''-methyl-4''-alkoxyphenylazo) benzoates were investigated by Naoum and co-workers (Naoum et al., 2015b). The mesomorphic behaviours of both azo-ester compounds with lateral methyl group attached to the position 2 or 3 of the same ring were compared with each other, as well as with lateral neat analogues (Figure 2.24). All homologues derivatives containing varied electron-donating groups i.e. (-H, -CH₃O and -CH₃) showed pure nematic mesophase. Dimorphic mesophases were observed for the lower homologue derivatives with electron-withdrawing substituent i.e. (-Br and -CN), while pure SmA mesophase observed for higher homologues. The mesophase stability decreased for lateral methyl substitution compounds (II_{n a-e} and III_{n a-e}) compared to the laterally neat compounds (I_{n a-e}) except for II₁₀, 12 chain length derivatives with -Br and -CN terminal groups. This result due to the steric effects of the

lateral methyl group, which caused variable conformations and enforced the molecules to become slightly twisted. The methyl substituted in position 2 of $\text{II}n_{a-e}$ analogues exhibited less steric effect compared to that substituted in position 3 of $\text{III}n_{a-e}$ analogues and thus showed higher mesophase stability than the other.

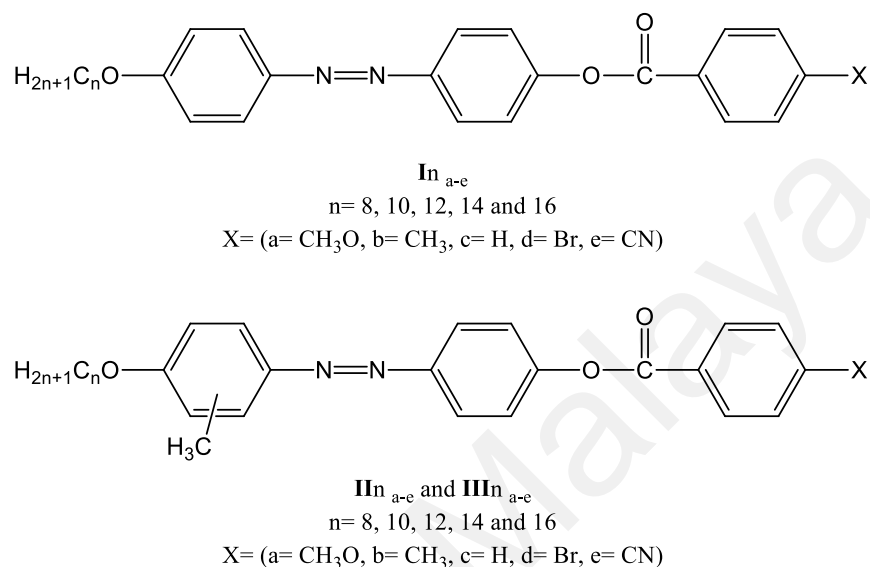


Figure 2.24: Azo-ester homologue compounds.

The effects of different lateral fluorine group position and alkoxy group with 8 or 16 carbons at the terminal of phenyl azo moieties and a polar substituent on the second terminal changes between electron-donating and electron-withdrawing groups (Figure 2.25) on the mesomorphic properties of the new azo-ester compounds were explored by Ahmed and co-workers (Ahmed et al., 2018). The effect of position of lateral fluorine group exhibited decreasing on the thermal stability of the smectic and nematic mesophases. The mesophase stability of derivatives with the lateral fluorine group substituted in position 2 is lower than those derivatives substituted in position 3 due to the resultant dipole moment, which changes depending on the polarity and position of the substituted groups.

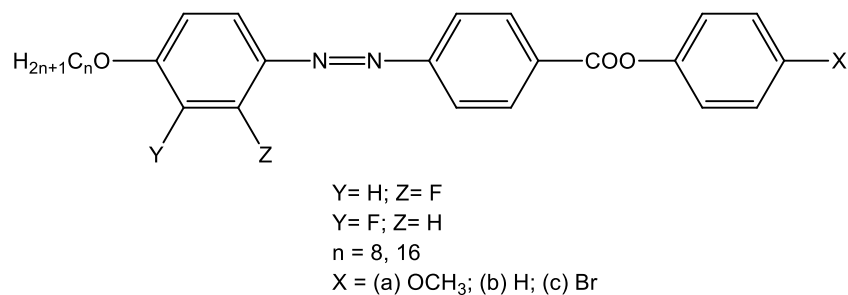


Figure 2.25: Liquid crystals substituted with lateral fluorine group.

Two liquid crystals compounds with different positions of two laterally fluorine atoms as shown in Figure 2.26 were synthesized and their effects on the mesomorphic properties were studied by Zaki and co-workers (Zaki et al., 2018). The compound bearing two fluorine atoms directed towards the core (compound I) exhibited nematic phase, while the smectic phase was observed for the compound substituted fluorine atoms directed outwards the molecular core (compound II). Compound I and II exhibited a broad mesophase temperature ranges, with higher melting and clearing temperatures for compound I than compound II. This could be related to the effect of the position and orientation of the fluorine atoms, which influences the resultant dipole moment of the compounds.

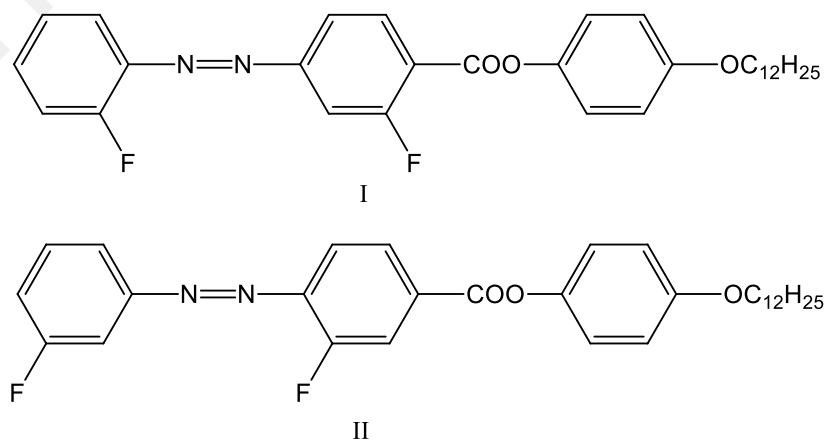


Figure 2.26: Liquid crystals compounds with different positions of two laterally fluorine atoms.

2.5.3 Effect of Terminal Group on Mesomorphic Properties

Naoum et al. prepared two series of 2 and 3 laterally methyl substituted derivatives 4-(4'-hexyloxyphenylazo)-2- (or 3-)methylphenyl-4''-substituted benzoates (I_{a-e} and II_{a-e}) and 4-(4'-substituted phenylazo)-2-(or 3-) methylphenyl-4''-hexyloxybenzoates (III_{a-e} and IV_{a-e}) (Figure 2.27). Mesomorphic properties and thermal stability for the synthesized compounds vary depending on the polarity and the position of terminal groups (X= -CH₃O, -CH₃, -Br, -NO₂, and -CN) and lateral methyl position. All compounds, irrespective of the positional and orientational of the lateral and terminal substituents, gave only nematic phase. Groups I and III, exhibits the same order of nematic stability CN > CH₃O > NO₂ > CH₃ > Br. Furthermore, groups I and II with different lateral methyl orientation exhibited lower nematic stability in parallel order, while group IV exchanged their order between CH₃ and CH₃O groups (Naoum et al., 2011).

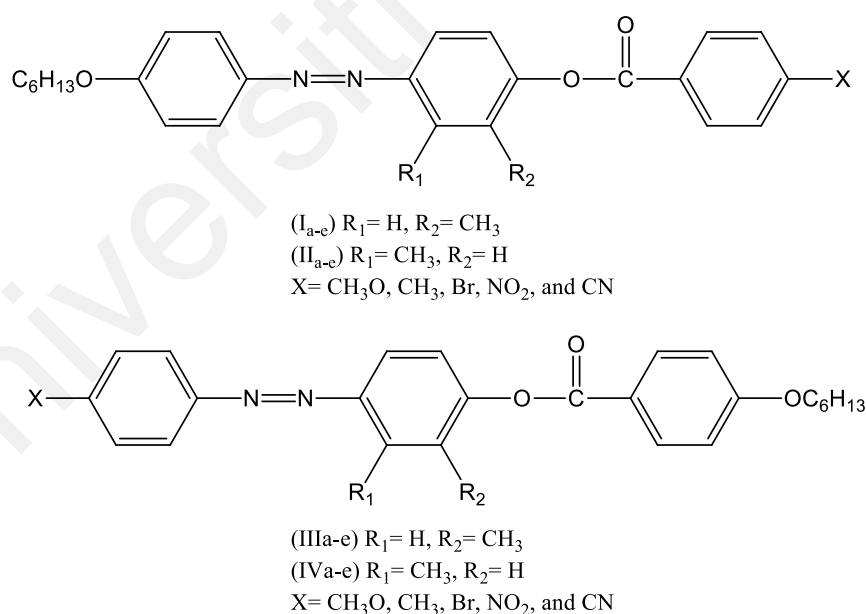
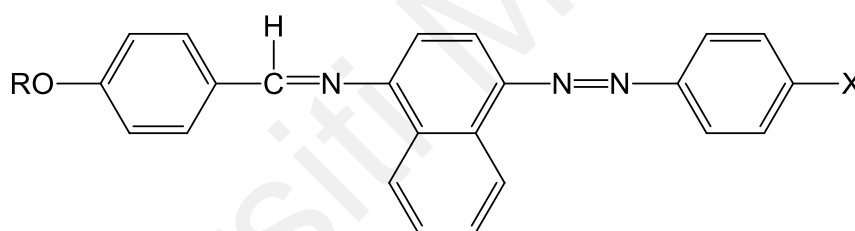


Figure 2.27: Two series of 2 and 3 laterally methyl substituted derivatives.

The effect of different terminal groups on the mesomorphic properties of new series of 4-(4'-n-alkoxy benzylidene amino)-naphthalene-4''-substituted-1-azo-benzene

liquid crystals were investigated (Thaker et al., 2010). The series consist of different terminal groups i.e. (-Cl, -Br, -CH₃ and -OCH₃) on one side and alkoxy octyl or hexadecyl group on the other terminal side (Figure 2.28). All synthesized compounds exhibited mesomorphic behaviours with smectic and nematic mesophases, except compounds A₁ and A₃ showed only nematic mesophase. The thermal stability of all compounds with respect of the terminal groups increase in order OCH₃ > Cl > Br > CH₃ > H. Therefore, the derivatives with OCH₃ group showed higher clearing temperature than that of other terminal groups. This might be explained by the fact that the lone pair of oxygen electrons is shielded by methyl group and the repulsive forces are thus greatly reduced, allowing nearby molecules to approach more closely, enhancing bonding forces and leading to an increase in thermal stability.



(Series A)

A₁-A₅: R = C₈H₁₇, X = H, CH₃, OCH₃, Cl, Br

A₆-A₁₀: R = C₁₆H₃₃, X = H, CH₃, OCH₃, Cl, Br

Figure 2.28: Two new series of azo-Schiff base and azo-ester liquid crystals.

Karim et al. described the synthesis of new liquid crystals containing varied terminal substituents (-H, -CH₃, -OCH₃ and -OC₂H₅) at the sixth position on azo benzothiazole chromophore with methacrylate terminal group (Figure 2.29). The terminal unsubstituted derivative exhibited a smectic phase, while the other derivatives with terminal -CH₃, -OCH₃ and -OC₂H₅ groups showed nematic and smectic mesophases. The terminal ethoxy analogue exhibited higher melting and clearing temperatures than the

other terminal analogues. The mesophase behaviours were strongly influenced by the terminal methacrylate moiety and the size of the sixth position substituents on benzothiazole ring (Karim et al., 2013).

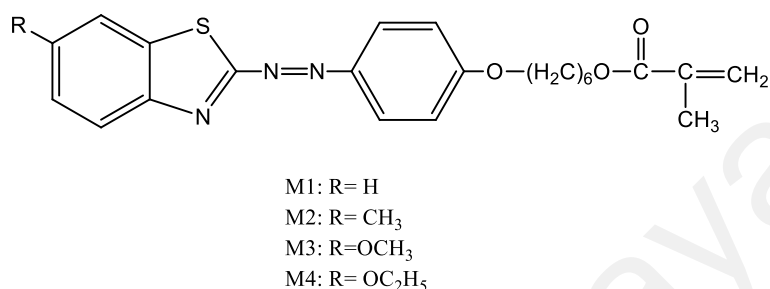


Figure 2.29: Azo benzothiazole chromophore compounds.

Two series of α -(4-benzylidene-substitutedaniline-4''-oxy)- ω -[pentyl-4-(4''-phenyl)benzoateoxy]hexane (Series I) and (*R,S*)-(benzylidene-4'-substitutedaniline)-2''-methylbutyl-4'''-(4''''-phenyloxy)benzoate-oxy)hexanoates (Series II) non-symmetric dimers (Figure 2.30) were reported (Yeap et al., 2011; Yeap et al., 2015). All compounds in series I containing -CH₃, -C₂H₅, -Cl, -Br, -F and -I terminal groups, except the unsubstituted compound, gave an enantiotropic nematic mesophase. SmA mesophase was observed for the bromo-terminated derivative of series I, as well as the halogen and ethyl-terminated compounds of series II. The size of the terminal substituents and its ability to interact with the mesogenic core plays an important role in enhancing the phase transition temperatures of the synthesized compounds.

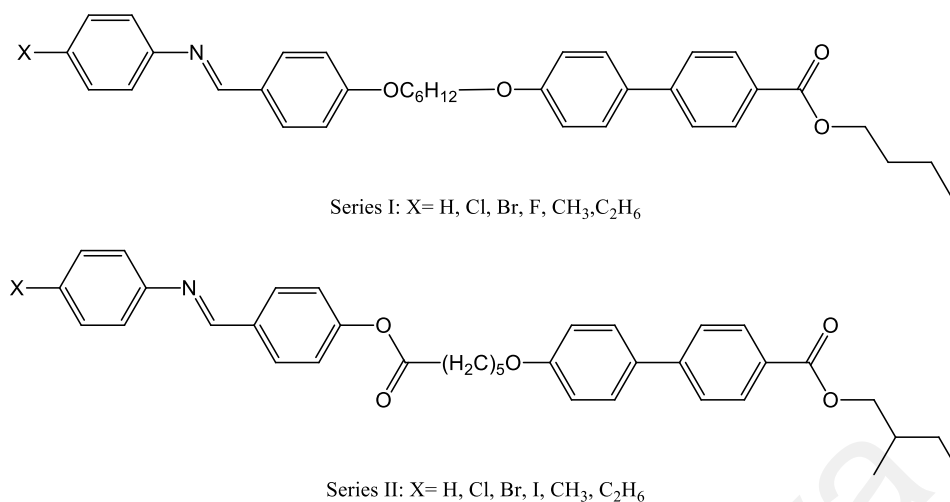


Figure 2.30: Two series of the non-symmetric dimers.

Three new series of 5-[2-(4-substituted phenyl)diazenyl]pyridin-2-yl 4'-alkoxybenzoate liquid crystals (Figure 2.31) were synthesized and their mesophase behaviours were investigated (Hagar et al., 2020). Within each series, the alkoxy group varies between 8, 10, 12, 14, and 16 carbons, whereas the substituent, X, changes between electron-donating group -OCH₃ and electron-withdrawing groups -Cl, including the unsubstituted terminal group. Compounds with -OCH₃ terminal substituent was found to be nematogenic, while the unsubstituted compounds were non-mesomorphic. Compounds with -Cl terminal withdrawing group exhibited either nematic mesophase, SmA mesophase or both depending on the alkoxy chain length. The presence and stability of the SmA and/or N phases is attributed to the elongated molecular length increasing the length-to-width ratio; permanent dipole moment across the longitudinal axis; polarity-to-polarisability ratio; and intermolecular dispersion forces.

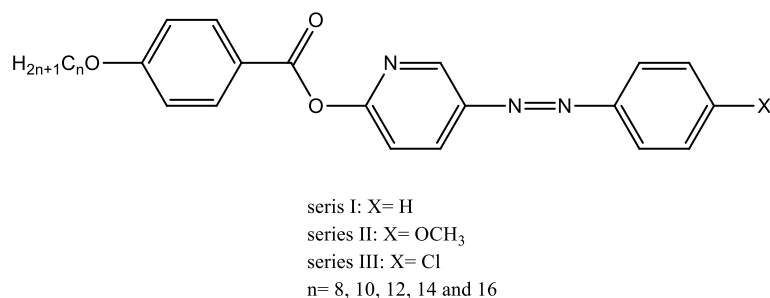
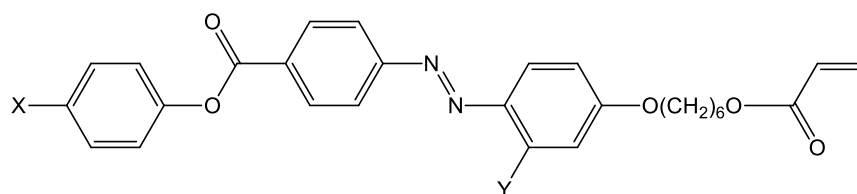


Figure 2.31: 5-[2-(4-substituted phenyl)diazenyl]pyridin-2-yl 4'-alkoxybenzoate liquid crystals.

Two series of azo-ester linked liquid crystal bearing polymerizable acrylate moiety and different terminal groups (-H, -Cl, -Br, -CN, -F, -OCH₃, -OC₂H₅, -OC₃H₇) were successfully synthesized and characterized (Figure 2.32) by Karim and co-workers (Karim et al., 2016). The effects of different electron-donating and electron-withdrawing terminal groups with laterally neat analogues on the mesomorphic behaviours were studied. The DSC and POM studies revealed that the terminal electron-donating derivatives (-OCH₃, -OC₂H₅ and -OC₃H₇) showed higher mesophase stability than those with terminal electron-withdrawing derivatives (-F, -Cl and -Br). This is due to the strong bonding forces formed between the neighbouring molecules, as the low repulsive forces between the lone pairs of oxygen atoms that are shielded by electron-donating groups. All compounds exhibited SmA and nematic mesophases which greatly influenced by the terminal substituents. Sardon and co-workers (Sardon et al., 2021) reported the effect of lateral methyl substituent with different (-H, -Cl, -Br and -CN) terminal groups on the mesomorphic and optical properties and compared them with the unsubstituted lateral analogues. The unsubstituted terminal compound (C7) showed nematic mesophase which undergo isotropization at lower temperature compared with electron-withdrawing terminated derivatives (C8, C9 and C10). The presence of lateral methyl substituent on the azo-ester mesogen exhibited lower melting and clearing temperatures than those of

lateral neat substituents. The lateral methyl substituted compounds showed blue emissions and red-shifted with the incorporation of terminal groups.



C1: X= F, Y= H	C2: X= Cl, Y= H
C3: X= Br, Y= H	C4: X= OCH ₃ , Y= H
C5: X= OC ₂ H ₅ , Y= H	C6: X= OC ₃ H ₇ , Y= H
C7: X= H, Y= CH ₃	C8: X= Cl, Y= CH ₃
C9: X= Br, Y= CH ₃	C10: X= CN, Y= CH ₃

Figure 2.32: Azo-ester linked mesogen bearing polymerizable acrylate end-group.

Recently, Al-Zahrani et al. studied the mesomorphic properties of newly synthesized azo-ester materials based on a central naphthalene group ($I_{n/x}$) bearing different length of alkoxy terminal group ($n = 6$ and 16 carbons) and a polar substituent ($-\text{OCH}_3$, $-\text{F}$, $-\text{Cl}$) on the opposite terminal side (Figure 2.33) (Al-Zahrani et al., 2021). All the prepared compounds possessed a purely enantiotropic nematic mesophase. For an electron-donating group ($-\text{OCH}_3$), the short length chain compound $I_{6/a}$ showed the highest thermal stability with the broadest nematic range, while the long chain compound $I_{16/a}$ displayed the lowest nematic stability. For an electron-withdrawing group ($-\text{F}$ and $-\text{Cl}$), the fluoro-substituted derivative $I_{6/b}$ exhibited lower melting temperature than the methoxy-substituted derivative $I_{6/a}$. On the other hand, the chloro-substituted derivative $I_{16/c}$ showed higher melting temperature than the methoxy-substituted derivative $I_{16/a}$. The introduction of a terminal polar substituent with different polarity and volume in the mesogenic core influenced the mesophase thermal stability.

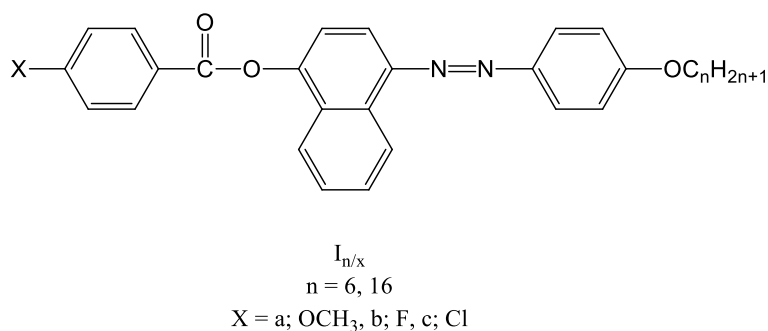


Figure 2.33: Azo-ester derivatives with central naphthalene group.

2.6 Application of Azo-Ester Liquid Crystal Compounds

Since the discovery of liquid crystals (LCs), investigations of physical and chemical properties have attracted considerable attention in numerous fields and applications i.e. chemical and biological sensing, optical storage and switching devices, display technology and so on (Arines, 2009; Bai & Abbott, 2012; Hrozhyk et al., 2010; Saha et al., 2012; Xu et al., 2010). Several researchers have synthesized azo-ester liquid crystal materials with varied functional groups to study their properties.

Yuvaraj et al. (Yuvaraj et al., 2014) have developed azo-ester liquid crystal dimers with varied spacers that are suitable for the application in photoswitching studies and optical storage devices. The photoswitching properties of these materials in solution exhibited similar *E-Z* isomerization at around 17 s for compound E1 with the aliphatic chain spacer and 18 s for compound E2 with the aromatic benzene ring spacer. Contrarily, their reverse process was dissimilar i.e. 13.25 h and 7.21 h for E1 and E2, respectively. Compound E1 was used for spectral research on solid cells because it had a high *E-Z* conversion efficiency in solution. In solid cell, compound E1 showed *E-Z* photoisomerization around 10 s and the reverse *Z-E* was observed at 382 min.

In 2016, the light-induced properties of resorcinol spacer based dimeric azobenzene in liquid crystalline were examined by Yuvaraj group (Yuvaraj et al., 2016) and their photoisomerization effect was assessed in both solution and solid state. Thermal

back relaxation was found at 11 h, whereas photosaturation was observed exactly at 18 s. The presence of resorcinol spacer substituted in bent-shaped molecules leads to a long duration of thermal back relaxation.

The liquid crystals monomers containing azobenzene chromophores, substituted or unsubstituted 1,3-phenylene bis-[4-(4-allyloxyphenylazo) benzoate] and substituted or unsubstituted 1,3-phenylene bis-[4-(4-allyloxy-3-fluorophenylazo) benzoate] were synthesized for optical storage devices application (Lutfor et al., 2009). UV-vis absorption for *trans*-form of these compounds exhibited a strong band in the region (355–366 nm), which is assigned to the π - π^* transition, and a weak band in region 455–465 nm corresponding to the n - π^* transition. The addition of bent core azo dye in liquid crystalline material (guest–host effect) has shown that these materials have a long thermal back relaxation time and could be used in optical image storage devices.

The optical properties for azo-based benzoate derivatives with different terminal substituents (-H, -F, -Br, -Cl, -I) on one side and 1-pentene on the other terminal side were studied by Hegde et al. (Hegde et al., 2016). Strong photoisomerisation was exhibited by both photochromic azo linking group and electronegative terminal substituents in which the longest thermal back relaxation period of 45 h after 82 s of UV irradiation was observed for the unsubstituted terminal derivative. Nevertheless, the incorporation of electronegative terminal group did not increase thermal back relaxation time in photocrosslinkable 1-pentene substituted azobenzene. The improved thermal back relaxation time suggested that the azo derivative with 1-pentene terminal group was photolocked under UV light and this feature could be useful in the manufacture of optical devices.

Photoswitching behaviour of a series of new azo-coumarin LC derivatives with varying aliphatic chain lengths has been investigated by Madiahlagan et al. (Madiahlagan et al., 2019). The addition of natural product groups to the azobenzene system resulted in

greater electron delocalization and mesophase properties. The coumarin-azo compounds required 46 s to reach photostationary state under UV irradiation and had a long thermal back relaxation time (16 h) in solutions. The research group also made device and studied the performance with respect to the alkyl chain length. The fabrication of optical information storage devices with coumarin substituted azobenzene LC materials was superior.

Universiti Malaya

CHAPTER 3: METHODOLOGY

3.1 Materials

All chemicals, reagents and solvents were purchased from suppliers without further purification unless otherwise stated. For the synthesis work, sulphuric acid (H₂SO₄, 98%) and hydrochloric acid (HCl, 95%) were acquired from R&M Chemicals. 1-Chloro-2-methylbutane (96%), *N,N*-dicyclohexylcarbodiimide (DCC, 99%), 3-fluorophenol (98%), 4-dimethylaminopyridine (DMAP, 99%) and phenol (99%) were purchased from Aldrich. Ethyl 4-aminobenzoate and 4-butoxyphenol (99%) were procured from Nacalai Tesque, Inc. and Acros Organics, respectively. Potassium carbonate (K₂CO₃), Potassium iodide (KI), sodium hydroxide (NaOH) and sodium nitrite (NaNO₂) were acquired from Friendemann Schmidt. 4-methoxyphenol (98%), 4-nitrophenol (99%), 4-bromophenol (99%) and *m*-cresol (98%) were supplied by Merck. Solvents including ethanol, hexane, ethyl acetate, dichloromethane (DCM) and *N,N*-dimethylformamide (DMF) were of reagent grade and procured from various commercial suppliers such as Merck, J.T. Baker and Friendemann Schmidt. DCM and DMF were kept anhydrous before use.

3.2 Synthesis of Liquid Crystal Compounds

In this work, two series of liquid crystal compounds with similar general structure but different mesogenic centre, lateral substituents and terminal groups were synthesized. The chemical structures were characterized by FT-IR, ¹H and ¹³C NMR spectroscopic techniques as well as elemental analysis. Some fluorinated azo-esters were also subject to ¹⁹F NMR spectroscopy. No attempts were made to separate the *R/S* chiral isomers of 1-chloro-2-methylbutane.

3.2.1 Synthesis of Two-Benzene-Ring Azo-Esters (T1, T2 and T3)

3.2.1.1 Ethyl 4-(4-Hydroxyphenylazo) Benzoate (T1-1)

In 500 mL reaction flask equipped with a magnetic stirrer, ethyl 4-aminobenzoate (5 g, 30 mmol) was dissolved in 1 M HCl solution (80 mL) and cooled in an ice bath to 0°C. To the resulting solution, 1 M sodium nitrate (NaNO₂) solution (6.3 g, 90 mmol) was added dropwise and the temperature of the mixture was kept below 5°C. Another set of ice cooled mixture of phenol (2.9 g, 30 mmol) dissolved in NaOH solution (90 mmol) was drop-wisely added into the latter mixture. The resulting mixture was stirred at the temperature below 5°C for 1 h and then acidified with 150 mL of 1 M HCl solution. The solid precipitate was filtered and recrystallized twice from ethanol. The resulting dull red product yield was 75%, m.p.: 160 °C, **FT-IR** (cm⁻¹): 3385 (OH, aromatic), 2978, 2929 (-C-H, aliphatic), 1689 (C=O in ester), 1592, 1505 (C=C, aromatic), 1429, 1401 (-N=N-), 1276, 1223 (-C-O), 1011, 844, 772 (C-H, aromatic). **¹H NMR** (400 MHz, DMSO-d₆) δ (ppm): 10.48 (s, 1H, Ar-OH), 8.06-8.04 (d, 2H, *J* = 8.7 Hz, Ar-H), 7.84-7.82 (d, 2H, *J* = 8.7 Hz, Ar-H), 7.81-7.78 (d, 2H, *J* = 8.7 Hz, Ar-H), 6.94-6.91 (d, 2H, *J* = 9.2 Hz, Ar-H), 4.31-4.26 (q, 2H, *J* = 7 Hz, -OCH₂-), 1.30-1.27 (t, 3H, *J* = 7.1 Hz, -CH₃). **¹³C NMR** (100 MHz, DMSO-d₆) δ (ppm): 165.7 (-C=O), 162.2, 155.2, 145.8, 131.3, 130.9, 125.9, 122.7, 116.6 (Ar-C), 61.5 (-OCH₂-), 14.6 (-H₂C-CH₃-).

3.2.1.2 (R,S)-Ethyl 4-(4-(2-Methylbutoxy)phenylazo) Benzoate (T1-2)

Compound **T1-1** (1 g, 3 mmol), 1-chloro-2-methylbutane (0.45 mL, 4 mmol), pinch of potassium iodide (KI) and potassium carbonate (K₂CO₃) (1 g, 7 mmol) were dissolved in 25 mL anhydrous DMF and refluxed for 72 h. The reaction mixture was diluted with ethyl acetate and the resultant mixture was washed three times with distilled water. The organic layer was separated, dried over anhydrous sodium sulphate (Na₂SO₄), and removed under reduced pressure. The red solid residue was purified through column

chromatography using silica gel as a stationary phase and ethyl acetate:hexane (1:10) as eluent. Finally, compound **T1-2** was recrystallized from hexane to give 51% yield, m.p.:85°C, **FT-IR** (cm^{-1}): 2963, 2931 (-C-H, aliphatic), 1708 (C=O in ester), 1601, 1584 (C=C, aromatic), 1498, 1473 (-N=N-), 1270, 1248 (-C-O), 1008, 863, 832, 774 (C-H, aromatic). **^1H NMR** (400 MHz, CDCl_3) δ (ppm): 8.19-8.17 (d, 2H, $J = 8.7$ Hz, Ar-H), 7.96-7.94 (d, 2H, $J = 8.7$ Hz, Ar-H), 7.92-7.90 (d, 2H, $J = 8.7$ Hz, Ar-H), 7.04-7.01 (d, 2H, $J = 9.2$ Hz, Ar-H), 4.45-4.39 (q, 2H, $J = 7$ Hz, CO-OCH₂-), 3.94-3.82 (q, 2H, $J = 6.0$ Hz, Ar-OCH₂-), 1.94-1.88 (m, 1H, OCH₂-CH), 1.64-1.59, 1.34-1.26 (m, 2H, CH-CH₂ *R,S*), 1.45-1.42 (t, 3H, $J = 7.1$ Hz, CO-OCH₂-CH₃), 1.06-1.05 (d, 3H, $J = 6.8$ Hz, CH-CH₃), 1.0-0.96 (t, 3H, $J = 7.4$ Hz, CH₂-CH₃). **^{13}C NMR** (100 MHz, CDCl_3) δ (ppm): 166.2 (-C=O), 162.5, 155.4, 146.9, 131.5, 130.6, 125.2, 122.3, 114.9 (Ar-C), 73.3 (Ar-OCH₂-), 61.2 (CO-OCH₂-), 34.7 (-OCH₂-CH), 26.2 (-CH-CH₂), 16.6 (-CH-CH₃), 14.4 (CO-OCH₂-CH₃), 11.4 (-H₂C-CH₃-).

3.2.1.3 (*R,S*)-4-(4-(2-Methylbutoxy)phenylazo) Benzoic Acid (**T1-3**)

Compound **T1-2** (0.9 g, 3 mmol) and 10% wt. NaOH (6 mmol) were added into a 250 mL round-bottom flask containing 50 mL absolute ethanol and the resultant mixture was refluxed for 6 h. The resultant mixture was poured into ice-cold water and then acidified with dilute HCl to give the desired compound **T1-3**. Color: orange. Yield: 90%, m.p.: 250°C, **FT-IR** (cm^{-1}): 3399 (O-H), 2961, 2918, 2874 (-C-H, aliphatic), 1677 (C=O in COOH), 1599, 1580 (C=C, aromatic), 1499, 1464 (-N=N-), 1291, 1247 (-C-O), 1012, 947, 867, 836 (C-H, aromatic). **^1H NMR** (400 MHz, DMSO-d_6) δ (ppm): 8.12-8.10 (d, 2H, $J = 8.7$ Hz, Ar-H), 7.90-7.89 (d, 4H, $J = 6.8$ Hz, Ar-H), 7.13-7.10 (d, 2H, $J = 9.2$ Hz, Ar-H), 3.94-3.82 (q, 2H, $J = 6.0$ Hz, Ar-OCH₂-), 1.85-1.78 (m, 1H, OCH₂-CH), 1.55-1.47, 1.26-1.19 (m, 2H, CH-CH₂ *R,S*), 0.95-0.94 (d, 3H, $J = 6.8$ Hz, -CH₃), 0.91-0.87 (t, 3H, $J = 7.4$ Hz, -CH₃). **^{13}C NMR** (100 MHz, DMSO-d_6) δ (ppm): 167.4 (-C=O), 162.7,

154.8, 146.6, 133.1, 131.08, 125.5, 122.7, 115.6 (Ar-C), 73.2 (Ar-OCH₂-), 34.5 (-OCH₂-CH), 26.01 (-CH-CH₂), 16.7 (-CH-CH₃), 11.6 (CH₂-CH₃).

3.2.1.4 (*R,S*)-Octyl 4-(4-(2-Methylbutoxy)phenylazo) Benzoate (T1)

Compound **T1-3** (1 g, 3 mmol) and 1-octanol (0.3 mL, 3 mmol) were dissolved in a mixed solvent of DCM/DMF with 5:1 volumetric mixing ratio. Then, *N,N'*-dicyclohexylcarbodiimide (DCC) (0.6 g, 3 mmol) and a small amount of *N,N'*-dimethylaminopyridine (DMAP) as a catalyst were added to the mixture and stirred at room temperature for 72 h. The resulted white solid was filtered off and the solvent was removed under reduced pressure. The solid residue was passed through column chromatography using silica gel as a stationary phase and DCM: hexane (10:5) as eluent. Finally, the compound was recrystallized from a mixture of DCM and ethanol (1:1). Color: orange. Yield: 70%. **FT-IR** (cm⁻¹): 2958, 2924, 2856 (-C-H, aliphatic), 1708 (C=O in ester), 1602, 1584 (C=C, aromatic), 1500, 1469 (-N=N-), 1273, 1251 (-C-O), 1009, 946, 864, 832 (C-H, aromatic). **¹H NMR** (400 MHz, CDCl₃) δ (ppm): 8.19-8.17 (d, 2H, *J* = 8.7 Hz, Ar-H), 7.96-7.90 (dd, 4H, *J* = 2.4, 11.5 Hz, Ar-H), 7.04-7.02 (d, 2H, *J* = 8.7 Hz, Ar-H), 4.37-4.33 (t, 2H, *J* = 7.1 Hz, OCH₂-CH₂), 3.94-3.82 (q, 2H, *J* = 6.0 Hz, Ar-OCH₂-), 1.96-1.88 (m, 1H, OCH₂-CH), 1.83-1.76 (m, 2H, OCH₂-CH₂), 1.63-1.57 (m, 2H, CH-CH₂ *R,S*), 1.50-1.43 (m, 2H, CH₂-CH₂), 1.36-1.25 (m, 8H, CH₂), 1.06-1.05 (d, 3H, *J* = 6.8 Hz, CH-CH₃), 1.00-0.96 (t, 3H, *J* = 7.4 Hz, CH₂-CH₃), 0.92-0.88 (t, 3H, *J* = 7.4 Hz, CH₂-CH₃). **¹³C NMR** (100 MHz, CDCl₃) δ (ppm): 166.3 (-C=O), 162.5, 155.3, 146.8, 131.5, 130.5, 125.2, 122.3, 114.8 (Ar-C), 73.2 (Ar-OCH₂-), 65.4 (OCH₂-CH₂), 34.7 (-OCH₂-CH), 31.8, 29.3, 29.2, 28.7, 26.1, 26.07, 22.7 (-CH₂), 16.5 (-CH-CH₃), 14.1 (CH₂-CH₃), 11.3 (CH-CH₂-CH₃). **Elemental Analysis for C₂₆H₃₆N₂O₃** (Calc.) Found: C (73.55) 73.66; H (8.55) 8.46; N (6.60) 6.37%.

3.2.1.5 Ethyl 4-(2-Fluoro-4-Hydroxyphenylazo) Benzoate (T2-1)

3-fluorophenol (3.4 g, 30 mmol) was used instead of phenol to synthesize compound **T2-1** by similar synthetic techniques described previously for the synthesis of **T1-1**. Color: dull red. Yield: 87%, m.p.: 202°C, **FT-IR** (cm^{-1}): 3357 (OH, aromatic), 2977, 2903 (C-H, aliphatic), 1691 (C=O in ester), 1599, 1497 (C=C, aromatic), 1474, 1437 (-N=N-), 1312, 1286, 1233 (-C-O), 1103 (C-F), 1010, 964, 861, 815 (C-H, aromatic). **^1H NMR** (400 MHz, DMSO- d_6) δ (ppm): 10.94 (s, 1H, Ar-OH), 8.09-8.06 (d, 2H, $J = 9.2$ Hz, Ar-H), 7.86-7.84 (d, 2H, $J = 8.7$ Hz, Ar-H), 7.71-7.66 (t, 1H, $J = 8.9$ Hz, Ar-H), 6.80-6.76 (dd, 1H, $J = 2.4, 15.1$ Hz, Ar-H), 6.73-6.71 (dd, 1H, $J = 2.4, 11.5$ Hz, Ar-H), 4.33-4.28 (q, 2H, $J = 7.1$ Hz, -OCH₂-), 1.32-1.28 (t, 3H, $J = 7.1$ Hz, -CH₃). **^{13}C NMR** (100 MHz, DMSO- d_6) δ (ppm): 165.6 (-C=O), 164.1, 163.3, 160.8, 155.3, 133.8, 131.6, 130.9, 122.9, 119.07, 113.2, 104.09 (Ar-C), 61.5 (-OCH₂-), 14.6 (-H₂C-CH₃-).

3.2.1.6 (R,S)-Ethyl 4-(2-Fluoro-4-(2-Methylbutoxy)phenylazo) Benzoate (T2-2)

Compound **T2-1** (0.9 g, 3 mmol) was used to synthesize compound **T2-2** by similar synthetic techniques described previously for the synthesis of **T1-2**. The red solid residue was passed through column chromatography (ethyl acetate/ hexane 1:10) and recrystallized from hexane. Color: red. Yield: 47%, m.p.: 61°C, **FT-IR** (cm^{-1}): 2963, 2934 (C-H, aliphatic), 1708 (C=O in ester), 1603, 1579 (C=C, aromatic), 1497, 1459 (-N=N-), 1272, 1238 (-C-O), 1104 (C-F), 1005, 965, 852, 819 (C-H, aromatic). **^1H NMR** (400 MHz, CDCl₃) δ (ppm): 8.19-8.17 (d, 2H, $J = 8.7$ Hz, Ar-H), 7.94-7.92 (d, 2H, $J = 8.7$ Hz, Ar-H), 7.84-7.80 (t, 1H, $J = 8.9$ Hz, Ar-H), 6.80-6.78 (dd, 2H, $J = 2.4, 7.5$ Hz, Ar-H), 6.77-6.75 (t, 2H, $J = 6$ Hz, Ar-H), 4.45-4.39 (q, 2H, $J = 7.1$ Hz, CO-OCH₂-), 3.92-3.80 (q, 2H, $J = 6$ Hz, Ar-OCH₂-), 1.93-1.88 (m, 1H, OCH₂-CH), 1.61-1.57, 1.32-1.26 (m, 2H, CH-CH₂ *R,S*), 1.45-1.41 (t, 3H, $J = 7.8$ Hz, CO-OCH₂-CH₃), 1.06-1.04 (d, 3H, $J = 8.7$ Hz, CH-CH₃), 1.0-0.96 (t, 3H, $J = 7.8$ Hz, CH₂-CH₃). **^{13}C NMR** (100 MHz, CDCl₃)

δ (ppm): 166.2 ($-\text{C}=\text{O}$), 163.9, 163.3, 160.8, 155.5, 134.9, 131.8, 130.6, 122.6, 118.6, 111.5, 102.5 ($\text{Ar}-\underline{\text{C}}$), 73.7 ($\text{Ar}-\text{O}\underline{\text{C}}\text{H}_2-$), 61.3 ($\text{CO}-\text{O}\underline{\text{C}}\text{H}_2-$), 34.6 ($-\text{O}\text{C}\text{H}_2-\underline{\text{C}}\text{H}$), 26.1 ($-\text{C}\text{H}-\underline{\text{C}}\text{H}_2$), 16.5 ($-\text{C}\text{H}-\underline{\text{C}}\text{H}_3$), 14.4 ($\text{CO}-\text{O}\text{C}\text{H}_2-\underline{\text{C}}\text{H}_3$), 11.3 ($-\text{H}_2\text{C}-\underline{\text{C}}\text{H}_3-$). ^{19}F NMR (100 MHz, CDCl_3) δ (ppm): 120.38 ($\text{C}-\underline{\text{F}}$).

3.2.1.7 (*R,S*)-4-(2-Fluoro-4-(2-Methylbutoxy)phenylazo) Benzoic Acid (T2-3)

Compound **T2-2** (1 g, 3 mmol) was used to synthesize compound **T2-3** by similar synthetic techniques described previously for the synthesis of **T1-3** to give the desired compound. Color: orange. Yield: 82%, m.p.: 235°C, FT-IR (cm^{-1}): 2929, 2872 (C-H, aliphatic), 1680 (C=O in COOH), 1601, 1580 (C=C, aromatic), 1461, 1423 ($-\text{N}=\text{N}-$), 1290, 1268, 1234 ($-\text{C}-\text{O}$), 1099 (C-F), 1027, 958, 868, 832 (C-H, aromatic). ^1H NMR (400 MHz, $\text{DMSO}-d_6$) δ (ppm): 8.12-8.10 (d, 2H, $J = 8.7$ Hz, $\text{Ar}-\underline{\text{H}}$), 7.90-7.87 (d, 2H, $J = 8.7$ Hz, $\text{Ar}-\underline{\text{H}}$), 7.75-7.71 (t, 1H, $J = 7.1$ Hz, $\text{Ar}-\underline{\text{H}}$), 7.10-7.06 (dd, $J = 2.4, 15.1$ Hz, 2H, $\text{Ar}-\underline{\text{H}}$), 6.89-6.86 (dd, 2H, $J = 2.4, 11.5$ Hz, $\text{Ar}-\underline{\text{H}}$), 3.94-3.82 (q, 2H, $J = 6$ Hz, $\text{Ar}-\text{O}\underline{\text{C}}\text{H}_2-$), 1.82-1.77 (m, 1H, $\text{O}\text{C}\text{H}_2-\underline{\text{C}}\text{H}$), 1.52-1.45, 1.24-1.17 (m, 2H, $\text{C}\text{H}-\underline{\text{C}}\text{H}_2$ *R,S*), 0.96-0.94 (d, 3H, $J = 8.7$ Hz, $-\underline{\text{C}}\text{H}_3$), 0.91-0.87 (t, 3H, $J = 7.8$ Hz, $-\underline{\text{C}}\text{H}_3$). ^{13}C NMR (100 MHz, $\text{DMSO}-d_6$) δ (ppm): 167.2 ($-\text{C}=\text{O}$), 164.3, 163.2, 160.65, 155.0, 134.5, 133.0, 131.1, 122.9, 118.7, 112.6, 102.9 ($\text{Ar}-\underline{\text{C}}$), 73.8 ($\text{Ar}-\text{O}\underline{\text{C}}\text{H}_2-$), 34.4 ($-\text{O}\text{C}\text{H}_2-\underline{\text{C}}\text{H}$), 25.9 ($-\text{C}\text{H}-\underline{\text{C}}\text{H}_2$), 16.6 ($-\text{C}\text{H}-\underline{\text{C}}\text{H}_3$), 11.5 ($\text{C}\text{H}_2-\underline{\text{C}}\text{H}_3$). ^{19}F NMR (100 MHz, $\text{DMSO}-d_6$) δ (ppm): 120.50 ($\text{C}-\underline{\text{F}}$).

3.2.1.8 (*R,S*)-Octyl 4-(2-Fluoro-4-(2-Methylbutoxy)phenylazo) Benzoate (T2)

Compound **T2-3** (1 g, 3 mmol) and 1-octanol (0.4 mL, 3 mmol) were dissolved in 25 mL dried DCM. The rest of the steps were conducted in the same manner as **T1**. Color: reddish orange. Yield: 65%. FT-IR (cm^{-1}): 2958, 2926, 2856 (C-H, aliphatic), 1716 (C=O in ester), 1611, 1585 (C=C, aromatic), 1495, 1460 ($-\text{N}=\text{N}-$), 1268, 1237 (C-

O), 1011, 962, 908, 835 (C–H, aromatic). **¹H NMR** (400 MHz, CDCl₃) δ (ppm): 8.19–8.16 (d, 2H, *J* = 8.7 Hz, Ar–H), 7.95–7.92 (d, 2H, *J* = 8.7 Hz, Ar–H), 7.84–7.80 (t, 2H, *J* = 8.9 Hz, Ar–H), 6.79–6.78 (d, 1H, *J* = 8.6 Hz, Ar–H), 6.76 (s, 1H, Ar–H), 4.37–4.33 (t, 2H, *J* = 7.1 Hz, OCH₂–CH₂), 3.91–3.80 (q, 2H, *J* = 6.0 Hz, Ar–OCH₂–), 1.94–1.87 (m, 1H, OCH₂–CH), 1.83–1.76 (m, 2H, OCH₂–CH₂), 1.63–1.56 (m, 2H, CH–CH₂ *R,S*), 1.50–1.43 (m, 2H, CH₂–CH₂), 1.36–1.27 (m, 8H, CH₂), 1.06–1.04 (d, 3H, *J* = 6.8 Hz, CH–CH₃), 1.00–0.96 (t, 3H, *J* = 7.4 Hz, CH₂–CH₃), 0.92–0.88 (t, 3H, *J* = 7.4 Hz, CH₂–CH₃). **¹³C NMR** (100 MHz, CDCl₃) δ (ppm): 165.2 (–C=O), 162.9, 162.8, 162.3, 159.7, 154.4, 133.8, 130.8, 129.5, 121.5, 117.5, 110.4, 101.2 (Ar–C), 72.6 (Ar–OCH₂–), 64.4 (OCH₂–CH₂), 33.5 (–OCH₂–CH), 30.8, 28.2, 28.1, 27.7, 25.03, 25.01, 21.6 (–CH₂), 15.4 (–CH–CH₃), 13.1 (CH₂–CH₃), 10.3 (CH–CH₂–CH₃). **Elemental Analysis for C₂₆H₃₅N₂O₃** (Calc.) Found: C (70.56) 70.34; H (7.97) 7.73; N (6.33) 6.31%.

3.2.1.9 Ethyl 4-((4-Hydroxy-2-Methylphenylazo) Benzoate (T3-1)

m-Cresol (3.3 g, 30 mmol) was used instead of phenol to synthesize compound **T3-1** by similar synthetic techniques described previously for the synthesis of **T1-1**. Color: dull red. Yield: 80%, m.p.: 167 °C, **FT-IR** (cm⁻¹): 3397 (OH, aromatic), 2980, 2906 (C–H, aliphatic), 1692 (C=O ester), 1602, 1582 (C=C, aromatic), 1480, 1474 (–N=N–), 1284, 1226 (–C–O), 1018, 949, 889, 858 (C–H, aromatic). **¹H NMR** (400 MHz, DMSO-d₆) δ (ppm): 10.30 (s, 1H, Ar–OH), 8.07–8.05 (d, 2H, *J* = 8.7 Hz, Ar–H), 7.85–8.82 (d, 2H, *J* = 9.2 Hz, Ar–H), 7.60–7.58 (d, 1H, *J* = 8.7 Hz, Ar–H), 6.77 (d, 1H, *J* = 2.5 Hz, Ar–H), 6.70–6.67 (dd, 1H, *J* = 2.4, 11.5 Hz, Ar–H), 4.32–4.27 (q, 2H, *J* = 7.1 Hz, –OCH₂–), 2.59 (s, 3H, Ar–CH₃), 1.32–1.28 (t, 3H, *J* = 7.1 Hz, –CH₃). **¹³C NMR** (100 MHz, DMSO-d₆) δ (ppm): 165.8 (–C=O), 162.2, 155.6, 143.9, 142.4, 131.1, 130.9, 122.8, 117.7, 117.6, 114.7 (Ar–C), 61.5 (–OCH₂–), 17.8 (Ar–C–CH₃), 14.7 (–H₂C–CH₃–).

3.2.1.10 (*R,S*)-Ethyl 4-((2-Methyl-4-(2-Methylbutoxy)phenylazo) Benzoate (T3-2)

Compound **T3-1** (0.9 g, 3 mmol) was used to synthesize compound **T3-2** by similar synthetic techniques described previously for the synthesis of **T1-2**. Color: red. Yield: 45%, m.p.: 50°C, **FT-IR** (cm^{-1}): 2960, 2926 (C-H, aliphatic), 1708 (C=O in ester), 1596 (C=C, aromatic), 1492, 1469 (N=N-), 1272, 1240 (C-O), 1002, 862, 821, 774 (C-H, aromatic). **^1H NMR** (400 MHz, CDCl_3) δ (ppm): 8.19-8.17 (d, 2H, $J = 8.7$ Hz, Ar-H), 7.92-7.90 (d, 2H, $J = 8.7$ Hz, Ar-H), 7.77-7.75 (d, 1H, $J = 8.7$ Hz, Ar-H), 6.85 (d, 2H, $J = 2.6$ Hz, Ar-H), 6.82-6.79 (dd, 2H, $J = 2.4, 11.5$ Hz, Ar-H), 4.45-4.39 (q, 2H, $J = 7.1$ Hz, CO-OCH₂-), 3.91-3.79 (q, 2H, $J = 6$ Hz, Ar-OCH₂-), 2.75 (s, 3H, Ar-CH₃), 1.92-1.88 (m, 1H, OCH₂-CH), 1.62-1.57, 1.34-1.27 (m, 2H, CH-CH₂ *R,S*), 1.45-1.42 (t, 3H, $J = 7.1$ Hz, CO-OCH₂-CH₃), 1.06-1.04 (d, 3H, $J = 8.7$ Hz, CH-CH₃), 1.0-0.96 (t, 3H, $J = 7.8$ Hz, CH₂-CH₃). **^{13}C NMR** (100 MHz, CDCl_3) δ (ppm): 166.3 (C=O), 162.6, 155.7, 144.9, 141.9, 131.3, 130.6, 122.5, 117.2, 116.0, 113.1 (Ar-C), 73.1 (Ar-OCH₂-), 61.2 (CO-OCH₂-), 34.8 (OCH₂-CH), 26.2 (CH-CH₂), 17.9 (Ar-C-CH₃), 16.6 (CH-CH₃), 14.4 (CO-OCH₂-CH₃), 11.4 (-H₂C-CH₃-).

3.2.1.11 (*R,S*)-4-((2-Methyl-4-(2-Methylbutoxy)phenylazo) Benzoic Acid (T3-3)

Compound **T3-2** (1 g, 3 mmol) was used to synthesize compound **T3-3** by similar synthetic techniques described previously for the synthesis of **T1-3** to give the desired compound. Color: orange. Yield: 85%, m.p.: 184°C, **FT-IR** (cm^{-1}): 2963, 2925, 2874 (C-H, aliphatic), 1675 (C=O in COOH), 1599, 1575 (C=C, aromatic), 1490, 1459 (N=N-), 1308, 1285, 1235 (C-O), 940, 867, 815, 778 (C-H, aromatic). **^1H NMR** (400 MHz, DMSO-d_6) δ (ppm): 8.07-8.05 (d, 2H, $J = 8.7$ Hz, Ar-H), 7.85-7.83 (d, 2H, $J = 8.7$ Hz, Ar-H), 7.62-7.60 (d, 1H, $J = 8.7$ Hz, Ar-H), 6.94 (d, 1H, $J = 2.3$ Hz, Ar-H), 6.84-6.81 (dd, 1H, $J = 2.4, 11.5$ Hz, Ar-H), 3.88-3.76 (q, 2H, $J = 6.1$ Hz, Ar-OCH₂-), 2.63 (s, 3H, Ar-CH₃), 1.77-1.74 (m, 1H, OCH₂-CH), 1.48-1.45, 1.20-1.17 (m, 2H, CH-CH₂ *R,S*),

0.93-0.92 (d, 3H, $J = 6.5$ Hz, $-\underline{\text{C}}\underline{\text{H}}_3$), 0.87-0.84 (t, 3H, $J = 7.8$ Hz, $-\underline{\text{C}}\underline{\text{H}}_3$). ^{13}C NMR (100 MHz, DMSO- d_6) δ (ppm): 167.4 ($-\text{C}=\text{O}$), 162.7, 155.4, 144.7, 142.1, 132.4, 131.1, 122.8, 117.3, 116.5, 113.8 ($\text{Ar}-\underline{\text{C}}$), 73.1 ($\text{Ar}-\text{O}\underline{\text{C}}\underline{\text{H}}_2-$), 34.6 ($-\text{O}\underline{\text{C}}\underline{\text{H}}_2-\underline{\text{C}}\underline{\text{H}}$), 26.0 ($-\text{C}\underline{\text{H}}-\underline{\text{C}}\underline{\text{H}}_2$), 17.9 ($\text{Ar}-\underline{\text{C}}-\underline{\text{C}}\underline{\text{H}}_3$), 16.7 ($-\text{C}\underline{\text{H}}-\underline{\text{C}}\underline{\text{H}}_3$), 11.6 ($\text{C}\underline{\text{H}}_2-\underline{\text{C}}\underline{\text{H}}_3$).

3.2.1.12 (*R,S*)-Octyl 4-(2-Methyl-4-(2-Methylbutoxy)phenylazo) Benzoate (T3)

Compound **T3-3** (1 g, 3 mmol) and 1-octanol (0.4 mL, 3 mmol) were dissolved in 25 mL dried DCM. The rest of the steps were conducted in the same manner as **T1**. Color: reddish orange. Yield: 75%. FT-IR (cm^{-1}): 2953, 2920, 2854 ($-\text{C}-\text{H}$, aliphatic), 1716 ($\text{C}=\text{O}$ in ester), 1596 ($\text{C}=\text{C}$, aromatic), 1489, 1454 ($-\text{N}=\text{N}-$), 1276, 1224 ($-\text{C}-\text{O}$), 1009, 956, 866, 847 ($\text{C}-\text{H}$, aromatic). ^1H NMR (400 MHz, CDCl_3) δ (ppm): 8.18-8.16 (d, 2H, $J = 8.7$ Hz, $\text{Ar}-\underline{\text{H}}$), 7.92-7.89 (d, 2H, $J = 8.7$ Hz, $\text{Ar}-\underline{\text{H}}$), 7.76-7.74 (d, 2H, $J = 8.7$ Hz, $\text{Ar}-\underline{\text{H}}$), 6.86-6.85 (d, 1H, $J = 2.3$ Hz, $\text{Ar}-\underline{\text{H}}$), 6.82-6.79 (dd, 1H, $J = 2.4, 11.5$ Hz, $\text{Ar}-\underline{\text{H}}$), 4.37-4.34 (t, 2H, $J = 7.1$ Hz, $\text{O}\underline{\text{C}}\underline{\text{H}}_2-\text{C}\underline{\text{H}}_2$), 3.92-3.80 (q, 2H, $J = 6.0$ Hz, $\text{Ar}-\text{O}\underline{\text{C}}\underline{\text{H}}_2-$), 2.75 (s, 3H, $\text{Ar}-\underline{\text{C}}\underline{\text{H}}_3$), 1.94-1.87 (m, 1H, $\text{O}\underline{\text{C}}\underline{\text{H}}_2-\underline{\text{C}}\underline{\text{H}}$), 1.83-1.76 (m, 2H, $\text{O}\underline{\text{C}}\underline{\text{H}}_2-\underline{\text{C}}\underline{\text{H}}_2$), 1.63-1.57 (m, 2H, $\text{C}\underline{\text{H}}-\underline{\text{C}}\underline{\text{H}}_2$ *R,S*), 1.50-1.43 (m, 2H, $\text{C}\underline{\text{H}}_2-\underline{\text{C}}\underline{\text{H}}_2$), 1.36-1.26 (m, 8H, $\text{C}\underline{\text{H}}_2$), 1.06-1.04 (d, 3H, $J = 6.8$ Hz, $\text{C}\underline{\text{H}}-\underline{\text{C}}\underline{\text{H}}_3$), 1.00-0.96 (t, 3H, $J = 7.4$ Hz, $\text{C}\underline{\text{H}}_2-\underline{\text{C}}\underline{\text{H}}_3$), 0.92-0.88 (t, 3H, $J = 7.4$ Hz, $\text{C}\underline{\text{H}}_2-\underline{\text{C}}\underline{\text{H}}_3$). ^{13}C NMR (100 MHz, CDCl_3) δ (ppm): 165.3 ($-\text{C}=\text{O}$), 161.6, 154.4, 143.7, 141.0, 130.3, 129.5, 121.4, 116.3, 114.9, 112.1 ($\text{Ar}-\underline{\text{C}}$), 72.1 ($\text{Ar}-\text{O}\underline{\text{C}}\underline{\text{H}}_2-$), 64.3 ($\text{O}\underline{\text{C}}\underline{\text{H}}_2-\text{C}\underline{\text{H}}_2$), 33.7 ($-\text{O}\underline{\text{C}}\underline{\text{H}}_2-\underline{\text{C}}\underline{\text{H}}$), 30.8, 28.2, 28.1, 27.7, 25.08, 25.04, 21.6 ($-\underline{\text{C}}\underline{\text{H}}_2$), 16.8 ($\text{Ar}-\underline{\text{C}}\underline{\text{H}}_3$), 15.5 ($-\text{C}\underline{\text{H}}-\underline{\text{C}}\underline{\text{H}}_3$), 13.1 ($\text{C}\underline{\text{H}}_2-\underline{\text{C}}\underline{\text{H}}_3$), 10.3 ($\text{C}\underline{\text{H}}-\underline{\text{C}}\underline{\text{H}}_2-\underline{\text{C}}\underline{\text{H}}_3$). **Elemental Analysis for $\text{C}_{27}\text{H}_{38}\text{N}_2\text{O}_3$** (Calc.) Found: C (73.94) 73.96; H (8.73) 8.57; N (6.39) 6.14%.

3.2.2 Synthesis of Three-Benzene-Ring Azo-Esters (S1, S2, S3, S4, S5, C1, C2, C3, C4, C5, C6, C7 and C8)

3.2.2.1 (*R,S*)-Phenyl 4-((4-(2-Methylbutoxy)phenylazo) Benzoate (S1)

Compound **T1-3** (1 g, 3 mmol) and phenol (0.3 g, 3 mmol) were dissolved in 25 mL dried DCM and 5 mL DMF. The rest of the steps were conducted in the same manner as **T1**. Color: reddish orange. Yield: 70%. **FT-IR** (cm^{-1}): 2962, 2933, 2875 (-C-H, aliphatic), 1724 (C=O in ester), 1599, 1581 (C=C, aromatic), 1489, 1465 (-N=N-), 1249, 1200 (-C-O), 1031, 913, 857, 837 (C-H, aromatic). **$^1\text{H NMR}$** (400 MHz, CDCl_3) δ (ppm): 8.27-8.25 (d, 2H, $J = 8.7$ Hz, Ar-H), 7.90-7.88 (dd, 4H, $J = 2.4, 11.5$ Hz, Ar-H), 7.39-7.35 (t, 2H, $J = 7.8$ Hz, Ar-H), 7.23-7.19 (t, 1H, $J = 7.8$ Hz, Ar-H), 7.18-7.16 (d, 2H, $J = 8.7$ Hz, Ar-H), 6.96-6.94 (d, 2H, $J = 8.7$ Hz, Ar-H), 3.86-3.74 (q, 2H, $J = 6.0$ Hz, Ar-OCH₂-), 1.86-1.81 (m, 1H, OCH₂-CH), 1.54-1.50, 1.25-1.21 (m, 2H, CH-CH₂ *R,S*), 0.98-0.97 (d, 3H, $J = 6.8$ Hz, CH-CH₃), 0.92-0.88 (t, 3H, $J = 7.4$ Hz, CH₂-CH₃). **$^{13}\text{C NMR}$** (100 MHz, CDCl_3) δ (ppm): 164.8 (-C=O), 162.7, 155.8, 150.9, 146.9, 131.2, 130.5, 129.5, 125.9, 125.3, 122.5, 121.7, 114.9 (Ar-C), 73.3 (Ar-OCH₂-), 34.7 (-OCH₂-CH), 26.1 (-CH-CH₂), 16.5 (-CH-CH₃), 11.3 (CH-CH₂-CH₃). **Elemental Analysis for C₂₄H₂₄N₂O₃** (Calc.) Found: C (74.21) 74.69; H (6.23) 6.23; N (7.21) 7.01%.

3.2.2.2 (*R,S*)-4-Methoxyphenyl 4-(4-(2-Methylbutoxy)phenylazo) Benzoate (S2)

Compound **T1-3** (1 g, 3 mmol) and 4-methoxyphenol (0.4 g, 3 mmol) were dissolved in 25 mL dried DCM and 5 mL DMF. The rest of the steps were conducted in the same manner as **T1**. Color: orange. Yield: 50%. **FT-IR** (cm^{-1}): 2962, 2924, 2875 (-C-H, aliphatic), 1727 (C=O in ester), 1599, 1582 (C=C, aromatic), 1499, 1466 (-N=N-), 1270, 1244, 1193 (-C-O), 1007, 861.5, 834, 811 (C-H, aromatic). **$^1\text{H NMR}$** (400 MHz, CDCl_3) δ (ppm): 8.34-8.32 (d, 2H, $J = 8.7$ Hz, Ar-H), 7.99-7.97 (d, 4H, $J = 8.7$ Hz, Ar-H), 7.19-7.16 (d, 2H, $J = 9.2$ Hz, Ar-H), 7.05-7.03 (d, 2H, $J = 8.7$ Hz, Ar-H), 6.98-6.96

(d, 2H, $J = 8.7$ Hz, Ar-H), 3.95-3.83 (q, 2H, $J = 6.0$ Hz, Ar-OCH₂-), 3.84 (s, 3H, O-CH₃), 1.95-1.90 (m, 1H, OCH₂-CH), 1.63-1.60, 1.34-1.30 (m, 2H, CH-CH₂ *R,S*), 1.07-1.06 (d, 3H, $J = 6.8$ Hz, CH-CH₃), 1.01- 0.97 (t, 3H, $J = 7.1$ Hz, CH₂-CH₃). ¹³C NMR (100 MHz, CDCl₃) δ (ppm): 165.2 (-C=O), 162.7, 157.4, 155.8, 146.9, 144.4, 131.2, 130.6, 125.3, 122.57, 122.53, 114.9, 114.6 (Ar-C), 73.3 (Ar-OCH₂-), 55.7 (O-CH₃), 34.7 (-OCH₂-CH), 26.2 (-CH-CH₂), 16.6 (-CH-CH₃), 11.4 (CH-CH₂-CH₃). **Elemental Analysis for C₂₅H₂₆N₂O₄** (Calc.) Found: C (71.75) 71.74; H (6.26) 6.50; N (6.69) 6.67%.

3.2.2.3 (*R,S*)-4-Butoxyphenyl 4-(4-(2-Methylbutoxy)phenylazo) Benzoate (S3)

Compound **T1-3** (1 g, 3 mmol) and 4-butoxyphenol (0.4 g, 3 mmol) were dissolved in 25 mL dried DCM and 5 mL DMF. The rest of the steps were conducted in the same manner as **T1**. Color: orange. Yield: 55%. **FT-IR** (cm⁻¹): 2960, 2932, 2872 (-C-H, aliphatic), 1722 (C=O in ester), 1599, 1580 (C=C, aromatic), 1501, 1465 (-N=N-), 1244, 1190 (-C-O), 1008, 862, 838, 816 (C-H, aromatic). ¹H NMR (400 MHz, CDCl₃) δ (ppm): 8.35-8.32 (d, 2H, $J = 9$ Hz, Ar-H), 7.99-7.97 (d, 4H, $J = 8.7$ Hz, Ar-H), 7.17-7.15 (d, 2H, $J = 8.7$ Hz, Ar-H), 7.05-7.03 (d, 2H, $J = 8.7$ Hz, Ar-H), 6.97-6.95 (d, 2H, $J = 8.7$ Hz, Ar-H), 4.00-3.97 (t, 2H, $J = 7.1$ Hz, Ar-OCH₂-CH₂), 3.95-3.83 (q, 2H, $J = 6.0$ Hz, O-CH₂), 1.96-1.90 (m, 1H, OCH₂-CH), 1.81-1.77 (m, 2H, CH₂-CH₂), 1.65-1.58, 1.36-1.30 (m, 2H, CH-CH₂ *R,S*), 1.55-1.50 (m, 2H, CH₂-CH₃), 1.08-1.06 (d, 3H, $J = 8.7$ Hz, -CH₃), 1.01-1.0 (t, 3H, $J = 7.1$ Hz, -CH₃), 0.99-0.98 (t, 3H, $J = 7.1$ Hz, -CH₃). ¹³C NMR (100 MHz, CDCl₃) δ (ppm): 165.2 (-C=O), 162.7, 157.07, 155.8, 146.9, 144.3, 131.2, 130.6, 125.3, 122.5, 122.4, 115.2, 114.9 (Ar-C), 73.3 (Ar-OCH₂-), 68.2 (Ar-OCH₂-CH₂), 34.7 (-OCH₂-CH), 31.4 (Ar-OCH₂-CH₂), 26.2 (-CH-CH₂), 19.3 (CH₂-CH₃), 16.6 (-CH-CH₃), 13.9 (CH₂-CH₃), 11.4 (CH-CH₂-CH₃). **Elemental Analysis for C₂₈H₃₂N₂O₄** (Calc.) Found: C (73.02) 73.02; H (7.00) 7.16; N (6.08) 6.21%.

3.2.2.4 (*R,S*)-4-Bromophenyl 4-(4-(2-Methylbutoxy)phenylazo) Benzoate (S4)

Compound **T1-3** (1 g, 3 mmol) and 4-bromophenol (0.6 g, 3 mmol) were dissolved in 25 mL dried DCM. The rest of the steps were conducted in the same manner as **T1**. Color: orange. Yield: 70%. **FT-IR** (cm^{-1}): 2963, 2927, 2874 (C-H, aliphatic), 1726 (C=O in ester), 1598, 1580 (C=C, aromatic), 1483, 1455 (-N=N-), 1252, 1199 (-C-O), 856, 836, 804, 765 (C-H, aromatic). **^1H NMR** (400 MHz, CDCl_3) δ (ppm): 8.33-8.31 (d, 2H, $J = 8.7$ Hz, Ar-H), 7.99-7.96 (dd, 4H, $J = 2.4, 11.5$ Hz, Ar-H), 7.58-7.56 (d, 2H, $J = 8.7$ Hz, Ar-H), 7.17-7.14 (d, 2H, $J = 8.7$ Hz, Ar-H), 7.05-7.03 (d, 2H, $J = 8.7$ Hz, Ar-H), 3.95-3.83 (q, 2H, $J = 6.0$ Hz, Ar-OCH₂-), 1.97-1.89 (m, 1H, OCH₂-CH), 1.67-1.56, 1.37-1.27 (m, 2H, CH-CH₂ *R,S*), 1.07-1.06 (d, 3H, $J = 6.8$ Hz, CH-CH₃), 1.01-0.97 (t, 3H, $J = 7.4$ Hz, CH₂-CH₃). **^{13}C NMR** (100 MHz, CDCl_3) δ (ppm): 163.4 (-C=O), 161.7, 154.8, 148.9, 145.8, 131.5, 130.2, 128.9, 124.3, 122.5, 121.5, 118.0, 113.8 (Ar-C), 72.2 (Ar-OCH₂-), 33.7 (-OCH₂-CH), 25.1 (-CH-CH₂), 15.5 (-CH-CH₃), 10.3 (CH-CH₂-CH₃). **Elemental Analysis for C₂₄H₂₃BrN₂O₃** (Calc.) Found: C (61.68) 61.43, H (4.96) 4.66, N (5.99) 5.80%.

3.2.2.5 (*R,S*)-4-Nitrophenyl 4-(4-(2-Methylbutoxy)phenylazo) Benzoate (S5)

Compound **T1-3** (1 g, 3 mmol) and 4-nitrophenol (0.4 g, 3 mmol) were dissolved in 25 mL dried DCM. The rest of the steps were conducted in the same manner as **T1**. Color: orange. Yield: 75%. **FT-IR** (cm^{-1}): 2964, 2934, 2878 (C-H, aliphatic), 1733 (C=O in ester), 1595, 1577 (C=C, aromatic), 1523, 1345 (N-O), 1501, 1463 (-N=N-), 1260, 1210 (-C-O), 863, 839, 765, 744 (C-H, aromatic). **^1H NMR** (400 MHz, CDCl_3) δ (ppm): 8.36-8.32 (dd, 4H, $J = 2.4, 11.5$ Hz, Ar-H), 8.01-7.97 (t, 4H, $J = 8.2$ Hz, Ar-H), 7.47-7.45 (d, 2H, $J = 8.7$ Hz, Ar-H), 7.05-7.03 (d, 2H, $J = 8.7$ Hz, Ar-H), 3.96-3.83 (q, 2H, $J = 6$ Hz, Ar-OCH₂-), 1.97-1.89 (m, 1H, OCH₂-CH), 1.66-1.52, 1.36-1.28 (m, 2H, CH-CH₂ *R,S*), 1.07-1.06 (d, 3H, $J = 8.7$ Hz, -CH₃), 1.0-0.97 (t, 3H, $J = 7.8$ Hz, -CH₃). **^{13}C**

NMR (100 MHz, CDCl₃) δ (ppm): 163.8 (–C=O), 162.8, 156.2, 155.7, 146.8, 145.5, 131.4, 129.3, 125.4, 125.3, 122.7, 114.9 (Ar–C), 73.3 (Ar–OCH₂–), 34.7 (–OCH₂–CH), 26.1 (–CH–CH₂), 16.5 (–CH–CH₃), 11.3 (CH–CH₂–CH₃). **Elemental Analysis for C₂₄H₂₃N₃O₅** (Calc.) Found: C (66.50) 66.12, H (5.35) 5.29, N (9.69) 9.50%.

3.2.2.6 (*R,S*)-Phenyl 4-(2-Fluoro-4-(2-Methylbutoxy)phenylazo) Benzoate (C1)

Compound **T2-3** (1 g, 3 mmol) and phenol (0.3 g, 3 mmol) were dissolved in 25 mL dried DCM and 5 mL DMF. The rest of the steps were conducted in the same manner as **T1**. Color: orange. Yield: 65%. **FT-IR** (cm⁻¹): 2962, 2933, 2875 (C-H, aliphatic), 1720 (C=O in ester), 1612, 1584 (C=C, aromatic), 1494, 1459 (–N=N–), 1262, 1240 (–C–O), 1077 (C-F), 961, 859, 833, 768 (C-H, aromatic). **¹H NMR** (400 MHz, CDCl₃) δ (ppm): 8.30-8.28 (d, 2H, *J* = 8.7 Hz, Ar–H), 7.97-7.94 (d, 2H, *J* = 8.7 Hz, Ar–H), 7.82-7.77 (t, 1H, *J* = 8.9 Hz, Ar–H), 7.43-7.39 (t, 2H, *J* = 7.8 Hz, Ar–H), 7.27-7.23 (t, 1H, *J* = 7.8 Hz, Ar–H), 7.22-7.20 (d, 2H, *J* = 8.7 Hz, Ar–H), 6.76-6.75 (dd, 1H, *J* = 2.4, 6.3 Hz, Ar–H), 6.74-6.72 (t, 1H, *J* = 5.2 Hz, Ar–H), 3.88-3.84 (q, 2H, *J* = 6 Hz, Ar–OCH₂–), 1.91-1.83 (m, 1H, OCH₂–CH), 1.58-1.50, 1.30-1.21 (m, 2H, CH–CH₂ *R,S*), 1.01-1.0 (d, 3H, *J* = 8.7 Hz, –CH₃), 0.95-0.91 (t, 3H, *J* = 7.8 Hz, –CH₃). **¹³C NMR** (100 MHz, CDCl₃) δ (ppm): 164.7 (–C=O), 164.1, 164.0, 163.4, 155.9, 150.9, 134.9, 131.2, 130.8, 129.5, 126.0, 122.8, 121.7, 118.6, 111.6, 102.5 (Ar–C), 73.7 (Ar–OCH₂–), 34.6 (–OCH₂–CH), 26.05 (–CH–CH₂), 16.5 (–CH–CH₃), 11.3 (CH–CH₂–CH₃). **¹⁹F NMR** (100 MHz, CDCl₃) δ (ppm): 120.1 (C–F). **Elemental Analysis for C₂₄H₂₃FN₂O₃** (Calc.) Found: C (70.92) 70.87, H (5.70) 5.69, N (6.89) 6.5%.

3.2.2.7 (*R,S*)-4-Methoxyphenyl 4-(2-Fluoro-4-2-Methylbutoxyphenylazo) Benzoate (C2)

Compound **T2-3** (1 g, 3 mmol) and 4-methoxyphenol (0.4 g, 3 mmol) were dissolved in 25 mL dried DCM and 5 mL DMF. The rest of the steps were conducted in the same manner as **T1**. Color: orange. Yield: 48%. **FT-IR** (cm⁻¹): 2965, 2939, 2835 (C-H, aliphatic), 1736 (C=O in ester), 1615, 1586 (C=C, aromatic), 1508, 1494 (-N=N-), 1267, 1239 (-C-O), 1073 (C-F), 1004, 965, 867, 840 (C-H, aromatic). **¹H NMR** (400 MHz, CDCl₃) δ (ppm): 8.34-8.32 (d, 2H, *J* = 8.7 Hz, Ar-H), 8.01-7.99 (d, 2H, *J* = 8.7 Hz, Ar-H), 7.87-7.82 (t, 1H, *J* = 8.9 Hz, Ar-H), 7.18-7.16 (d, 2H, *J* = 8.7 Hz, Ar-H), 6.98-6.95 (d, 2H, *J* = 8.7 Hz, Ar-H), 6.81-6.80 (dd, 1H, *J* = 2.4, 6.3 Hz, Ar-H), 6.78-6.77 (t, 1H, *J* = 5.2 Hz, Ar-H), 3.93-3.81 (q, 2H, *J* = 6 Hz, Ar-OCH₂-), 3.84 (s, 3H, O-CH₃), 1.92-1.88 (m, 1H, OCH₂-CH), 1.63-1.56, 1.35-1.27 (m, 2H, CH-CH₂ *R,S*), 1.07-1.05 (d, 3H, *J* = 8.7 Hz, -CH₃), 1.0-0.97 (t, 3H, *J* = 7.8 Hz, -CH₃). **¹³C NMR** (100 MHz, CDCl₃) δ (ppm): 165.1 (-C=O), 164.1, 164.0, 163.4, 160.90, 157.4, 155.8, 144.4, 134.9, 131.2, 130.9, 122.8, 122.5, 118.6, 114.6, 111.6, 102.5 (Ar-C), 73.7 (Ar-OCH₂-), 55.7 (O-CH₃), 34.6 (-OCH₂-CH), 26.1 (-CH-CH₂), 16.5 (-CH-CH₃), 11.3 (CH-CH₂-CH₃). **¹⁹F NMR** (100 MHz, CDCl₃) δ (ppm): 120.13 (C-F). **Elemental Analysis for C₂₅H₂₅FN₂O₄** (Calc.) Found: C (68.79) 68.73, H (5.77) 5.84, N (6.42) 6.67%.

3.2.2.8 (*R,S*)-4-Butoxyphenyl 4-(2-Fluoro-4-2-Methylbutoxy phenylazo) Benzoate (C3)

Compound **T2-3** (1 g, 3 mmol) and 4-butoxyphenol (0.5 g, 3 mmol) were dissolved in 25 mL dried DCM and 5 mL DMF. The rest of the steps were conducted in the same manner as **T1**. Color: orange. Yield: 55%. **FT-IR** (cm⁻¹): 2960, 2932, 2873 (C-H, aliphatic), 1728 (C=O in ester), 1614, 1600 (C=C, aromatic), 1505, 1464 (-N=N-), 1269, 1236, 1189 (-C-O), 1071 (C-F), 1008, 963, 864, 834 (C-H, aromatic). **¹H NMR**

(400 MHz, CDCl₃) δ (ppm): 8.34-8.32 (d, 2H, $J = 8.7$ Hz, Ar-H), 8.01-7.99 (d, 2H, $J = 8.7$ Hz, Ar-H), 7.87-7.82 (t, 1H, $J = 8.9$ Hz, Ar-H), 7.17-7.14 (d, 2H, $J = 8.7$ Hz, Ar-H), 6.96-6.94 (d, 2H, $J = 8.7$ Hz, Ar-H), 6.79-6.78 (dd, 1H, $J = 2.4, 6.3$ Hz, Ar-H), 6.79-6.77 (t, 1H, $J = 5.2$ Hz, Ar-H), 4.0-3.97 (t, 2H, $J = 6.4$ Hz, Ar-OCH₂-CH₂), 3.92-3.81 (q, 2H, $J = 6$ Hz, O-CH₂), 1.94-1.90 (m, 1H, OCH₂-CH), 1.82-1.76 (m, 1H, CH₂-CH₂), 1.63-1.57, 1.34-1.27 (m, 2H, CH-CH₂ *R,S*), 1.55-1.48 (m, 2H, CH₂-CH₃), 1.07-1.05 (d, 3H, $J = 8.7$ Hz, -CH₃), 1.02 (t, 3H, $J = 7.3$ Hz, -CH₃), 0.97 (t, 3H, $J = 7.3$ Hz, -CH₃). ¹³C NMR (100 MHz, CDCl₃) δ (ppm): 165.1 (-C=O), 164.1, 163.5, 160.9, 157.0, 155.8, 144.2, 134.9, 131.2, 130.9, 122.8, 122.4, 118.6, 115.2, 111.6, 102.5 (Ar-C), 73.7 (Ar-OCH₂-), 68.2 (Ar-OCH₂-CH₂), 34.6 (-OCH₂-CH), 31.4 (Ar-OCH₂-CH₂), 26.1 (-CH-CH₂), 19.3 (CH₂-CH₃), 16.5 (-CH-CH₃), 13.9 (CH₂-CH₃), 11.4 (CH-CH₂-CH₃). ¹⁹F NMR (100 MHz, CDCl₃) δ (ppm): 120.15 (C-F). **Elemental Analysis for C₂₈H₃₁FN₂O₄** (Calc.) Found: C (70.27) 70.20, H (6.53) 6.74, N (5.85) 6.18%.

3.2.2.9 (*R,S*)-4-Bromophenyl 4-(2-Fluoro-4-(2-Methylbutoxy)phenylazo) Benzoate (C4)

Compound **T2-3** (1 g, 3 mmol) and 4-bromophenol (0.5 g, 3 mmol) were dissolved in 25 mL dried DCM. The rest of the steps were conducted in the same manner as **T1**. Color: orange. Yield: 65%. **FT-IR** (cm⁻¹): 2961, 2927, 2874 (C-H, aliphatic), 1722 (C=O in ester), 1610, 1583 (C=C, aromatic), 1483, 1457 (-N=N-), 1261, 1239, 1206 (-C-O), 1064 (C-F), 858, 831, 802, 767 (C-H, aromatic). ¹H NMR (400 MHz, CDCl₃) δ (ppm): 8.33-8.30 (d, 2H, $J = 8.7$ Hz, Ar-H), 8.01-7.99 (d, 2H, $J = 9.06$ Hz, Ar-H), 7.86-7.82 (t, 1H, $J = 9.06$ Hz, Ar-H), 7.58-7.56 (d, 2H, $J = 8.7$ Hz, Ar-H), 7.17-7.14 (d, 2H, $J = 8.7$ Hz, Ar-H), 6.81-6.80 (t, 1H, $J = 2.4$ Hz, Ar-H), 6.79-6.77 (s, 1H, Ar-H), 3.93-3.81 (q, 2H, $J = 6.0$ Hz, Ar-OCH₂-), 1.96-1.88 (m, 1H, OCH₂-CH), 1.62-1.55, 1.37-1.27 (m, 2H, CH-CH₂ *R,S*), 1.07-1.05 (d, 3H, $J = 6.8$ Hz, CH-CH₃), 1.0-0.97 (t, 3H, $J = 7.4$ Hz,

CH₂-CH₃). ¹³C NMR (100 MHz, CDCl₃) δ (ppm): 163.3 (–C=O), 162.4, 159.8, 154.9, 148.8, 133.8, 131.5, 130.2, 129.2, 122.5, 121.8, 118.1, 117.5, 110.5, 101.2 (Ar–C), 72.6 (Ar–OCH₂–), 33.5 (–OCH₂–CH), 25.0 (–CH–CH₂), 15.4 (–CH–CH₃), 10.3 (CH–CH₂–CH₃). ¹⁹F NMR (100 MHz, CDCl₃) δ (ppm): 120.05 (C–F). **Elemental Analysis for C₂₄H₂₂BrFN₂O₃** (Calc.) Found: C (59.39) 58.98, H (4.57) 4.25, N (5.77) 5.54%.

3.2.2.10 (*R,S*)-4-Nitrophenyl 4-(2-Fluoro-4-(2-Methylbutoxy)phenylazo) Benzoate (C5)

Compound **T2-3** (1 g, 3 mmol) and 4-nitrophenol (0.4 g, 3 mmol) were dissolved in 25 mL dried DCM. The rest of the steps were conducted in the same manner as **T1**. Color: orange. Yield: 70%. **FT-IR** (cm⁻¹): 2963, 2935, 2878 (C–H, aliphatic), 1739 (C=O in ester), 1612, 1582 (C=C, aromatic), 1520, 1343 (N–O), 1493, 1456 (–N=N–), 1262, 1238, 1212 (–C–O), 1065 (C–F), 862, 839, 764, 745 (C–H, aromatic). **¹H NMR** (400 MHz, CDCl₃) δ (ppm): 8.36-8.32 (dd, 4H, *J* = 2.4, 11.5 Hz, Ar–H), 8.03-8.0 (d, 2H, *J* = 9.06 Hz, Ar–H), 7.87-7.82 (t, 1H, *J* = 9.06 Hz, Ar–H), 7.47-7.45 (d, 2H, *J* = 8.7 Hz, Ar–H), 6.81-6.80 (t, 1H, *J* = 2.4 Hz, Ar–H), 6.78 (s, 1H, Ar–H), 3.93-3.81 (q, 2H, *J* = 6 Hz, Ar–OCH₂–), 1.96-1.88 (m, 1H, OCH₂–CH), 1.65-1.54, 1.35-1.26 (m, 2H, CH–CH₂ *R,S*), 1.07-1.05 (d, 3H, *J* = 8.7 Hz, –CH₃), 1.0-0.97 (t, 3H, *J* = 7.8 Hz, –CH₃). **¹³C NMR** (100 MHz, CDCl₃) δ (ppm): 164.3 (–C=O), 163.8, 161.0, 156.3, 155.7, 145.6, 134.9, 131.5, 129.7, 125.4, 123.0, 122.7, 118.6, 111.7, 102.5 (Ar–C), 73.7 (Ar–OCH₂–), 34.7 (–OCH₂–CH), 26.1 (–CH–CH₂), 16.5 (–CH–CH₃), 11.4 (CH–CH₂–CH₃). **¹⁹F NMR** (100 MHz, CDCl₃) δ (ppm): 119.9 (C–F). **Elemental Analysis for C₂₄H₂₂FN₃O₅** (Calc.) Found: C (63.85) 63.53, H (4.91) 4.98, N (9.31) 8.90%.

3.2.2.11 (*R,S*)-Phenyl 4-((2-Methyl-4-(2-Methylbutoxy)phenylazo) Benzoate (C6)

Compound **T3-3** (1 g, 3 mmol) and phenol (0.3 g, 3 mmol) were dissolved in 25

mL dried DCM. The rest of the steps were conducted in the same manner as **T1**. Color: orange. Yield: 75%. **FT-IR** (cm^{-1}): 2961, 2929, 2874 (-C-H, aliphatic), 1721 (C=O in ester), 1590 (C=C, aromatic), 1488, 1456 (-N=N-), 1244, 1201 (-C-O), 910, 848, 826, 766 (C-H, aromatic). **$^1\text{H NMR}$** (400 MHz, CDCl_3) δ (ppm): 8.26-8.24 (d, 2H, $J = 8.7$ Hz, Ar-H), 7.90-7.88 (d, 2H, $J = 8.7$ Hz, Ar-H), 7.72-7.70 (d, 1H, $J = 8.7$ Hz, Ar-H), 7.40-7.36 (t, 2H, $J = 7.1$ Hz, Ar-H), 7.24-7.20 (t, 1H, $J = 7.8$ Hz, Ar-H), 7.18-7.16 (d, 2H, $J = 7$ Hz, Ar-H), 6.79 (d, 1H, $J = 2.3$ Hz, Ar-H), 6.73-6.72 (dd, 1H, $J = 2.4, 11.5$ Hz, Ar-H), 3.84-3.72 (q, 2H, $J = 6.0$ Hz, Ar-OCH₂-), 2.68 (s, 3H, Ar-CH₃), 1.85-1.80 (m, 1H, OCH₂-CH), 1.57-1.51, 1.24-1.19 (m, 2H, CH-CH₂ *R,S*), 0.98-0.96 (d, 3H, $J = 6.4$ Hz, -CH₃), 0.92-0.88 (t, 3H, $J = 7.8$ Hz, -CH₃). **$^{13}\text{C NMR}$** (100 MHz, CDCl_3) δ (ppm): 164.8 (-C=O), 162.7, 156.1, 150.9, 144.9, 142.1, 131.2, 130.2, 129.5, 125.9, 122.6, 121.7, 117.2, 115.9, 113.1 (Ar-C), 73.1 (Ar-OCH₂-), 34.7 (-OCH₂-CH), 26.1 (-CH-CH₂), 17.9 (Ar-C-CH₃), 16.5 (-CH-CH₃), 11.3 (CH-CH₂-CH₃). **Elemental Analysis for C₂₅H₂₆N₂O₃** (Calc.) Found: C (74.60) 75.03; H (6.51) 6.37; N (6.96) 6.56%.

3.2.2.12 (*R,S*)-4-Methoxyphenyl-4-(2-Methyl-4-(2-Methylbutoxy)phenylazo)

Benzoate (C7)

Compound **T3-3** (1 g, 3 mmol) and 4-methoxyphenol (0.4 g, 3 mmol) were dissolved in 25 mL dried DCM. The rest of the steps were conducted in the same manner as **T1**. Color: orange. Yield: 55%. **FT-IR** (cm^{-1}): 2961, 2933, 2875 (-C-H, aliphatic), 1728 (C=O in ester), 1592 (C=C, aromatic), 1488, 1463 (-N=N-), 1270, 1240, 1194 (-C-O), 1029, 863, 827, 771 (C-H, aromatic). **$^1\text{H NMR}$** (400 MHz, CDCl_3) δ (ppm): 8.34-8.32 (d, 2H, $J = 8.7$ Hz, Ar-H), 7.98-7.96 (d, 2H, $J = 8.7$ Hz, Ar-H), 7.80-7.78 (d, 1H, $J = 8.7$ Hz, Ar-H), 7.19-7.16 (d, 2H, $J = 9.2$ Hz, Ar-H), 6.98-6.96 (d, 2H, $J = 8.7$ Hz, Ar-H), 6.87 (d, 1H, $J = 2.4$ Hz, Ar-H), 6.83-6.81 (dd, 1H, $J = 2.4, 11.5$ Hz, Ar-H), 3.93-3.81 (q, 2H, $J = 6.0$ Hz, Ar-OCH₂-), 3.85 (s, 3H, O-CH₃), 2.77 (s, 3H, Ar-CH₃), 1.94-1.88 (m,

1H, OCH₂-CH), 1.64-1.60, 1.33-1.27 (m, 2H, CH-CH₂ *R,S*), 1.07-1.05 (d, 3H, *J* = 6.4 Hz, -CH₃), 0.99-0.97 (t, 3H, *J* = 7.1 Hz, -CH₃). ¹³C NMR (100 MHz, CDCl₃) δ (ppm): 165.2 (-C=O), 162.7, 157.4, 156.1, 144.9, 144.5, 142.2, 131.2, 130.4, 122.7, 122.5, 117.3, 116.0, 114.6, 113.2 (Ar-C), 73.2 (Ar-OCH₂-), 55.7 (O-CH₃), 34.8 (-OCH₂-CH), 26.2 (-CH-CH₂), 17.9 (Ar-C-CH₃), 16.6 (-CH-CH₃), 11.4 (CH-CH₂-CH₃). **Elemental Analysis for C₂₆H₂₈N₂O₄** (Calc.) Found: C (72.20) 72.41; H (6.53) 6.78; N (6.48) 6.51%.

3.2.2.13 (*R,S*)-4-Butoxyphenyl 4-(2-Methyl-4-(2-Methylbutoxy)phenylazo) Benzoate (C8)

Compound **T3-3** (1 g, 3 mmol) and 4-butoxyphenol (0.5 g, 3 mmol) were dissolved in 25 mL dried DCM. The rest of the steps were conducted in the same manner as **T1**. Color: orange. Yield: 60%. **FT-IR** (cm⁻¹): 2962, 2939, 2873 (-C-H, aliphatic), 1723 (C=O in ester), 1594 (C=C, aromatic), 1505, 1455 (-N=N-), 1242, 1190 (-C-O), 1009, 859, 822, 796 (C-H, aromatic). ¹H NMR (400 MHz, CDCl₃) δ (ppm): 8.34-8.31 (d, 2H, *J* = 8.7 Hz, Ar-H), 7.98-7.96 (d, 2H, *J* = 8.7 Hz, Ar-H), 7.81-7.78 (d, 1H, *J* = 8.7 Hz, Ar-H), 7.17-7.15 (d, 2H, *J* = 8.7 Hz, Ar-H), 6.97-6.95 (d, 2H, *J* = 8.7 Hz, Ar-H), 6.88-6.87 (d, 1H, *J* = 2.4 Hz, Ar-H), 6.84-6.81 (dd, 1H, *J* = 2.4, 11.5 Hz, Ar-H), 4.01-3.97 (t, 2H, *J* = 7.1 Hz, Ar-OCH₂-), 3.93-3.81 (q, 2H, *J* = 6.0 Hz, Ar-OCH₂), 2.77 (s, 3H, Ar-CH₃), 1.94-1.91 (m, 1H, OCH₂-CH), 1.83-1.76 (m, 2H, OCH₂-CH₂), 1.62-1.55, 1.34-1.28 (m, 2H, CH-CH₂ *R,S*), 1.54-1.49 (m, 2H, CH₂-CH₂), 1.07-1.05 (d, 3H, *J* = 6.4 Hz, CH₂-CH₃), 1.01 (t, 3H, *J* = 7.1 Hz, -CH₃), 0.97 (t, 3H, *J* = 7.1 Hz, -CH₃). ¹³C NMR (100 MHz, CDCl₃) δ (ppm): 165.2 (-C=O), 162.7, 157.0, 156.1, 145.0, 144.3, 142.2, 131.2, 130.4, 122.7, 122.5, 117.3, 116.0, 115.2, 113.2 (Ar-C), 73.2 (Ar-OCH₂-), 68.2 (Ar-OCH₂-CH₂), 34.8 (-OCH₂-CH), 31.4 (Ar-OCH₂-CH₂), 26.2 (-CH-CH₂), 19.3 (CH₂-CH₃), 17.9 (Ar-C-CH₃), 16.6 (-CH-CH₃), 13.9 (CH₂-CH₃), 11.4 (CH-CH₂-CH₃). **Elemental Analysis for C₂₉H₃₄N₂O₄** (Calc.) Found: C (73.39) 73.28; H (7.22) 7.28; N

(5.90) 6.11%.

3.3 Characterisation Methods and Instrumentation

3.3.1 Fourier Transform Infrared Spectroscopy (FT-IR)

Fourier transform infrared spectroscopy (FT-IR) measures the electromagnetic radiation in the infrared region, which has a lower frequency and a longer wavelength than visible light. It is measurable in a sample when submitted to infrared radiation. The sample is irradiated with infrared light, and the transmitted light is analysed in infrared spectroscopy, which allows structural analysis and quantification. The amount of light absorption by the sample molecules is measured using absorbance analysis, which is dependent on wavelength. Interatomic chemical bonds in a molecule can stretch as if they were springs. Because the energy associated with such stretching vibrations is similar to that of infrared light, molecules absorb it and vibrate. Infrared light can only induce vibrations that require a change in dipole moment. When the vibrations of atoms bonds cancel each other, infrared absorption does not occur (Mohamed et al., 2017). Figure 3.1 shows the schematic diagram of the FT-IR spectrometer.

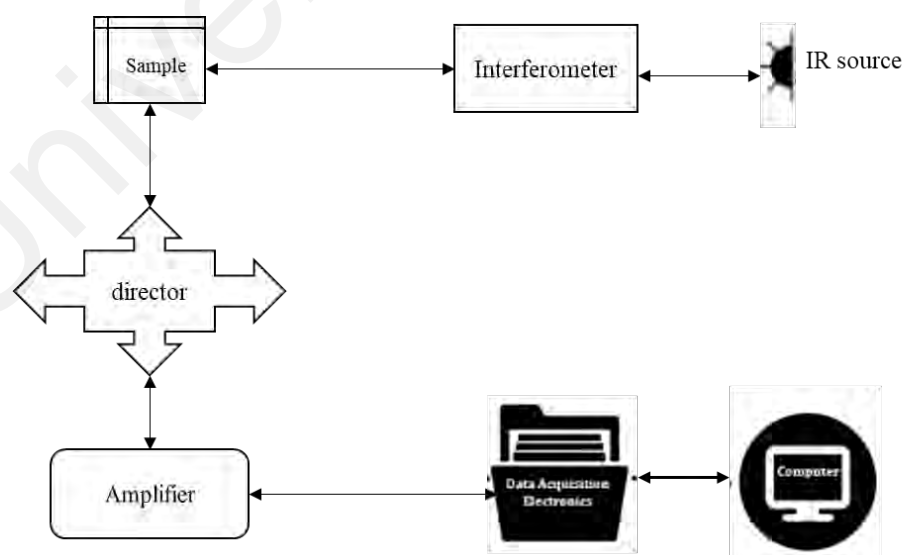


Figure 3.1: Schematic diagram of FT-IR spectrometer.

Measurement

Samples placed in the infrared beam's path will absorb and transmit light, and the light signal is then passed to the detector through the sample. The detector determines the radiation's intensity that moves into the sample and the radiation transmitting through it. The output as a function of time has been converted by a computer using a Fourier transform method into a plot of absorption against wavenumber. The FT-IR spectra were recorded with a Spotlight 400 Perkin Elmer spectrometer (Waltham, MA, USA) using the attenuated total reflectance (ATR) method. The light beam's penetration depth using the ATR technique in the sample is approximately 0.5–3 μm . A minimum amount of sample was placed over the ATR crystal and maximum pressure was applied using the slip-clutch mechanism. The spectrum was obtained in the region of 4000 to 450 cm^{-1} , with a resolution of 4 cm^{-1} and collected after 4 scans. All data processing was performed using the instrument's built in Spectrum v6.3.1.0132 software.

3.3.2 Nuclear Magnetic Resonance Spectroscopy (NMR)

NMR spectroscopy provides a representation of single atoms, molecules and solid-state in solution in several media. It is non-destructive and produces a molar reaction that enables structural elucidation and quantification and details the organic molecules' chemical structure and dynamics. The principle behind NMR is that there is spin in some nuclei and electric charging of all nuclei. If an additional magnetic field is applied, the transfer of energy between the base energy level to a higher energy level is possible (generally, a single energy gap). Many atoms' nuclei start acting like small magnets when molecules are placed in a strong magnetic field. The nuclei can resonate at their own frequencies if a broad spectrum of radiofrequency waves is applied to the sample. Magnetic interactions with covalent bindings between NMR-active nuclei along with result in spin-spin (n-J) couplings. Because of the low-energy level excitation, NMR

spectroscopy has a distinct relaxation and sensitivity when compared to other spectroscopic methods.

In order to understand the NMR data evaluation within the experiment, the rotating coordinate system is a valuable method. During the acquisition time, the NMR data are reported in the y and x-direction. The macroscopic magnetisation would fall back into the equilibrium state during the acquisition time of the NMR experiment. This effect is called spin-lattice relaxation. In an exponential curve, the measurable magnetisation tends towards zero. High or lower frequency resonances with various protons can be present. The free induction decay is the raw data calculated in the NMR experiment. The actual signals are increased during data collection, while the statistical noise was disappeared. The condition for such a strategy is that the equilibrium state is achieved before the next excitation. Therefore, it is important to understand the relaxation mechanism. Under the restrictions of quantum mechanics, an excited state's energy must be returned to the surroundings, called transversal relaxation (Günther, 2013; Jacobsen, 2016; Pavia et al., 2014). Figure 3.2 illustrates the schematic diagram of NMR spectrometer.

Through 1D NMR experiments, all compounds were examined to determine the presence of proton and carbon atoms via ^1H and ^{13}C NMR. Various nuclei can be also considered by NMR spectroscopy i.e. fluorine atom via ^{19}F NMR. The ^{13}C NMR spectrum revealed all of the carbon atoms in the compounds, but it did not distinguish between signals for quaternary carbon (C), methine (CH), methylene (CH_2), or methyl (CH_3). The Distortionless Enhancement by Polarization Transfer (DEPT) NMR experiment is usually used to determine primary, secondary, and tertiary carbon by selecting varied angle parameters. The (DEPT-45) gives all attached carbons signal in a positive phase, (DEPT-90) shows only CH groups, while (DEPT-135) illustrates CH and CH_3 in a positive phase and CH_2 in a negative phase. In APT (Attached Proton Test)

NMR experiment, both CH and CH₃ appear as positive signals in the spectrum, while quaternary C and CH₂ appear as negative signals. In the DEPT-135 experiment, quaternary carbons' signals are suppressed but in the APT experiment, the signals are observed.

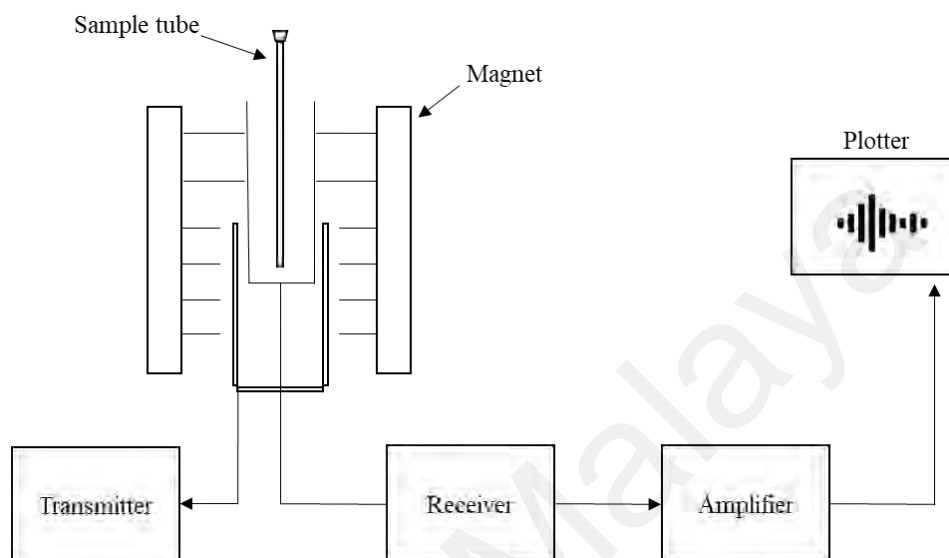


Figure 3.2: Schematic diagram of NMR spectrometer. Redrawn from (Günther, 2013).

Measurement

For this study, ¹H NMR, ¹³C NMR and ¹⁹F NMR measurements were performed using a JEOL ECA 400 MHz spectrometer (Tokyo, Japan) and a Bruker AVN 400 MHz spectrometer (Fällanden, Switzerland). All compounds with weight 10 mg and 20 mg for ¹H NMR and ¹³C NMR analyses respectively were dissolved in suitable deuterated chloroform (CDCl₃) or deuterated dimethyl sulfoxide (DMSO-d₆) solvent in NMR tube with depth 4.5 cm. The samples were prepared and measured at room temperature. The concentration of the sample was kept at 2.5% (w/v) for ¹H and ¹⁹F NMR and 15% (w/v) for ¹³C NMR. The CDCl₃ peaks were set at 7.27 ppm and 77.0 ppm for ¹H NMR and ¹³C NMR, respectively. The dimethyl sulfoxide (DMSO) peaks for ¹H NMR were set at 3.34 and 2.4 ppm, while the peak for ¹³C NMR was set at 40.6 ppm. Commonly used solvents do not contain fluorine atoms, so they do not affect the ¹⁹F NMR signals.

3.3.3 Elemental Analysis CHN/O

The carbon (C), hydrogen (H) and nitrogen (N) elemental content of the final compounds were determined using a Perkin Elmer CHNS/O 2400 Series II Analyzer. This instrument calculates the percentages of elemental concentrations based the Pregl-Dumas method principle, in which the samples were combusted in a pure oxygen environment, with the resultant combustion gases measured in an automated fashion. A tin capsule is used to measure the sample under inspection. The sample is placed in the autosampler after folding the capsule (which resembles wrapped tin foil). The tin capsule containing the sample falls into the reactor chamber, which has previously been filled with excess oxygen. At about 990 °C, the material is "mineralised". The formation of carbon monoxide is likely at this temperature, even under these conditions of excess oxygen. The gaseous reaction products pass through a tungsten trioxide catalyst which completes the oxidation. As a result, the resulting mixture should contain H₂O, CO₂ and NO. The product gas mixture is passed through a silica tube that is filled with copper granules. Remaining oxygen is bound, and nitric/nitrous oxides are reduced in this zone, which is kept at around 500 °C. The analytically important species of CO₂, H₂O and N₂ are present in the leaving gas stream. Eventually, included SO₂ or hydrohalogenides absorb in appropriate traps. High purity helium (Quality 5.0) is used as a carrier gas. Finally, the gas mixture is brought to a specific pressure/volume ratio before being passed through a gas chromatographic system. The species are separated using a technique known as zone chromatography. In this technique, a staircase type signal is registered. Step height is proportional to the substance amount in the mixture (Thompson, 2008). Figure 3.3 shows a schematic diagram of CHNS/O elemental analyzer.

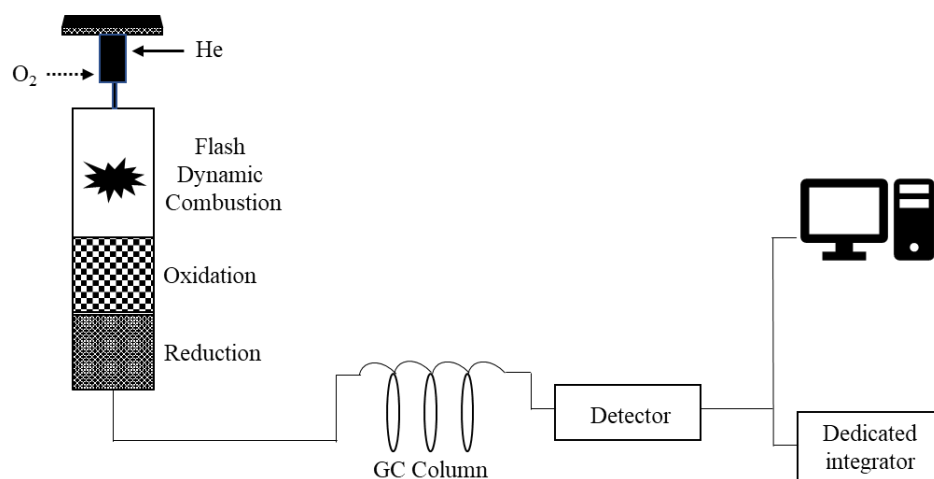


Figure 3.3: Schematic diagram of CHNS/O Elemental Analyzer. Redrawn from (Thompson, 2008).

Measurement

The compounds were weighed 1 mg in a tin capsule and wrapped according to the instrument packing steps. Elemental analyses were obtained using Perkin Elmer CHNS/O Elemental Analyzer 2400 Series II. Acetanilide was used as calibration standard for all analyses.

3.3.4 Thermogravimetric Analysis (TGA)

TGA is a technique used by monitoring the changes in weight that occur when a sample is constantly heated to determine the thermal stability, oxidative stability, chemical composition of a substance, and its fraction of volatile components. TGA is a thermal analysis method in which a sample's mass is determined over time as the temperature increases. TGA analysis is carried out by raising a sample's temperature in a furnace gradually as its weight is weighed on an analytical balance that remains outside the furnace. In TGA, mass loss is observed when the loss of a volatile component involves a thermal event. In order to illustrate thermal transitions in the material, the sample weight

is plotted against temperature or time, such as loss of solvents and plasticisers in polymers; hydration of water in inorganic materials; and decomposition of the material (Haines, 2012). The basic setup of a thermogravimetric analyser is shown in Figure 3.4.

TGA instrument is typically loaded with a sample mass of 4–15 mg, depending on the sample's density, the sample's pan size, and the purpose of the analysis. The first derivative of the TGA curve with derivative thermogravimetry (DTG) is another type of representation of results. It defines the rate at which mass changes take place. DTG is often used to detect more subtle effects or when investigating kinetic parameters. The DTG is typically plotted as mg/min or percent/min because the TGA signal is recorded in mg or percent (100 percent is the initial mass at time zero). Both the TGA and DTG curves were obtained from a thermogravimetric test of a sample performed in a nitrogen atmosphere and a constant heating rate. The TGA curve describes the compounds thermal decomposition which occur at different temperatures. A constant slope characterises from the various steps of thermal decomposition can be observed from a TGA plot. The DTG plot helps to identify transformations that correlate with or are associated with low loss of mass (Prime et al., 2009).

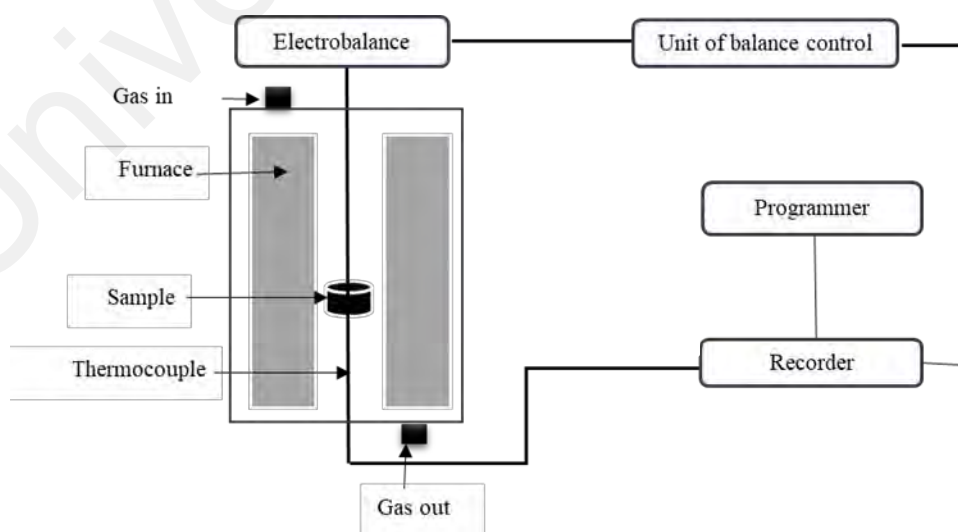


Figure 3.4: Basic setup of TGA analyser. Redrawn from (Haines, 2012).

Measurement

Thermal decomposition data were obtained using SDT Q600 thermogravimetric analyzer (New Castle, USA). In this experiment, samples of approximately 3-5 mg were transferred to the aluminium pan and loaded into the sample holder. Thermogravimetric analysis was recorded under a nitrogen atmosphere at a heating rate of $20^{\circ}\text{C min}^{-1}$. The data analysis was performed using Pyris software.

3.3.5 Differential Scanning Calorimetry (DSC)

DSC is used to measure enthalpy changes and phase transition temperature as a function of time or temperature. It is very sensitive, fast and easy to use. Generally, DSC measures the heat flow rate difference between a reference sample and a sample while the sample is subjected to a temperature-controlled programme (Höhne et al., 2003). DSC can be used to determine the temperature of glass transition (T_g), purity, melting and crystallisation temperature, measurement of heat capacity, characterisation of thermosets, and liquid crystal transition measurement. In order to provide details on the phase-type of the formed liquid crystalline structures, DSC analysis is used to complement POM. Figure 3.5 illustrates the schematic diagram of a differential scanning calorimeter and a typical DSC curve.

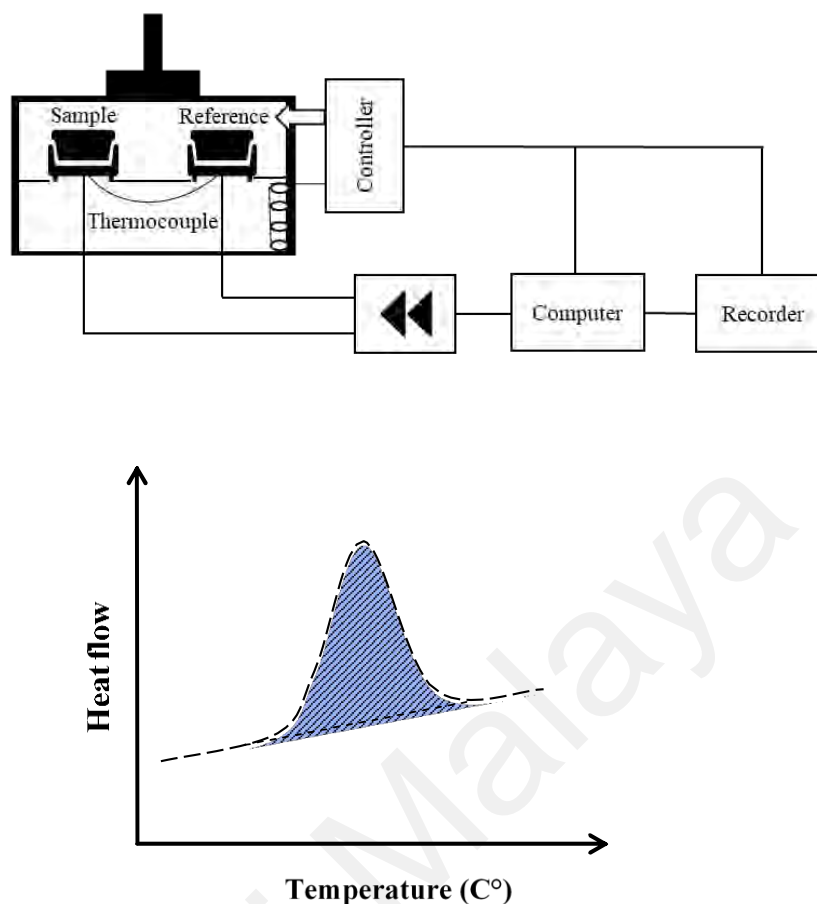


Figure 3.5: Schematic diagram of a differential scanning calorimeter and a typical DSC curve. Redrawn from (Höhne et al., 2003).

Measurement

Differential scanning calorimetry (DSC) measurements were recorded using a Mettler Toledo DSC 822^e calorimeter (Columbus, OH, USA) equipped with Haake EK90/MT intercooler. Indium was used as the standard sample to calibrate the temperature and enthalpy accuracy. The calorimetric measurements were carried out for two cycles at heating and cooling scanning rates of 10 °C min⁻¹ under nitrogen atmosphere. Samples of 4–6 mg were placed into 40- μ L sealed aluminium pans. The data were analyzed using STAR^e Thermal Analysis System software.

3.3.6 Polarized Optical Microscopy (POM)

POM is a technique used to determine textures in differentiating phases in both the lyotropic and thermotropic behaviour of LC compounds. POM is also a convenient way to identify the liquid crystalline compounds transition temperature. The major function of POM is to distinguish between anisotropic and isotropic media (Ellis et al., 2020). Figure 3.6 displays a typical setup of polarized optical microscope. There are two important components: i) the objective lens that collects lights diffracted by the sample to form the magnified actual image and ii) the condenser lens that focuses the light onto a small area of the specimen from the illuminator. The image is magnified by the objective lens and is captured by the eyepiece to produce an image. It also can be recorded directly as real image onto a camera. Polarizer acts like a filter to allow only light oscillating in one orientation to pass (Bellare et al., 1990).

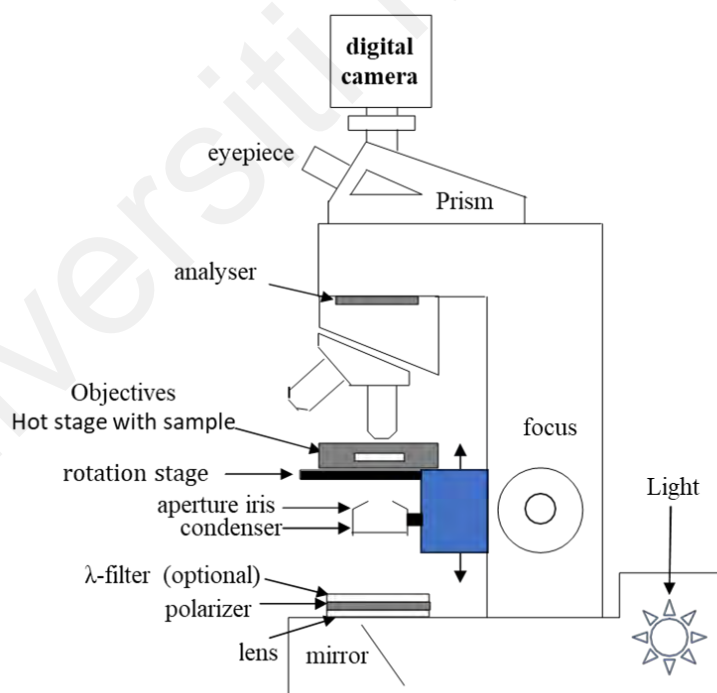


Figure 3.6: Basic setup of polarized optical microscope. Redrawn from (Dierking, 2003).

Measurement

The liquid crystalline textures and phase transitions were identified by POM experiments using an Olympus BX51 polarized light microscope (Tokyo, Japan) attached to a Mettler Toledo FP82HT hot stage (Columbus, OH, USA) and a temperature controller (FP90 central processor). The microscope was connected to an Olympus camera for image capture, and cell- Sens microscope imaging software was used for image analysis and storage. Each sample was placed between a non-treated glass slide and coverslip, then heated until it reached its isotropic phase and then cooled down to room temperature. The phase transition temperature was recorded during the second heating and the liquid crystalline textures formed were taken upon the second cooling at a rate of 2 °C min⁻¹.

3.3.7 Small- and Wide-Angle X-ray Scattering (SWAXS)

SWAXS measurements were performed to determine the structural properties of the identified mesophases. The measurement of SWAXS confirmed the liquid crystal phase determined by POM (Li et al., 2016). Small-angle X-ray scattering (SAXS) is a technique determining the intensity of X-rays scattered by a sample due to the scattering angle. Measurements are made at very tiny angles, typically between 0.1 to 5 degrees (De Bruyn Ouboter et al., 2011). From the law of Bragg as shown in Equation 3.1, it is assumed that as the scattering angle decreases, increasingly structural features will be investigated. A SAXS signal is detected when a material has structural characteristics, typically in the range of 1-100 nm on the nanometers length scale (Kikhney & Svergun, 2015).

$$n\lambda = 2d\sin \theta \qquad \text{Equation (3.1)}$$

where λ represent the X-ray radiation wavelength, the different peak order ($n = 1, 2$) represents the integer, d is the inter-plane distance (d-spacing), and θ is the angle of the incident rays to the surface of the sample. Wide-angle X-ray scattering (WAXS) is the study of Bragg peaks scattered at wide angles, which are created by structures smaller than a nanometer ($d < 1$ nm), such as atoms and interatomic distances. The detector is placed away from the sample in SAXS experiments. In contrast, in WAXS experiments, the detector is situated close to the sample in order to observe maxima at larger angles (Podorov et al., 2006). Figure 3.7 shows a schematic diagram of the SWAXS technique.

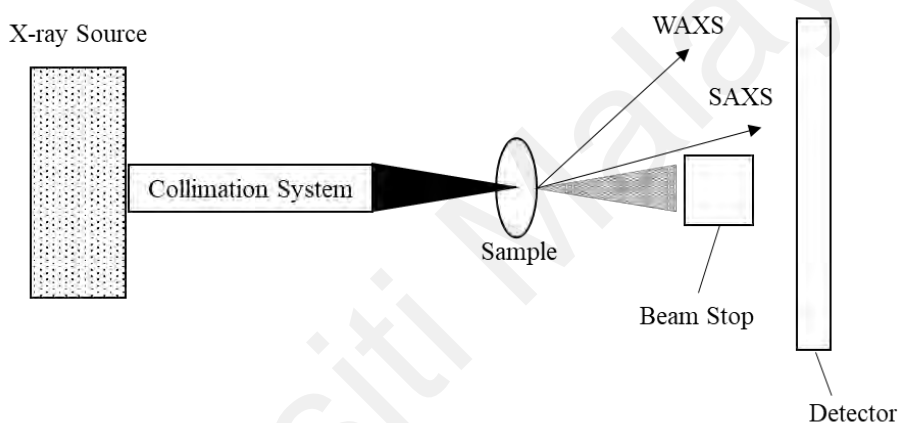


Figure 3.7: Schematic diagram of SWAXS technique.

Measurement

An analytical SWAXS from SAXSpace (Anton Paar, Austria) was equipped with an X-ray tube (DX-Cu 12 × 0.45, SERFERT) generating Cu-K α radiation beam with wavelength $\lambda = 0.1542$ nm at 40 kV and 50 mA. The measurements were carried out in line collimation mode under vacuum with the detector distance of 121 mm. Silver behenate ($\lambda = 5.84$ nm) was used as a calibrant for all measurements. Each sample was transferred to a solid sample holder and loaded into the X-ray machine. The sample was then heated to its isotropic state and allowed to cool at room temperature. The measurement at a selected temperature was conducted upon second heating using a Peltier

System (TCStage 300) to control the sample temperature with an accuracy of ± 0.1 °C. Each sample was equilibrated for 10 min at the designated temperature followed by 10 min exposure time for the measurement. The data were calibrated by normalizing the primary beam using SAXStreat software.

3.3.8 Ultraviolet-Visible Spectroscopy (UV-Vis)

UV-Vis spectroscopy is a type of absorption spectroscopy in which a molecule absorbs light from the UV-Vis region. The absorption of UV-Vis radiation leads to the excitation of electrons from the ground to a higher energy state. In many applications, UV-Vis is simple, inexpensive and easy to use in various fields, primarily for routine measurements, such as in the food industry, hospitals, the petrochemical industry and laboratories for water quality control. UV-Vis is currently one of the most frequently used techniques in both chemical and pharmaceutical laboratories for the quantitative determination of various inorganic and organic compounds in solution. This instrument may also be used to determine the purity of a compound (Penner, 2017).

The principle of UV-Vis Spectroscopy is based on the absorption by chemical compounds of ultraviolet or visible light, resulting in a different spectrum. The theory follows the Beer-Lambert Law. UV-Vis has several applications e.g. detect the extent of conjugation in polyenes, the absence or chromophore presence in a complex compound, functional group (Baldock & Hutchison, 2016). Figure 3.8 shows a schematic diagram of the UV-Vis spectrophotometer.

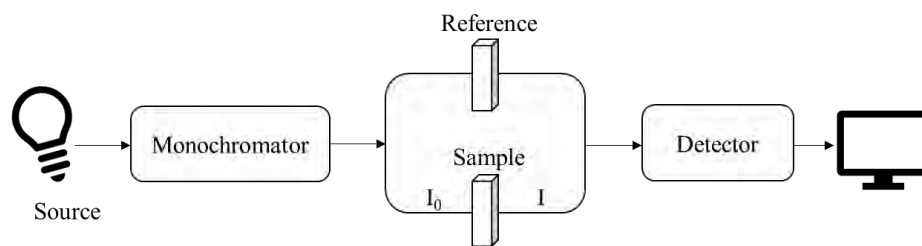


Figure 3.8: Schematic diagram of UV-Vis spectrophotometer. Redrawn from (Hof, 2003).

Measurement

The compound solution (5×10^{-5} M) in CHCl_3 was prepared and fresh CHCl_3 was used as a blank. The solution was placed into a 1-cm path-length quartz cuvette at room temperature. UV-vis absorption spectra were recorded using a Cary 60 UV-Vis spectrophotometer with medium scan rate from 200 nm to 600 nm.

3.3.9 Photoluminescence Spectroscopy (PL)

PL spectroscopy is the study of how the light energy, or photons, induce the emission of a photon from any matter. Light is guided to a sample, where it is absorbed and where there might be a process called photo-excitation. The photo-excitation causes the material to jump to a higher electronic state and then release energy (photons) as it relaxes and returns to a lower energy level. PL is a quantum mechanical mechanism in which a photon is absorbed into a substance and transferred to a ground electron and excited in a femtosecond timescale (Aoki, 2019).

Luminescence, divided into fluorescence and phosphorescence, is the spontaneous emission of light from electronically excited states of any material. Sir George Gabriel Stokes, a physicist and mathematics professor, introduced the first type of luminescence, fluorescence, in the middle of the 19th century. Phosphorescence is the second type of luminescence, in which excited triplet states emit light. As the ground-

state electron, the orbital electron has the same spin orientation (Obodovskiy, 2019). The Jablonski diagram depicts the processes that occur between light absorption and emission as shown in Figure 3.9.

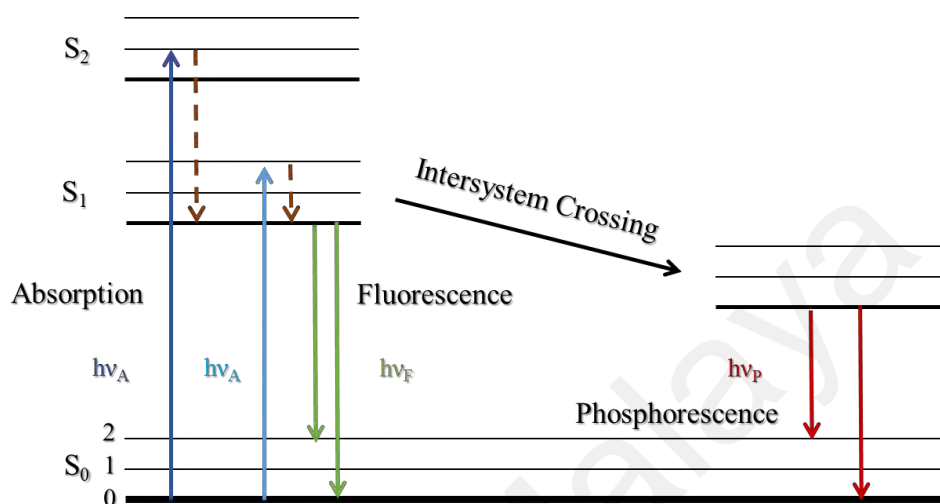


Figure 3.9: A typical Jablonski diagram. Redrawn from (Lakowicz, 2013).

Fluorescence is a powerful instrument at the molecular or supramolecular level for investigating the dynamics of matter, structure and living systems. It is used to measure the concentrations of various substance, including neutral and ionic. It is useful as probes for estimating local parameters such as molecular mobility, fluidity, polarity, and electrical potential in diverse systems like biological membranes, polymers, nucleic acids, surfactant solutions, proteins, and even living cells (Chattopadhyay, 2003). Figure 3.10 illustrates schematic diagram of fluorescence spectrometer.

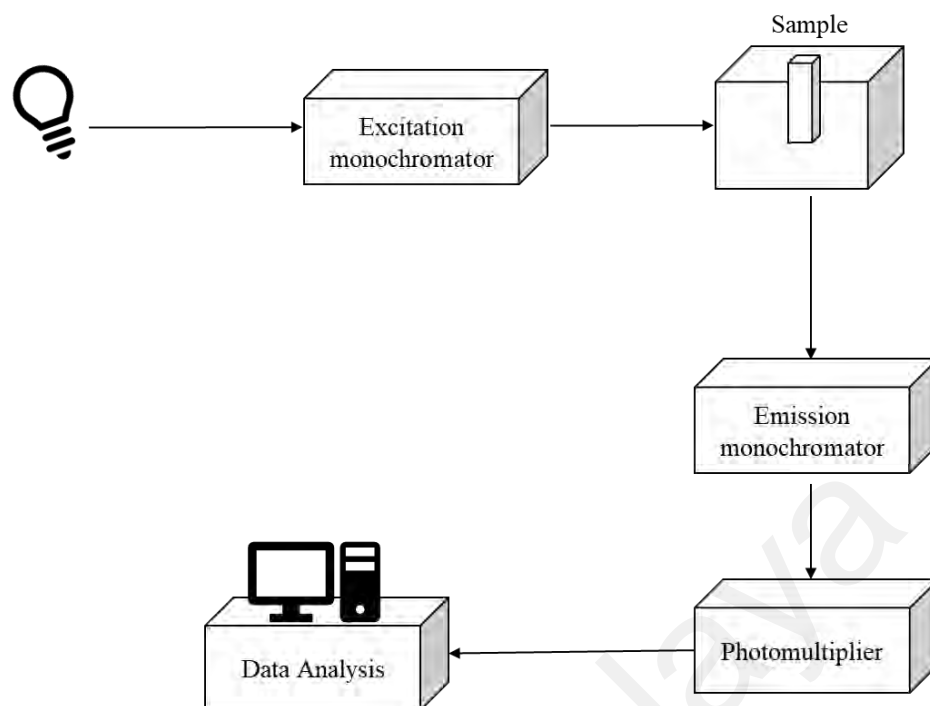


Figure 3.10: Schematic diagram of fluorescence spectrometer. Redrawn from (Lakowicz, 2013).

Measurement

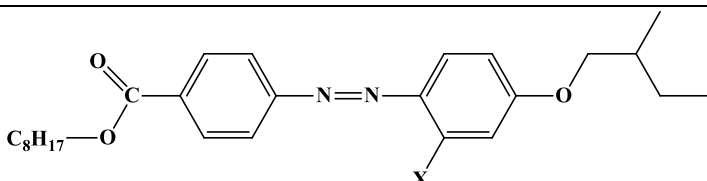
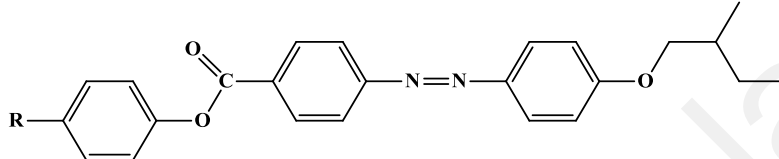
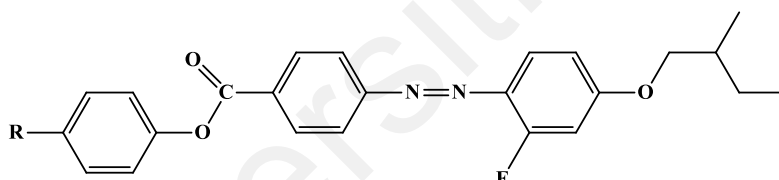
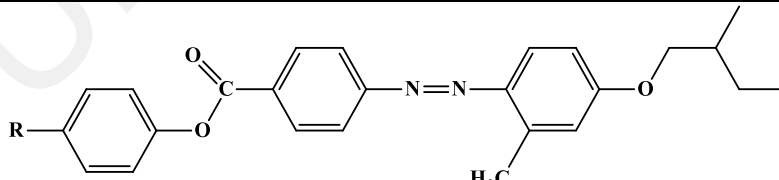
The corresponding fluorescence spectra were obtained using Photon Technology International EL-1000 spectrofluorometer. Samples were measured from 370 to 700 nm in a 1-cm path-length quartz cuvette at room temperature.

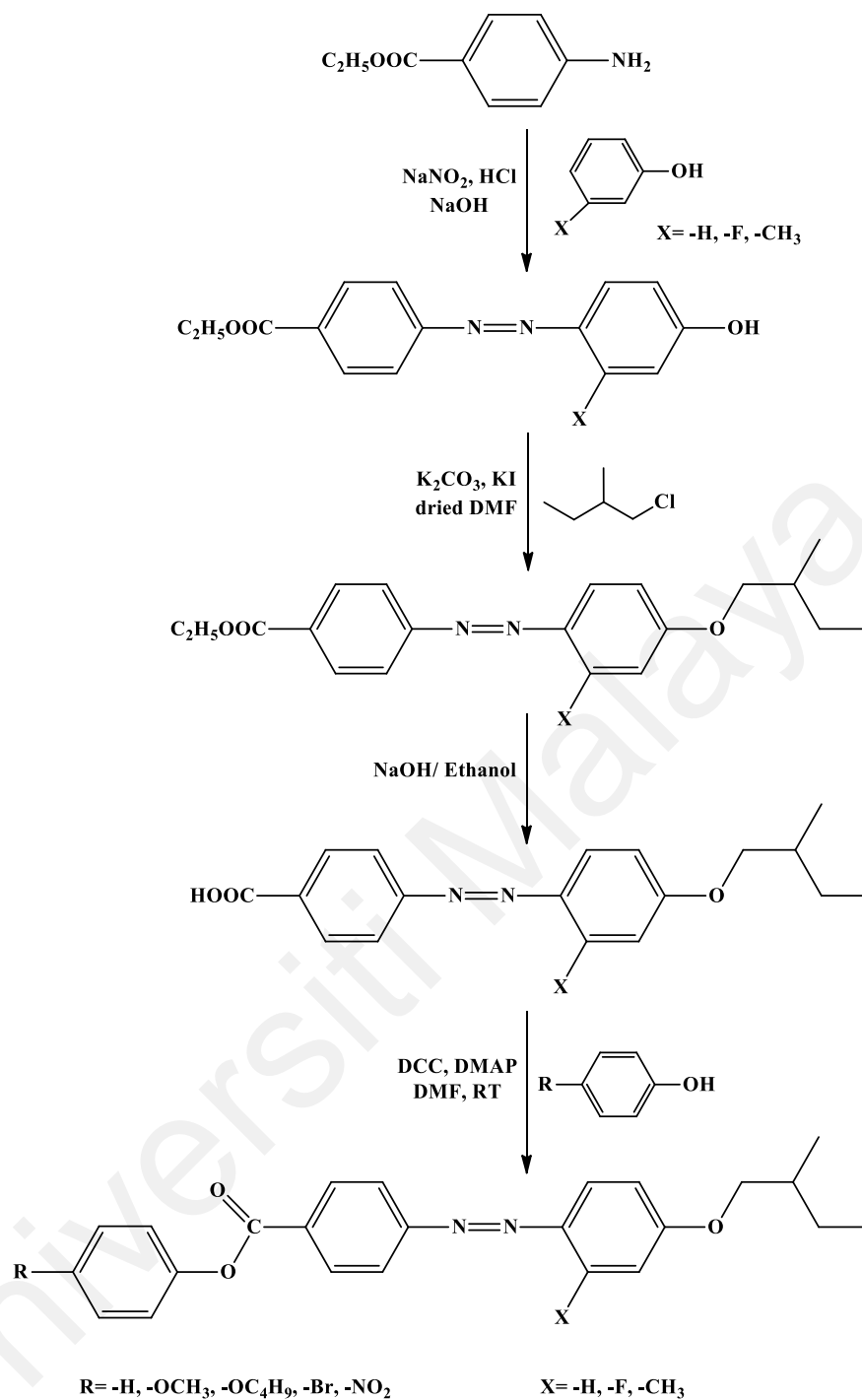
CHAPTER 4: RESULTS AND DISCUSSION

4.1 Synthesis

A series of two and three-benzene-ring molecular core of azo-ester compounds have been successfully synthesized. Table 4.1 shows the molecular structure and percentage yield of the synthesised compounds. All compounds required four steps from their common precursor, i.e. ethyl-4-aminobenzoate. These four steps are the diazotization, Williamson etherification, hydrolysis and esterification as shown in Scheme 4.1. The common structural feature of these azo-ester compounds is the 2-methylbutoxy terminal group on the phenylazo side with changes between lateral fluorine and methyl substituents at the 2-position of the azo-linkage and the unsubstituted lateral analogues. For the two-benzene-ring molecular core azo-esters, the second terminal group within each set of laterally-neat, laterally fluorinated and laterally methyl analogues bear octyl chain. On the other hand, for the three-benzene-ring molecular core azo-esters, the second terminal group at the phenyl ester ring had either electron-donating or electron-withdrawing groups within each lateral set.

Table 4.1: The molecular structure and percentage yield of two and three-benzene-ring molecular core of azo-ester compounds

Molecular Structure	Compound	Yield (%)
 <p>X= -H, (T1) X= -F, (T2) X= -CH₃, (T3)</p>	T1	70%
	T2	65%
	T3	75%
 <p>R= -H, (S1) R= -OCH₃, (S2) R= -OC₄H₉, (S3) R= -Br, (S4) R= -NO₂, (S5)</p>	S1	70%
	S2	50%
	S3	55%
	S4	70%
	S5	75%
 <p>R= -H, (C1) R= -OCH₃, (C2) R= -OC₄H₉, (C3) R= -Br, (C4) R= -NO₂, (C5)</p>	C1	65%
	C2	48%
	C3	50%
	C4	65%
	C5	70%
 <p>R= -H, (C6) R= -OCH₃, (C7) R= -OC₄H₉, (C8)</p>	C6	75%
	C7	55%
	C8	60%

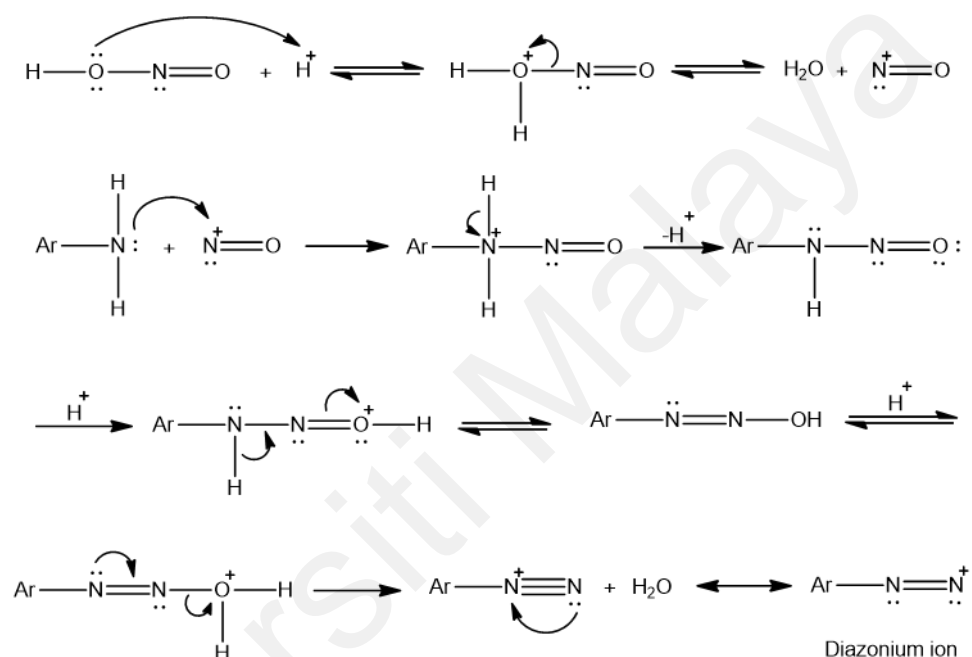


Scheme 4.1: Synthetic route of the three-benzene-ring azo-esters.

4.1.1 Diazotization Reaction

The diazotization reaction starts with the generation of a nitrosonium ion (NO^+) by the reaction of nitrous acid with the other acid. The nitrous acid was generated from sodium nitrate with mineral acid. Then, the nucleophilic addition reaction of the aromatic

ring attaches to the amine group with nitrosonium ion to form a new nitrogen-nitrogen bond. The nitrosamine is produced after the subsequent deprotonation and then converted into a diazohydroxide in the acid medium via protonation and subsequent deprotonation. This is followed by the removal of water from the diazohydroxide compound to give the diazonium ion as shown in Scheme 4.2, which can easily react with another aromatic ring (Heines, 1958).



Scheme 4.2: Reaction mechanism of diazotization reaction.

4.1.2 Williamson Etherification

Williamson etherification is an organic reaction developed by Alexander Williamson in 1850 (Williamson, 1850). The reaction involves an organohalide which reacts with deprotonated alcohol via an $\text{S}_{\text{N}}2$ bimolecular nucleophilic substitution mechanism forming an ether (Singh, 2004). Alkoxide ions are highly reactive and are mostly prepared in an in-situ reaction. Synthesis is typically achieved using a carbonate base or potassium hydroxide. A typical Williamson ether synthesis is generated at around

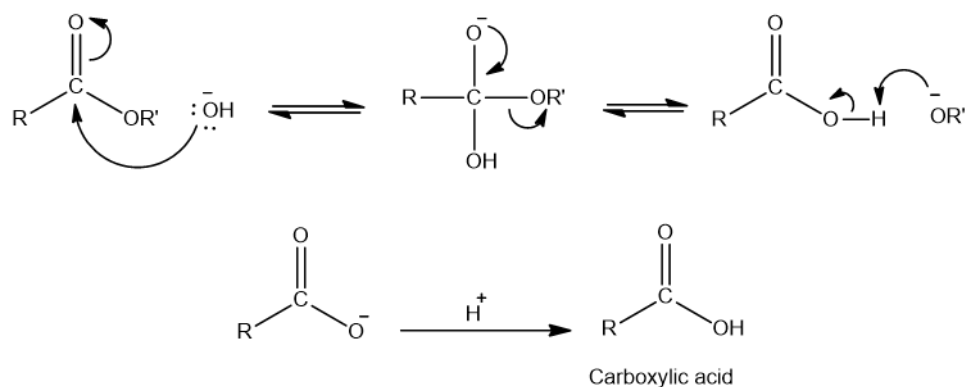
100 °C. The complete disappearance of the reactants is difficult to accomplish, and side reactions are common. A soluble iodide salt catalyst is used with the unreactive alkylating agent (e.g. alkyl chloride) to improve the rate of the reaction. Mechanistically, the formation of ether through Williamson etherification is shown in Scheme 4.3. In the reaction an alkoxide ion (nucleophile) attacks the electrophilic carbon of the alkyl halide (leaving group) to form an ether. The reaction conditions (temperature, reaction time and solvent) are strongly affecting the product yields. N,N-dimethylformamide solvent is normally used, because the protic solvents and a polar solvents tend to slow the reaction rate (Mosher, 1992).



Scheme 4.3: The general reaction mechanism of Williamson etherification.

4.1.3 Base Hydrolysis of Esters

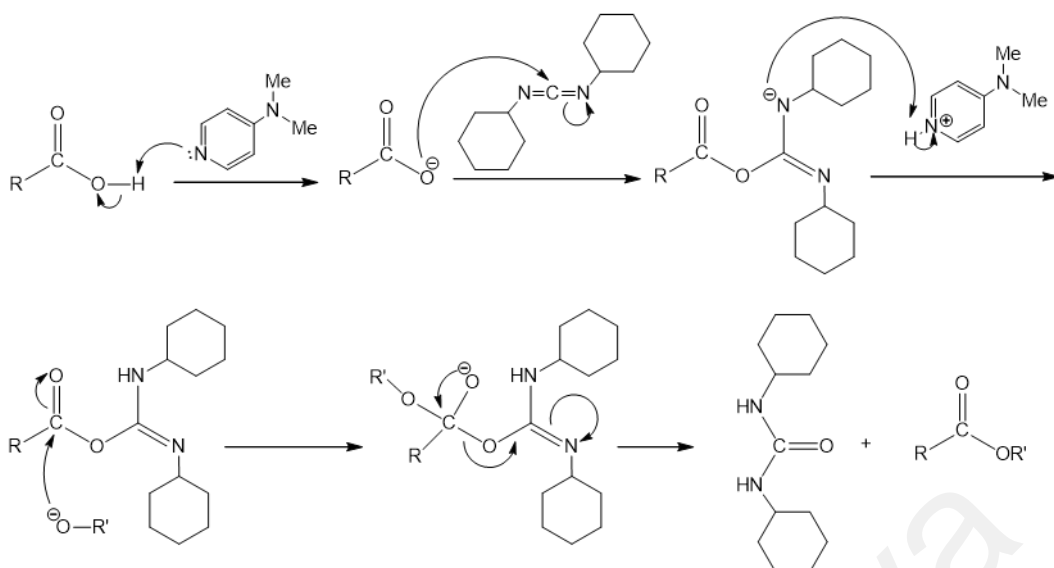
Esters are hydrolysed to give the corresponding carboxylic acid and an alcohol. Usually, aqueous acid (e.g. H₂SO₄/ heat), or aqueous base (e.g. NaOH/ heat) reagents are used in this reaction. Scheme 4.4 shows the nucleophile (-OH) attacks the electrophilic carbon of the carbonyl, breaking the π bond and generating the tetrahedral intermediate. Then, the C=O reforms and the alkoxide group leaves the molecules to form the carboxylic acid. At equilibrium, alkoxide functions as a base deprotonating the carboxylic acid, while acidification by an excess of a strong acid like dilute hydrochloric acid directs the reaction to the carboxylic acid forming (Stoker, 2015).



Scheme 4.4: Base hydrolysis of esters mechanism.

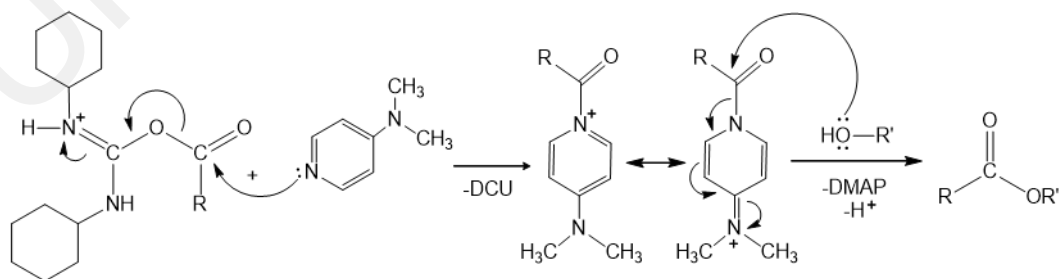
4.1.4 Steglich Esterification Reaction

The esterification reaction was first described by Wolfgang Steglich in 1978 (Neises & Steglich, 1978). The ester linkage in the formation of azo-ester mesogen has been generated by using *N,N'*-dicyclohexylcarbodiimide (DCC) as a coupling reagent and 4-dimethylaminopyridine (DMAP) as a catalyst in Steglich esterification reaction. The general esterification reaction mechanism is illustrated in Scheme 4.5. The reaction of the carboxylic acid with DCC forming the more reactive *O*-acylisourea intermediate than the free acid. After that, the phenol attacks the intermediate compound to form an ester and *N,N'*-dicyclohexylurea (DHU) by-product.



Scheme 4.5: Steglich esterification reaction mechanism.

However, the 1,3-rearrangement of the *O*-acyl intermediate forms a side-product of an *N*-acylurea, which reduces the final yield or complicates the purification of the product. This side-reaction is unable to further react with the alcohol. To inhibit this side reaction, DMAP is used to act as an acyl transfer reagent, as described in Scheme 4.6. The nucleophilic attack of the *O*-acylisourea by DMAP forms a reactive intermediate, that react rapidly with the phenol and produce the ester at around a 60% yield (Neises & Steglich, 1978).



Scheme 4.6: The use of DMAP in the esterification reaction.

4.2 Structural Determination

The structural determination of all the synthesized compounds were done by FTIR and NMR analysis. ^1H NMR, ^{13}C NMR and ^{19}F NMR were used to confirm the structure of synthesised azo esters.

4.2.1 FT-IR Spectra

The main vibrational band frequencies of all synthesized compounds are listed in Table 4.2. Generally, all the compounds exhibited similar FT-IR spectral behaviours with slightly shifted vibrational frequencies due to the influence of lateral and terminal substituents.

The FT-IR spectra of these azo-esters showed absorption bands between 2835 and 2965 cm^{-1} which were due to the asymmetric and symmetric C-H stretching vibrations of the methylene ($-\text{CH}_2-$) groups in the alkyl chain. The very sharp stretching peak between 1708 and 1739 cm^{-1} was assigned to the C=O stretching vibration of the ester group. The laterally neat and fluorinated analogues exhibited medium intensity bands between 1577 and 1615 cm^{-1} region due to the C=C stretching vibration of aromatic benzene groups. For the laterally methyl-substituted analogues, the characteristic peak of the C=C aromatic benzene groups vibration appeared in the 1590–1596 cm^{-1} region. Furthermore, all compounds exhibited the vibration bands within the 1454–1508 cm^{-1} region due to N=N stretching of azo group.

Table 4.2: FT-IR spectral data of the synthesized compounds

Compound	X	R	FT-IR (ν , cm^{-1})			
			-C-H	C=O	C=C	-N=N-
T1	H	-	2958, 2924, 2856	1708	1602, 1584	1500, 1469
T2	F	-	2958, 2926, 2856	1716	1611, 1585	1495, 1460
T3	CH ₃	-	2953, 2920, 2854	1716	1596	1489, 1454
S1	H	H	2962, 2933, 2875	1724	1599, 1581	1489, 1465
S2	H	OCH ₃	2962, 2924, 2875	1727	1599, 1582	1499, 1466
S3	H	OC ₄ H ₉	2960, 2932, 2872	1722	1599, 1580	1501, 1465
S4	H	Br	2963, 2927, 2874	1726	1598, 1580	1483, 1455
S5	H	NO ₂	2964, 2934, 2878	1733	1595, 1577	1501, 1463
C1	F	H	2962, 2933, 2875	1720	1612, 1584	1494, 1459
C2	F	OCH ₃	2965, 2939, 2835	1736	1615, 1586	1508, 1494
C3	F	OC ₄ H ₉	2960, 2932, 2873	1728	1614, 1600	1505, 1464
C4	F	Br	2961, 2927, 2874	1722	1610, 1583	1483, 1457
C5	F	NO ₂	2963, 2935, 2878	1739	1612, 1582	1493, 1456
C6	CH ₃	H	2961, 2929, 2874	1721	1590	1488, 1456
C7	CH ₃	OCH ₃	2961, 2933, 2875	1728	1592	1488, 1463
C8	CH ₃	OC ₄ H ₉	2962, 2939, 2873	1723	1594	1505, 1455

4.2.2 ¹H NMR Spectra

The chemical shifts of all the protons in the compounds are in agreement with their expected molecular structure. Figure 4.1 illustrates the ¹H NMR spectra for compound T1 with its molecular structure. The signals between δ 7.02-8.19 ppm are ascribed to the aromatic protons on the two phenyl rings connected by the azo groups. The most de-shielded doublet signal at δ 8.17-8.19 ppm represent the protons on the phenyl ring (9) due to its connecting to the ester withdrawing group. The signal at δ 7.90-

7.96 ppm is due to the protons (7 and 8) on the phenyl ring linked by the azo group. The doublet protons (6) at 7.02-7.04 ppm are attributed to the butoxy groups attached to the phenyl ring. The signal of protons (10 and 5) on the carbon attached to the single-bonded oxygen ($-\text{OCH}_2-$) assigned at 4.33-4.37 ppm and 3.82-3.94 ppm, respectively, are due to the influence of the high electronegativity of the oxygen atom. The signals in the range of 1.96 to 0.88 ppm involved aliphatic protons of the terminal alkyl chains. On the other hand, ^1H NMR of compounds **T2** and **T3** showed similar spectral data as **T1** with slightly shifted chemical shifts, due to the presence of lateral fluorine and methyl substituents at the 2-position of the azo linkage.

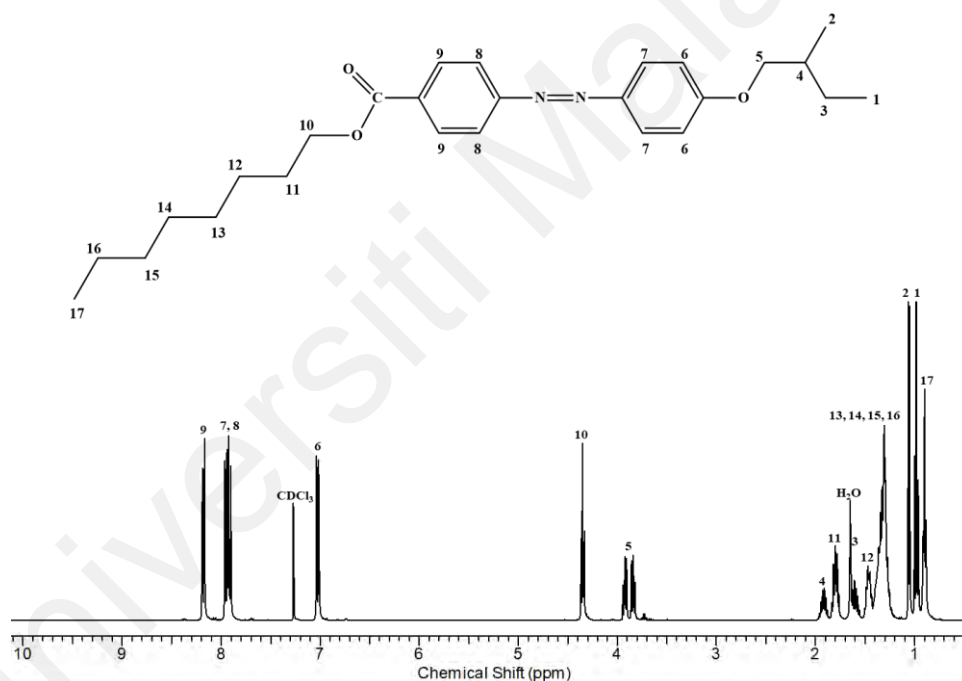


Figure 4.1: ^1H NMR spectrum of T1.

The ^1H NMR spectrum of compound **S1** with its molecular structure is showed in Figure 4.2. The signals appearing at δ 6.94-8.27 ppm are due to the aromatic protons of three-benzene-ring linked by azo and ester groups. The most de-shielded doublet signal at δ 8.25-8.27 ppm is attributed to the protons (9) connecting to the ester group. The

signals at δ 7.88-7.90 ppm are due to the protons (7 and 8) on phenyl ring linked by azo group. The two triplet signals appearing at δ 7.19-7.39 ppm and doublet signal at δ 7.18 ppm are attributed to (10, 11 and 12) protons on the terminal phenyl ring. The doublet protons (6) appearing at 6.94-6.96 ppm are due to the presence of butoxy group attached to the phenyl ring. Aromatic protons signals are de-shielded due to the large anisotropic field of the aromatic rings created by the circulation of π electrons. The signal of the protons on the carbon attached to the single-bonded oxygen ($-\text{OCH}_2-$) appeared at 3.74-3.86 ppm (5). The signals in the range of 0.88 to 1.86 ppm were assigned to the aliphatic protons (1, 2, 3 and 4). The two signals of protons (3) are formed due to the independent coupling of *S* and *R* configuration of proton (4) on the chiral centre where each proton splits the peak into a separate signal. Independent coupling occurs when protons are not rotated freely, as in the case of the presence of chiral centre (Anderson et al., 2004).

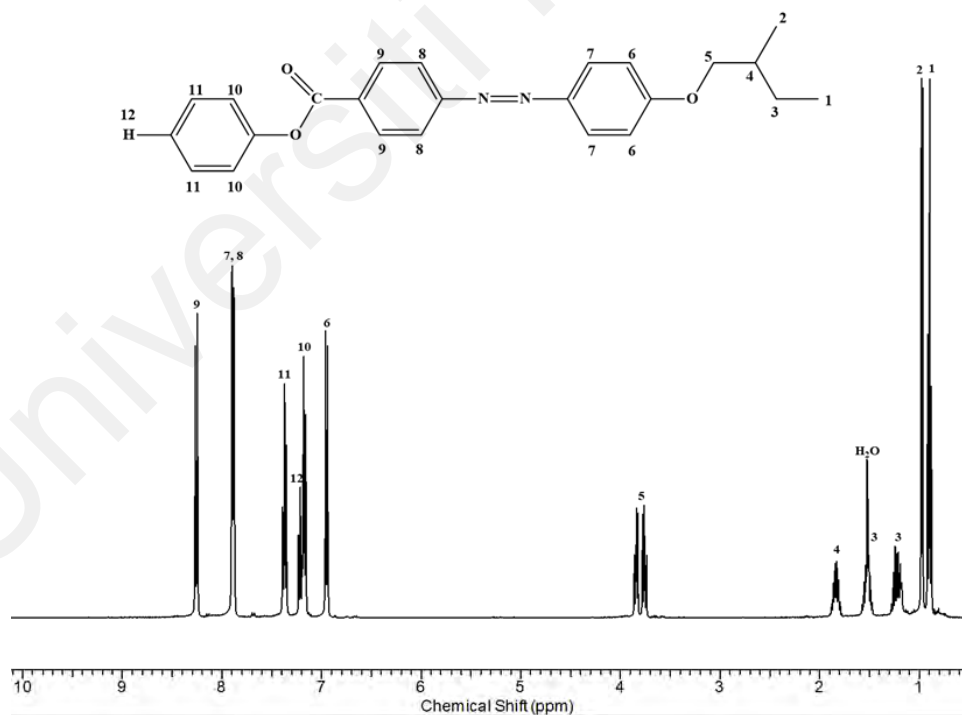


Figure 4.2: ^1H NMR spectrum of S1.

Figure 4.3 shows the ^1H NMR spectrum of compound **S2** with its molecular structure. The doublet signals appeared at most de-shielded signals at δ 8.34, δ 7.96 and δ 6.96-7.16 ppm are due to the aromatic protons on phenyl rings linked by an azo and ester groups. The protons on the carbon attached to the single-bonded oxygen (5) appeared at 3.95 ppm due to the influence of the high electronegativity of the oxygen atom. The intense signal of the terminal methoxy group attached to the phenyl ring resonate at 3.83 ppm. The signals in the range of 0.97 to 1.95 ppm are attributed to the aliphatic protons (1, 2, 3 and 4).

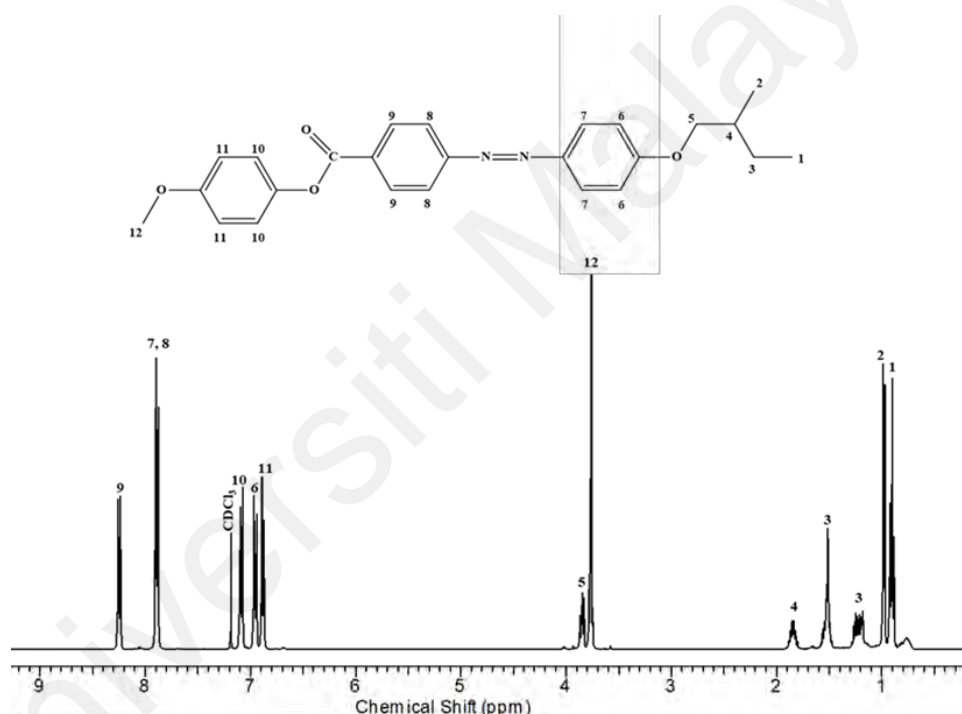


Figure 4.3: ^1H NMR spectrum of S2.

The ^1H NMR spectrum of compound **S3** with its molecular structure is illustrated in Figure 4.4. The most de-shielded doublet signal at δ 8.32-8.35 ppm is due to the aromatic protons (9) on phenyl ring linked to ester group, while the adjacent aromatic protons (7 and 8) on phenyl ring linked to azo group appeared at δ 7.97-7.99 ppm. The other aromatic protons (6, 10 and 11) are located at 6.97 to 7.17 ppm due to anisotropic

field of π electrons in the phenyl rings and the electron-donating effect of oxygen atom (Pavia et al., 2014). The methylene protons' signals (5 and 12) on the carbon attached to single-bonded oxygen ($-\text{OCH}_2-$) appeared at δ 3.83- 3.95 ppm. The signals that appeared at δ 1.36 to 1.96 ppm are attributed to CH and CH_2 aliphatic protons of the butoxy terminal group, whereas the signals of three CH_3 methyl protons terminal groups (1, 2 and 15) shifted to upfield δ 0.98 to 1.08 ppm.

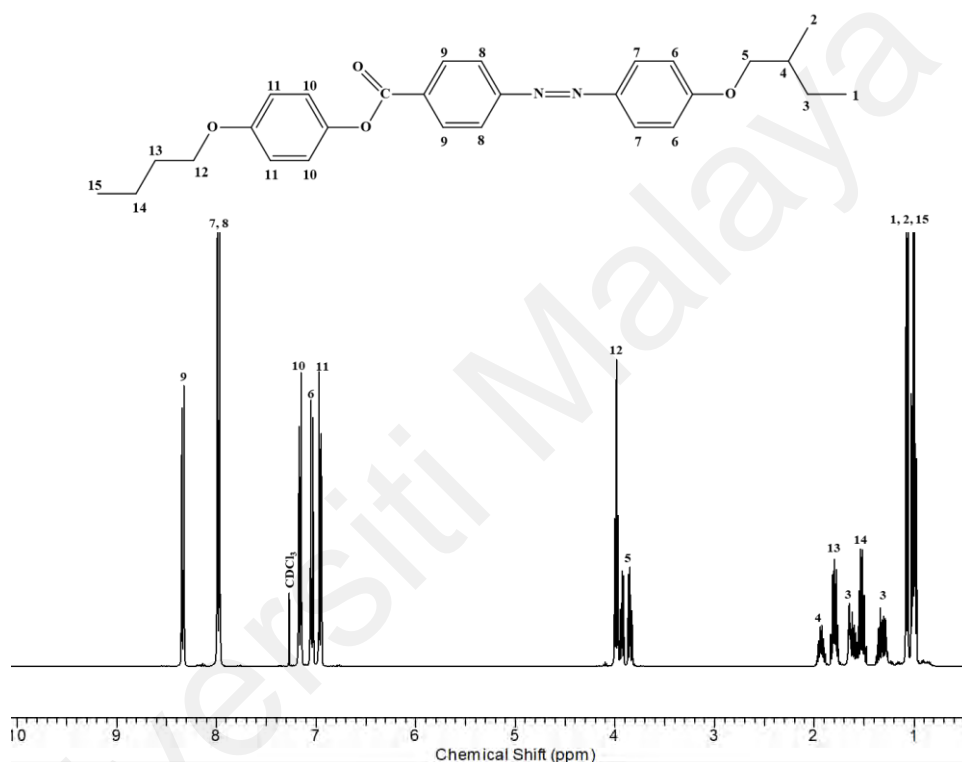


Figure 4.4: ^1H NMR spectrum of **S3**.

Figure 4.5 and Figure 4.6 illustrate the ^1H NMR spectrum of compounds **S4** and **S5** with their molecular structure, respectively. The signals of aliphatic and aromatic protons of compounds **S4** and **S5** appeared at similar chemical shifts of compounds **S1**, **S2** and **S3** due to their structural similarity. However, the aromatic protons (11) are shifted to a lower the chemical shift in the terminal bromo and nitro substituent (**S4** and **S5**), due to its electron-withdrawing effect.

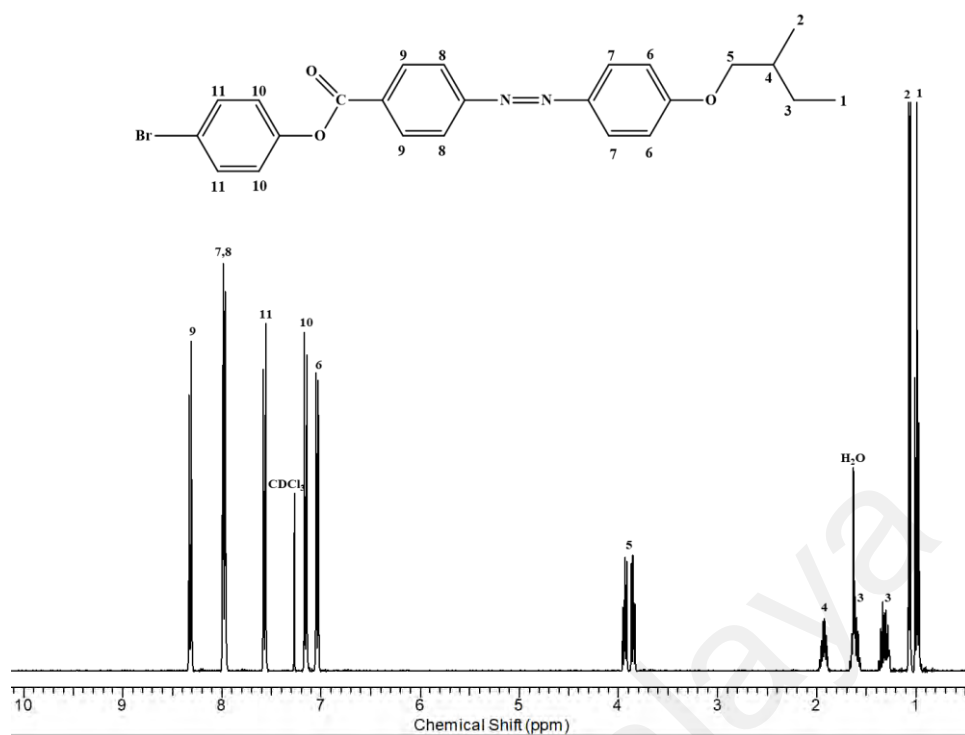


Figure 4.5: ¹H NMR spectrum of S4.

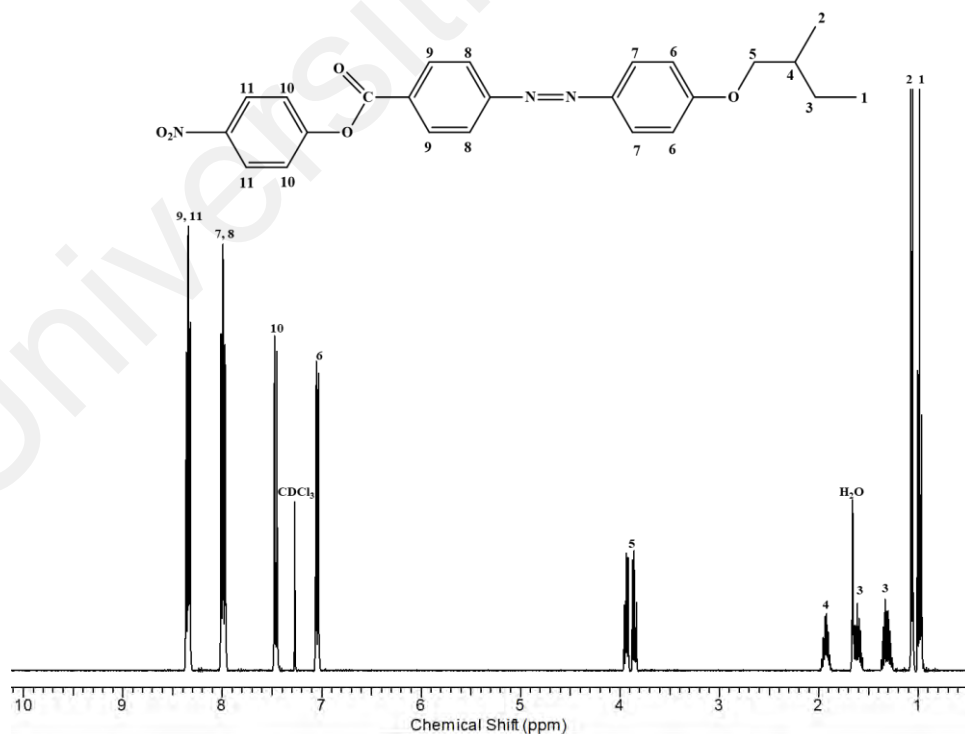


Figure 4.6: ¹H NMR spectrum of S5.

As the compounds **C1** to **C5** bear structural similarities of **S1** to **S5** except for the lateral fluorine group in the mesogen, they showed similar ^1H NMR spectral properties. Figure 4.7 shows the ^1H NMR spectrum of compound **C1** with its molecular structure. All protons signal appeared almost in the same chemical shift of **S1** except the aromatic protons on the phenyl ring with lateral fluorine derivatives. The triplet signal of the aromatic proton (7) on the carbon linked to the azo moiety appeared at δ 7.77-7.82 ppm region. The aromatic protons (6 and 8) shifted to lower chemical shifts 6.72-6.76 ppm due to the fluorine atom effect (Pavia et al., 2014).

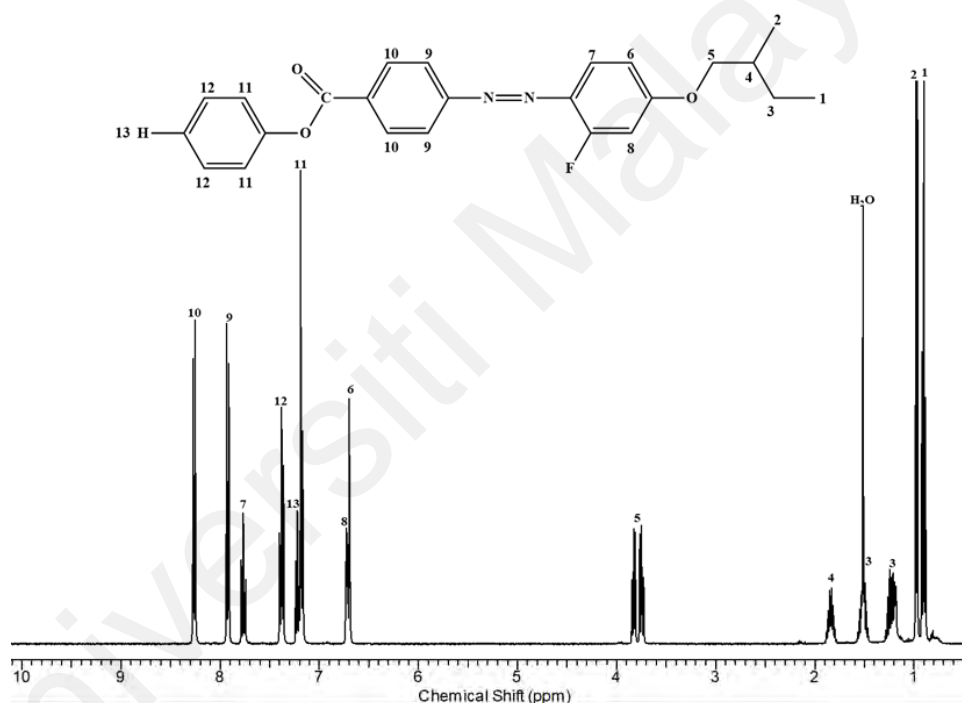


Figure 4.7: ^1H NMR spectrum of **C1**.

As the compounds **C6**, **C7** and **C8** have structural similarities of **S1**, **S2** and **S3** except for the lateral methyl group in the mesogen, they showed similar ^1H NMR spectral properties. Figure 4.8 shows the ^1H NMR spectrum of compound **C6** with its molecular structure. All protons signal of **C6** almost appeared in the same chemical shift of **S1** except for the aromatic protons on the laterally methyl-substituted phenyl ring. The

intense singlet signal at δ 2.68 ppm is due to the methyl protons (9) bonded to the phenyl ring. The doublet signal of the aromatic proton (7) on the carbon linked to the azo moiety shifted to δ 7.70-7.72 ppm, due to the electron-donating effect of methyl group. Furthermore, the aromatic protons (6 and 8) shifted to lower chemical shifts at 6.72- 6.79 ppm region.

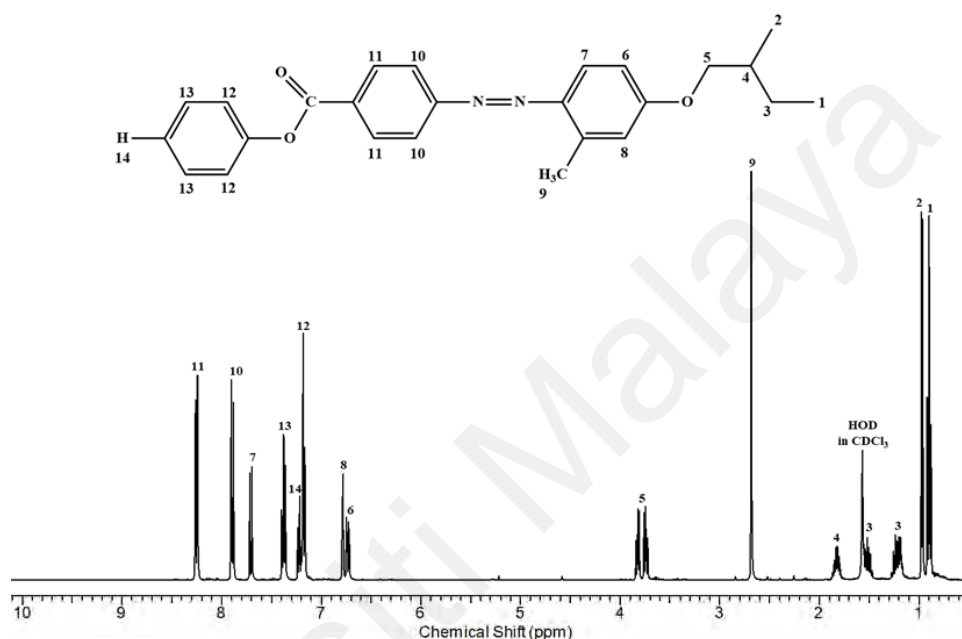


Figure 4.8: ^1H NMR spectrum of C6.

4.2.3 ^{13}C NMR Spectra

The chemical shifts of all the carbons in the compounds are in agreement with their expected molecular structure. The proton decoupled ^{13}C NMR spectrum of compound T1 is presented in Figure 4.9 together with its molecular structure. The signal of the carbonyl carbon (14) resonates at the most downfield region at 166.3 ppm. The sp^2 hybridization effect of the double bond and the electronegative oxygen directly attached to the carbonyl carbon de-shielding the signal to the highest chemical shifts (Pavia et al., 2014). The signals assigned at the high frequency region between 114.8 and 162.5 ppm are due to the two-phenyl-ring carbons. The signals of the carbon on an alkyl chain

attached to an oxygen atom (5 and 15) are appeared at 73.2 and 65.4 ppm, respectively. These carbons were shifted to a relatively high chemical shift due to the electron-withdrawing effect of the oxygen atom as well as the diamagnetic anisotropy effect of the aromatic ring (Pavia et al., 2014). The signals appeared at a low frequency between 11.3-34.7 ppm are ascribed to the aliphatic carbon atoms attached to the alkyl chain. However, due to the differences in lateral substituent at the 2-position to the phenyl azo ring, similar spectral behaviours were observed for compounds **T2** and **T3**, with slight shifting on the chemical shift.

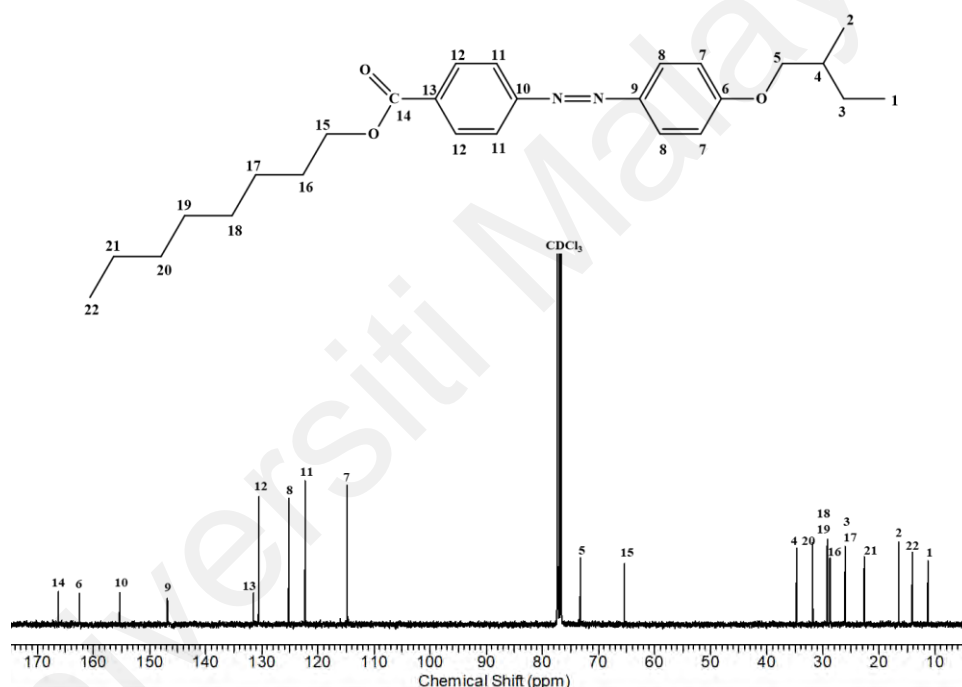


Figure 4.9: ^{13}C NMR spectrum of **T1**.

Figure 4.10 illustrates the ^{13}C NMR spectrum of compound **S1** together with its molecular structure. The signal of the carbonyl carbon (14) resonates at the most downfield region at 164.8 ppm. The aromatic carbons signals were assigned at the low field region between 114.9-162.7 ppm due to the sp^2 hybridization and diamagnetic anisotropy. The signal at 73.3 ppm is assigned to carbon (5), which is carbon on an alkyl

chain attached to an oxygen atom. The signals appeared upfield between 11.3-34.7 ppm attributable to the carbon atoms attached to the alkyl chain. The strongest intensity signals of alkyl chain carbons are attributed to the interaction of spin-spin dipoles that operate through space (NOE effect) (Pavia et al., 2014).

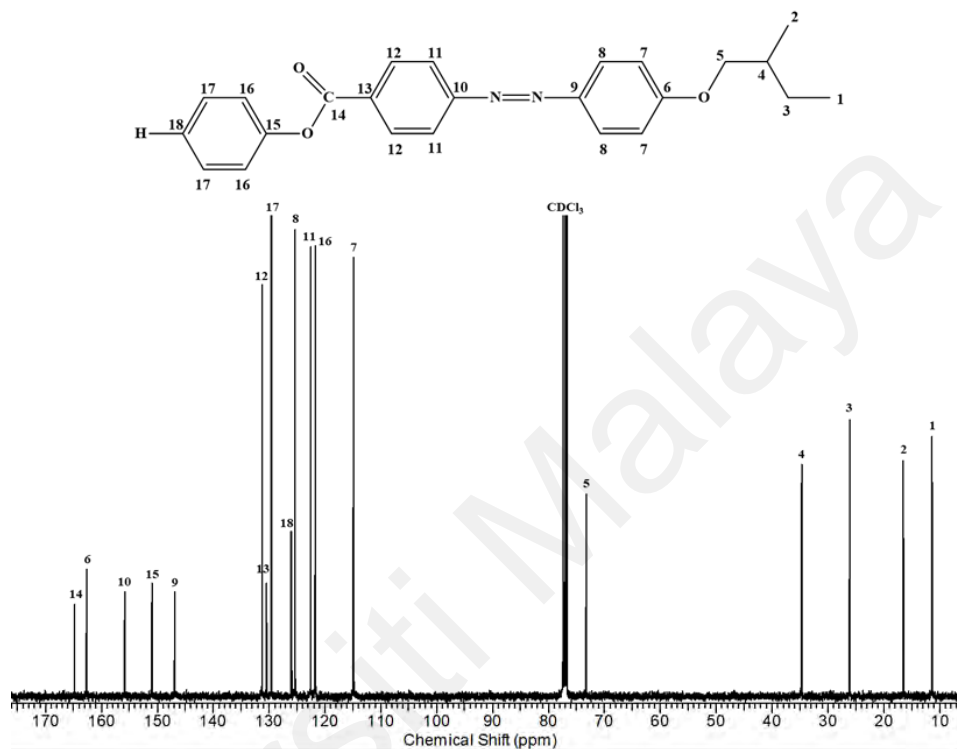


Figure 4.10: ¹³C NMR spectrum of S1.

Figure 4.11 illustrates the ¹³C NMR and DEPT-135 NMR spectra of compound S2 together with its molecular structure. The most downfield region signals in ¹³C NMR are attributed to quaternary carbons and carbonyl group, which do not appear in the DEPT NMR spectrum. The signals that appeared at the region 114.6 to 131.2 ppm are attributed to aromatic carbons. The sp² hybridization and diamagnetic anisotropy of the phenyl rings shifted the aromatic carbons to the downfield region. The aromatic carbons and carbonyl carbon (14) have low intensity signals compared to the other aromatic carbons due to the substituent attached directly to these carbons (*ipso* carbons). Furthermore, long relaxation time and the effect of weak nuclear overhauser enhancement make these carbons' signals

very weak. The signal at 73.3 ppm is assigned for carbon (5) attached to an oxygen atom attached to the aromatic ring. The signals located at the most upfield chemical shift are the more shielded carbon atoms. Therefore, the carbon atoms that are attached to the alkyl groups (4 and 3) resonated at 26.2-34.7 ppm. The methyl carbons (2 and 1) appeared at 16.6 and 11.4 ppm, respectively, whereas the methoxy carbon (19) resonated at 55.7 ppm. The methyl group's carbons were observed at a high field compared to methoxy carbon due to the high electronegative of the oxygen atom that attracts a bonding pair of the carbon electrons. On DEPT-135 NMR spectra, the signals of the methylene CH₂ carbon (3 and 5) appeared on the opposite side of the other carbons signal, which proves the ¹³C NMR signals analysis.

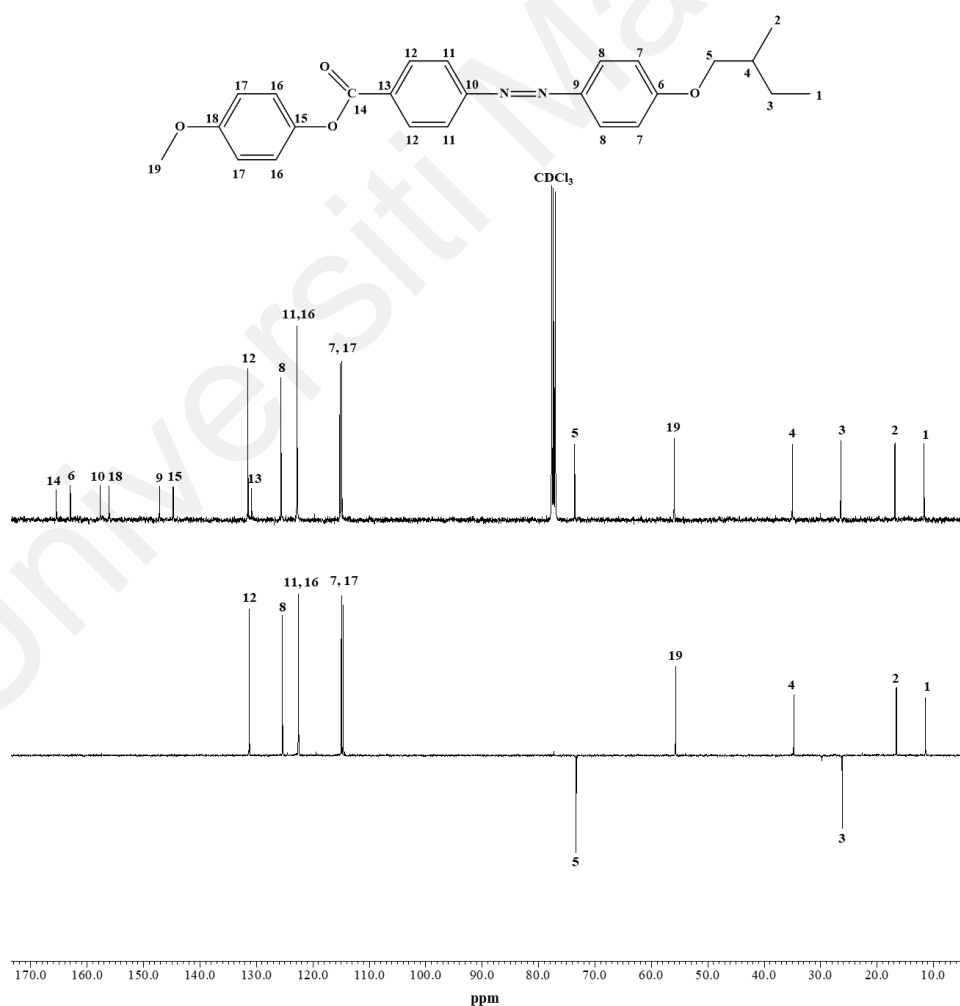


Figure 4.11: ¹³C NMR and DEPT-135 NMR spectra of S2.

The ^{13}C NMR and APT NMR spectra of compound **S3** are presented in Figure 4.12. The APT NMR experiments used to aid elucidating structures with ^{13}C NMR spectra. All signals of compound **S3** are similar to compound **S2** signals due to the structural similarities except for the terminal butoxy chain. The signal at 68.2 ppm is assigned to carbon on the alkyl chain (19), which is attached to oxygen. The other signals at 31.4, 19.3, 13.9 ppm are attributed to methylene carbons (20 and 21) and methyl terminal carbon atoms (22) on the butoxy chain, respectively. Additionally, compounds **S4** and **S5** exhibited similar spectra with the other lateral unsubstituted derivatives **S1**, **S2** and **S3** with shifting of aromatic carbons adjacent to the terminal bromo and nitro electron-withdrawing groups.



Figure 4.12: ^{13}C NMR and APT NMR spectrum of **S3**.

Compounds **C1-C8** are structurally similar to **S1-S5** derivatives except for the lateral group on the rigid mesogen. The ^{13}C NMR spectrum for **C1** is shown in Figure 4.13. The signals that appeared at 118.6, 111.6 and 102.5 ppm are assigned for carbons (8, 7 and 10), while carbons (6 and 9) appeared at 164.1 and 134.9 ppm, respectively. The carbon (11) attached to the fluorine atom is appeared as doublet peaks at 164.0- 163.4 ppm. This pattern appeared because ^{13}C spectra are normally acquired decoupled from ^1H , so they appear as singlets, while the same pulse sequence does not decouple ^{19}F . This carbon shifted to down field as compared with compound **S1** due to the high electronegativity effect of fluorine atom. However, the other signals of the compound were observed in the relatively same chemical shift of compound **S1**.

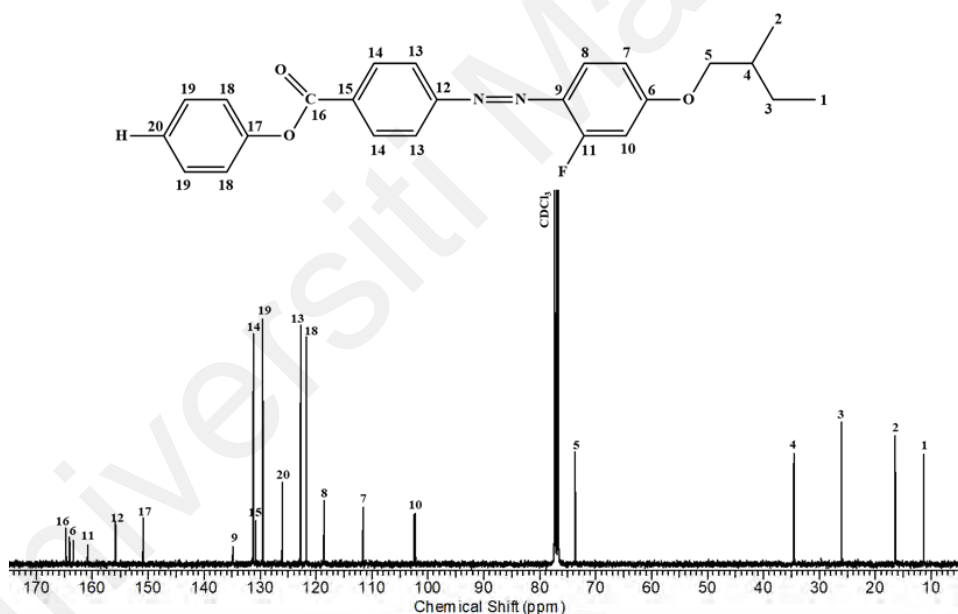


Figure 4.13: ^{13}C NMR spectrum of **C1**.

Figure 4.14 shows ^{13}C NMR spectrum for compound **C6** together with its molecular structure. The methyl carbon (11) substituted laterally on mesogen is assigned at 17.9 ppm. The signals that appeared at 115.9 and 113.1 ppm are due to the aromatic carbon (9 and 7), respectively. The carbons (6 and 12) showed signals at 162.7 and 144.9

ppm chemical shifts. Carbon (8 and 10) give signals at 117.2, 142.1 ppm due to the electron-donating methyl group effect, which shifted the signal to a lower chemical shift compared to S1 and C1, respectively.

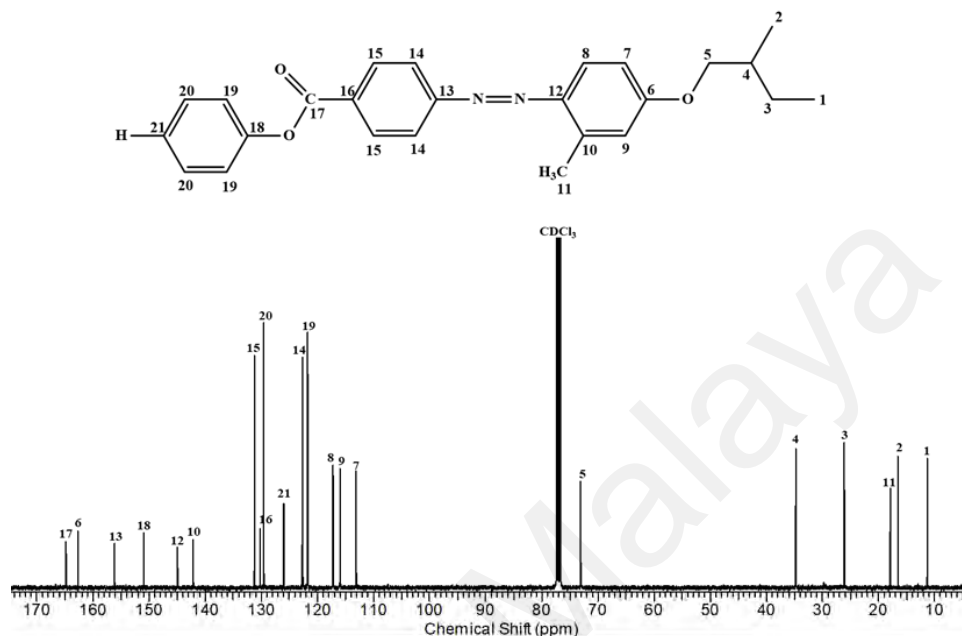


Figure 4.14: ^{13}C NMR spectrum of C6.

4.3 Physico-Chemical Characterization

4.3.1 Thermal Stability

The thermal stability of all azo-ester compounds have been investigated by TGA within a temperature range of 50–900°C under nitrogen atmosphere. Table 4.3 summarizes the TGA data of all compounds which includes the temperature at 5% of weight loss ($T_d, 5\%$) and the temperature of maximum decomposition rate (T_{max}). Taking $T_d, 5\%$ as criteria for stability, the $T_d, 5\%$ value for the two-benzene-ring compounds were shown to be in the range 267–341 °C, while the three-benzene-ring compounds were shown to be above 315 °C, which indicating that the thermal stability of the synthesized compounds is relatively high. All azo-ester compounds of either two or three-phenyl-ring exhibited a single-stage thermal decomposition as shown in Figure 4.15 as examples.

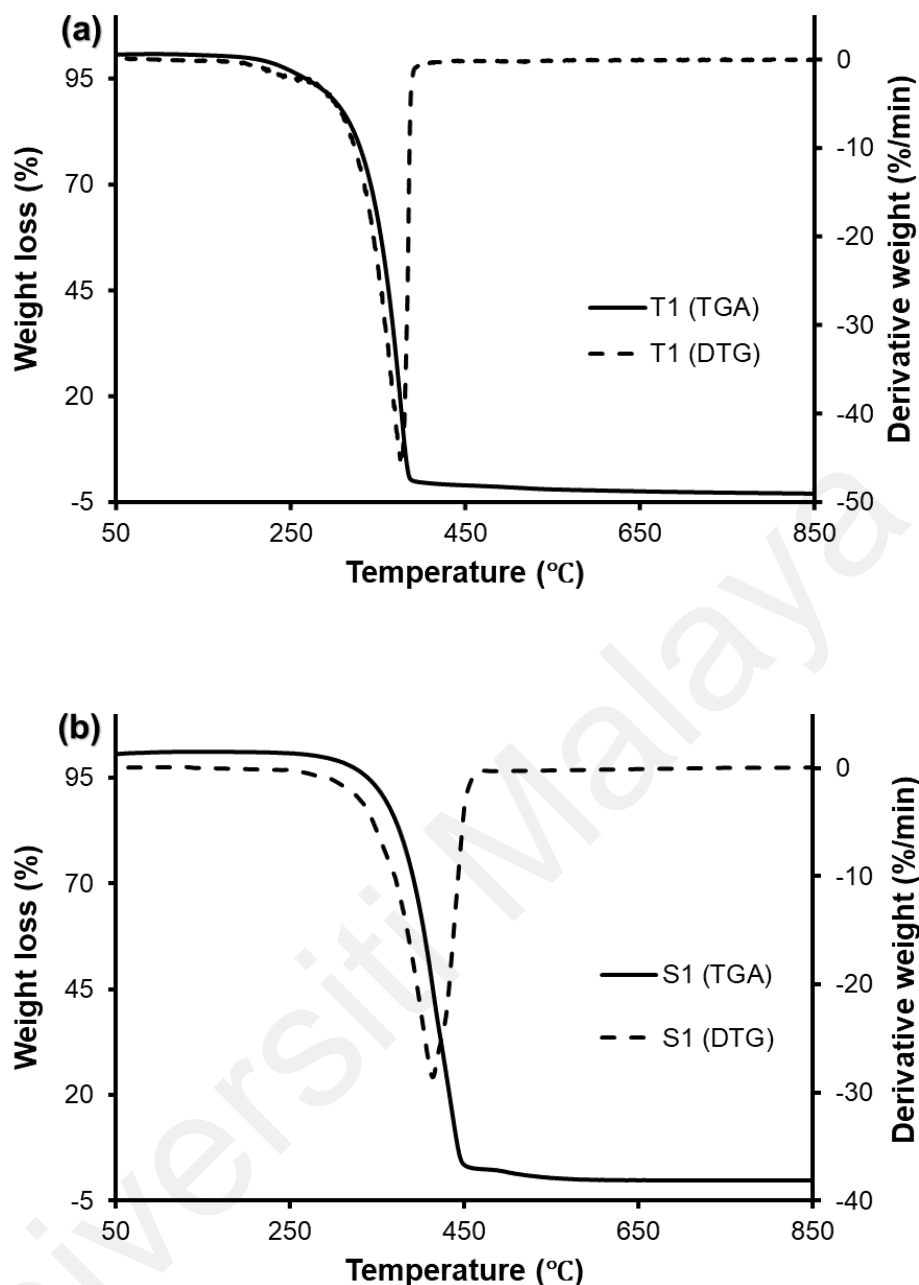


Figure 4.15: TGA curve and its corresponding derivative (DTG) of (a) T1 and (b) S1 at heating rate of $20^{\circ}\text{C min}^{-1}$ under nitrogen atmosphere.

From Table 4.3, the laterally unsubstituted two-phenyl-ring derivative **T1** showed the highest weight loss of 99% within a temperature range 260–440°C ($T_{\text{max}} = 375^{\circ}\text{C}$). A weight loss of $\sim 80\%$ for laterally fluorine and methyl derivatives (**T2** and **T3**) occurred around 275–470°C with T_{max} 384°C and 380°C, respectively.

For the three-phenyl-ring, the unsubstituted derivative **S1** gave a weight loss of 97% between 270–450°C ($T_{\max} = 413^{\circ}\text{C}$), with the remaining residue completely decomposed around 500°C. With the presence of alkoxy substituent on the second terminal group i.e. $-\text{OCH}_3$ and $-\text{OC}_4\text{H}_9$ for **S2** and **S3**, respectively, a weight loss of 75% was observed between 260–456°C ($T_{\max} \sim 435^{\circ}\text{C}$) for both compounds. As for the laterally fluoro-substituted derivatives, the unsubstituted terminal analogue **C1** showed a weight loss of 72% within a temperature range of 260–460°C ($T_{\max} = 450^{\circ}\text{C}$). In the terminally methoxy- (**C2**) and butoxy-substituted (**C3**) derivatives a weight loss of 65 and 62%, respectively, were observed around 260–450°C with $T_{\max} \sim 420^{\circ}\text{C}$ for both compounds. For the electron-withdrawing groups i.e. bromo- and nitro-substituted derivatives, the laterally unsubstituted compounds **S4** and **S5** exhibited a weight loss of 70% ($T_{\max} = 400^{\circ}\text{C}$) and 75% ($T_{\max} = 370^{\circ}\text{C}$), respectively, with the remaining weight completely lost around 800°C. A weight loss of 67% ($T_{\max} = 390^{\circ}\text{C}$) and 72% ($T_{\max} = 370^{\circ}\text{C}$) occurred in the temperature range of 260–440°C for the laterally fluorinated compounds **C4** and **C5**, respectively. As for the laterally methyl-substituted compounds **C6**, **C7** and **C8**, a rapid weight loss of 61–68% occurred around 260–450°C with T_{\max} at 412, 424 and 413°C, respectively.

The rapid weight loss within the mentioned temperature range for all compounds may be attributed to the thermal cleavage of the azo group (Rameshbabu & Kannan, 2004; Zhao et al., 2017) and the aliphatic chains (Lam et al., 2000). Subsequently, the remaining weight loss took place gradually until 900°C, due to the thermal cleavage of aromatic moiety, including those containing lateral fluorine or lateral methyl substituents as well as degradation of the carbonyl group (Amer et al., 2013; Dzulkharnien et al., 2017; Karim et al., 2014).

Table 4.3: TGA data of all azo-esters

Compound	X	R	T _{d,5%} (°C)	Decomposition stage		Char yield at 850°C (%)
				T _{max} (°C)	Weight loss (%)	
T1	H	-	267	375	99	0
T2	F	-	287	384	81	8
T3	CH ₃	-	341	380	85	7
S1	H	H	338	413	97	0
S2	H	OCH ₃	351	437	75	4
S3	H	OC ₄ H ₉	373	435	75	5
S4	H	Br	315	400	70	0
S5	H	NO ₂	331	370	75	0
C1	F	H	374	450	72	7
C2	F	OCH ₃	361	421	65	2
C3	F	OC ₄ H ₉	381	420	62	13
C4	F	Br	319	390	67	5
C5	F	NO ₂	328	370	72	20
C6	CH ₃	H	345	412	63	3
C7	CH ₃	OCH ₃	377	424	61	8
C8	CH ₃	OC ₄ H ₉	349	413	68	2

Table 4.3 shows that at 850°C, the decomposition processes were completed for laterally unsubstituted either two or three-phenyl-ring compounds **T1**, **S1**, **S4** and **S5** but not for the other derivatives. The remaining residues for **S2** and **S3** are 4 and 5%, respectively, and for those laterally fluorinated compounds **T2** and **C1-C5** are in range of 2 to 20%, respectively. The remaining residues for laterally methyl compounds **T3**, **C6**, **C7** and **C8** were reported to be 7, 3, 8, 2%, respectively. These results indicate good thermal stability for the synthesized compounds above the isotropic temperatures (Naoum et al., 2015a).

4.3.2 Mesomorphic Behaviour

The thermal and mesomorphic properties were investigated by DSC, POM and SWAXS. Table 4.4 shows the phase transition temperatures and enthalpy changes for the two and three-phenyl-ring compounds. Their mesomorphic properties were determined from the second heating and cooling cycles to avoid the thermal history of compounds.

Figure 4.16 shows the DSC thermograms during the second heating scan of the two-phenyl-ring compounds **T1**, **T2** and **T3** at scanning rate of $10\text{ }^{\circ}\text{C min}^{-1}$. The compounds exhibited one endothermal transition peak, which is ascribed to the melting phase transition from solid to liquid, without a trace of phase transition into liquid crystalline phase. Except for compound **T1**, compound **T2** and **T3** did not showed any transition peak on cooling scan due to slow crystalline formation. The presence of only two benzene rings did not provide sufficient rigidity to compensate the flexible octyl chain, consequently preventing the formation of the mesophase in the two-benzene ring azo-esters. On the other hand, the presence of lateral fluorine and methyl groups in compounds **T2** and **T3** widen the molecular core and further reduces the molecular length-to-width ratio, leading to decrease in the melting temperature to $42\text{ }^{\circ}\text{C}$ and $39\text{ }^{\circ}\text{C}$, respectively compared with that of the laterally unsubstituted derivative **T1** (Ha et al., 2009; Ha et al., 2010).

Table 4.4: Phase transition temperatures and enthalpy changes of the synthesized compounds upon the second heating and cooling runs at a scan rate of 10 °C min⁻¹ by DSC

Compound	X	R	Scan	Phase transitions temperature (°C) [Enthalpy changes (kJ mol ⁻¹)]	
				Heating	Cooling
T1	H	-	Heating Cooling	Cr 62 [30.7] I I 45 [29.6] Cr	
T2	F	-	Heating Cooling	Cr 42 [11.3] I n.d.	
T3	CH ₃	-	Heating Cooling	Cr 39 [3.5] I n.d.	
S1	H	H	Heating Cooling	Cr 128 [29.7] I I 119[-31.1] Cr	
S2	H	OCH ₃	Heating Cooling	Cr 124 [35.5] N 206 [0.8] I I 205 [-0.9] N 93 [-32.3] Cr	
S3	H	OC ₄ H ₉	Heating Cooling	Cr 135 [36.9] N 207 [1.5] I I 205 [-1.4] N 110 [-35.4] Cr	
S4	H	Br	Heating Cooling	Cr 148 [29.0] N _x 202 [2.7] N 211 [0.5] I I 210 [-0.6] N 200 [-2.7] N _x 129 [-28.0] Cr	
S5	H	NO ₂	Heating Cooling	Cr 168 [31.5] N 238 [0.3] I I 236 [-0.6] N 146 [-30.5] Cr	
C1	F	H	Heating Cooling	Cr 104.1 [25.8] I I 78.3 [-26.9] Cr	
C2	F	OCH ₃	Heating Cooling	Cr 95 [30.3] N 190 [1.0] I I 189 [-1.0] N 30 [-17.2] Cr	
C3	F	OC ₄ H ₉	Heating Cooling	Cr 117 [37.7] N 184 [1.2] I I 182 [-1.4] N 73 [-32.4] Cr	
C4	F	Br	Heating Cooling	Cr 115 [33.0] N 175 [0.4] I I 174 [-0.4] N 112 [-0.2] N _x 83 [-31.8] Cr	
C5	F	NO ₂	Heating Cooling	Cr 164 [31.1] N 215 [0.3] I I 213 [-0.4] N 146 [-32.1] Cr	
C6	CH ₃	H	Heating Cooling	Cr 105 [33.7] I I 72 [-29.3] Cr	
C7	CH ₃	OCH ₃	Heating Cooling	Cr 105 [36.2] N 160 [0.6] I I 159 [-0.8] N	
C8	CH ₃	OC ₄ H ₉	Heating Cooling	Cr 107 [26.5] N 160 [1.0] I I 159 [-0.9] N 49 [-22.6] Cr	

Abbreviations: Cr = crystalline phase; N_x = nematic X phase; N = nematic phase; I = isotropic phase, n.d. (not detected).

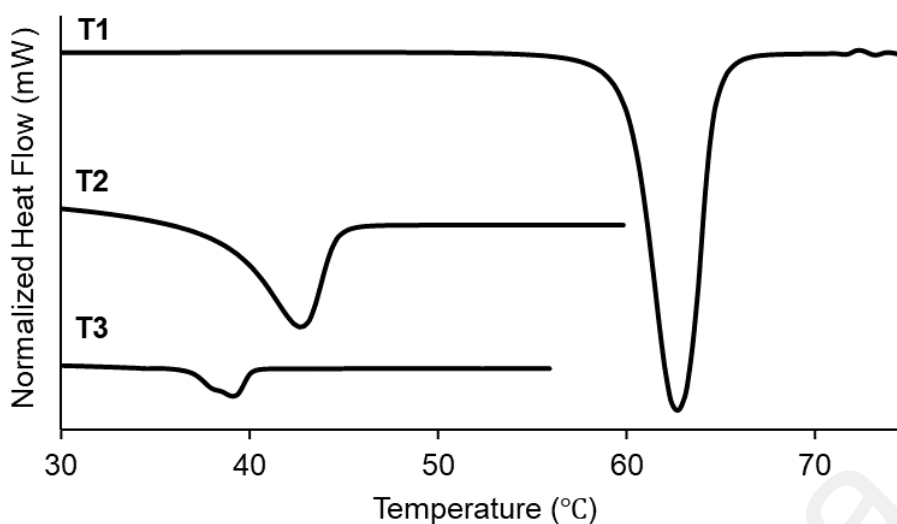


Figure 4.16: DSC thermograms at the scanning rate of $10^{\circ}\text{C min}^{-1}$ of compounds T1, T2 and T3 upon heating.

Figure 4.17 shows the DSC thermograms during the second heating and cooling cycles of compound S1, S2 and S3 at a scanning rate of $10^{\circ}\text{C min}^{-1}$. From the thermogram, compound S1 does not possess liquid crystalline properties. The absence of liquid crystalline behaviour may be attributed to the absence of substituted lateral and terminal groups that diminishes the mesomorphic properties in compound S1 (Ha et al., 2009; Ha et al., 2010). The replacement of terminal hydrogen by the electron-donating methoxy and butoxy groups significantly increases the molecular length-to-width ratio to give mesomorphic behavior in S2 and S3, respectively (Ha et al., 2009; Ha et al., 2010). On heating, compounds S2 and S3 exhibited nematic mesophase at 124 and 135°C with isotropic transition temperature at 206 and 207°C, respectively. On cooling, two peaks at 205 and 93°C were observed for S2 which are associated with isotropic-mesophase and mesophase-crystalline transitions, respectively. As for compound S3, isotropic-mesophase and mesophase-crystalline transitions were observed at 205 and 110°C, respectively. The incorporation of methoxy electron-donating group on a substituted aromatic ring increases the π -electron density of the ring, which reduces the phase

transition temperature (Salleh et al., 2013). The effect of increasing the terminal alkoxy length chain from methoxy to butoxy significantly affects the mesomorphic stability. The melting temperature increases with the increase of the terminal alkoxy-chain length from methoxy (e.g. 124°C for **S2**) to butoxy (e.g. 135°C for **S3**) due to the higher van der Waals association between the hydrophobic tails with an increase in the alkyl chain length. This argument is valid for shorter alkoxy chains (methoxy- and butoxy-chain), as in our case. However, such a trend was not apparent for those with long alkoxy chains ($n \geq 6$) as observed in other molecular cores. This could be explained on the basis that all the members of a homologous series ($n \geq 6$) shown to possess the same dipole moments, irrespective of the alkoxy chain length (Naoum et al., 2016; Saad et al., 2019; Thaker et al., 2010). Conversely, there is no considerable change in the clearing point with the increase of the terminal alkoxy chain length. This may be due to the shorter alkoxy chains used in the present work. Nonetheless, it has been reported that the nematic-to-isotropic transition temperatures decrease with increasing alkoxy-chain length due to the dilution of the interaction between the mesogenic units (Imrie & Taylor, 1989; Naoum et al., 2016; Saad et al., 2019).

Figure 4.18 shows the POM textures of compound **S2** at different temperatures. When the compound was cooled to 211°C the small droplets of nematic texture started to appear from the isotropic temperature as shown in Figure 4.18 (a). Upon further cooling, more droplets formed as observed at 206°C (Figure 4.18 (b)). The marble nematic texture was formed when the compound was cooled to 200°C (Figure 4.18 (c)). Upon further cooling to 84°C, the nematic phase changed to a lumber-like mosaic crystalline phase (Figure 4.18 (d)).

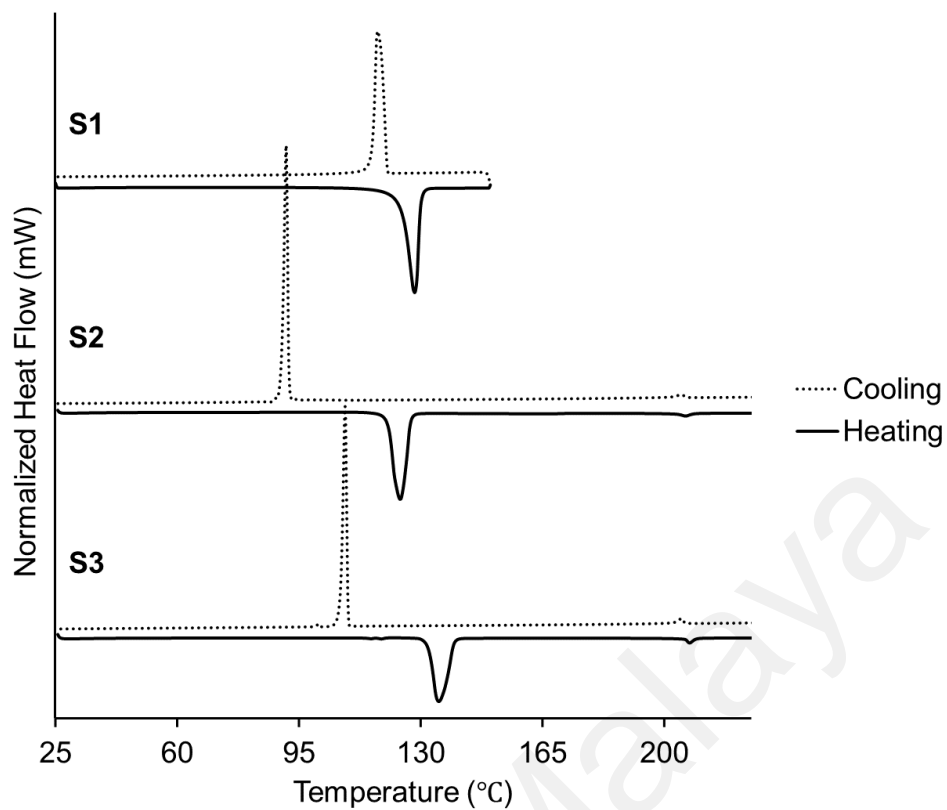


Figure 4.17: DSC thermograms at the scanning rate of $10^{\circ}\text{C min}^{-1}$ of compounds S1, S2 and S3.

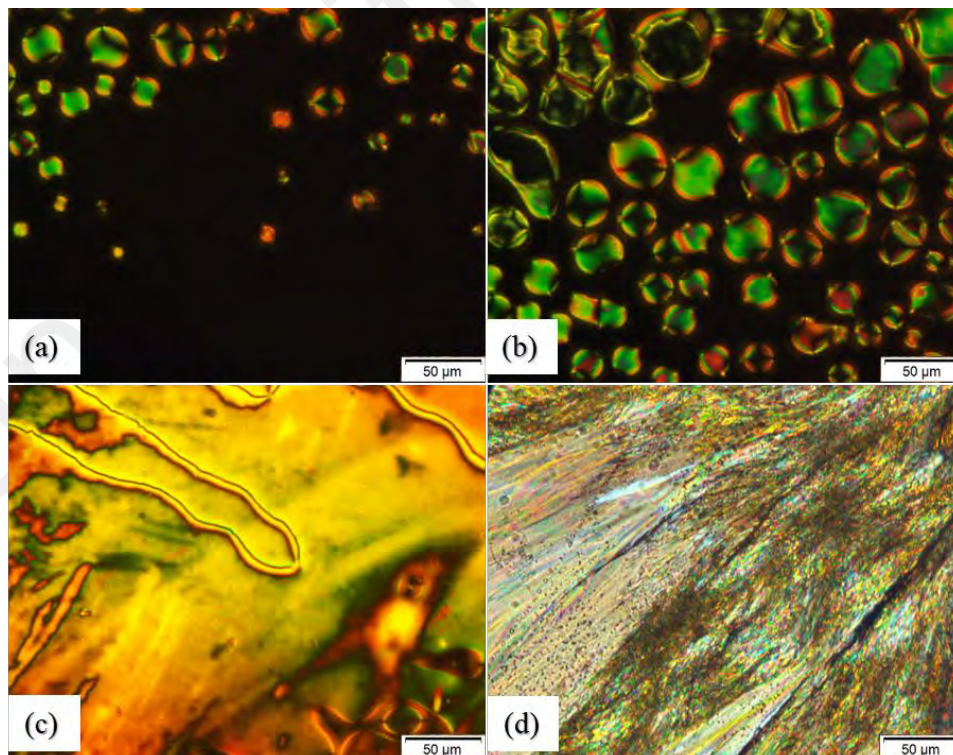


Figure 4.18: POM textures of S2 upon cooling from isotropic liquid at (a) 211°C , (b) 206°C , (c) at 200°C and (d) 84°C .

Figure 4.19 shows the POM textures of compound **S3** at different temperatures. Compound **S3** exhibited multi-coloured droplets characteristic of nematic texture when the compound was cooled to 207°C from the isotropic phase (Figure 4.19 (a)). Upon cooling to 203°C, the droplets grew to form the Schlieren nematic texture (Figure 4.19 (b)). When the compound cooled from its nematic phase to 110°C, its crystalline phase completely formed (Figure 4.19 (c)).

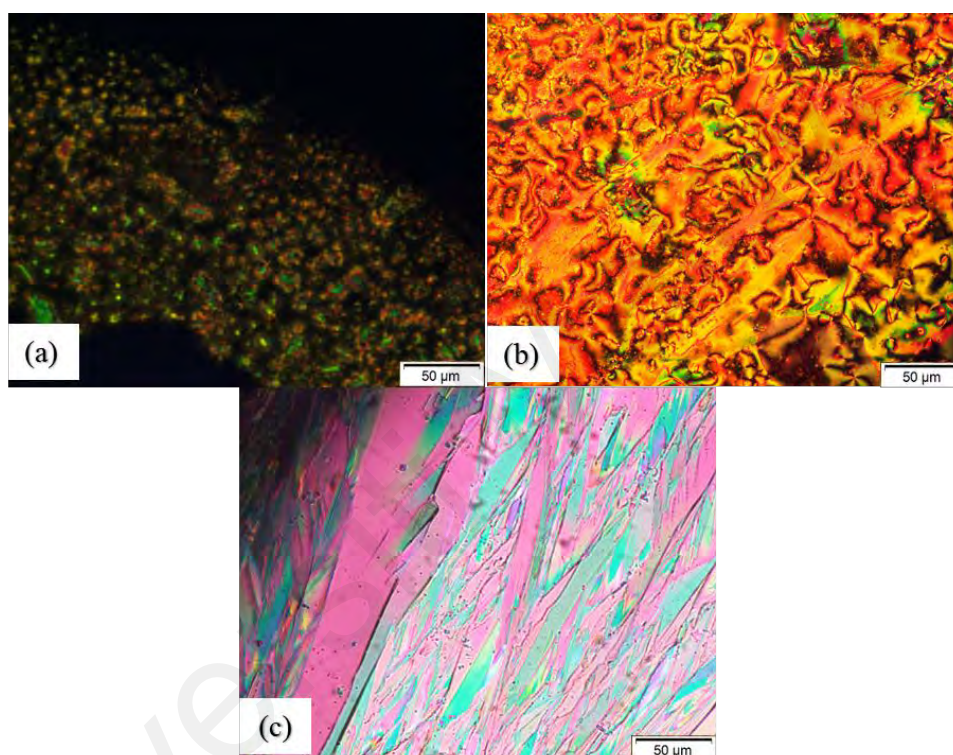


Figure 4.19: POM textures of S3 upon cooling from isotropic liquid at (a) 207°C, (b) 203°C and (c) 110°C.

The incorporation of lateral substitutions to the rigid mesogenic core of low molar mass liquid crystals have strongly affect their mesomorphic properties (Collings, 2002). The shielding of a lateral substituent by a steric or polar effect may lead to an increase or decrease in the phase transition temperature (Ahmed et al., 2018; Dixit & Intwala, 2016; Karim et al., 2016; Naoum et al., 2015c). To investigate the effect of introducing lateral fluorine group at the 2-position to the azo phenyl ring, the mesomorphic properties of the

synthesized compounds **C1**, **C2** and **C3** which contain a lateral fluorine group and terminal unsubstituted or electron-donating groups on the mesogen have been compared with the lateral unsubstituted compounds **S1**, **S2** and **S3**.

Figure 4.20 shows the DSC thermograms during second heating and cooling cycles of compound **C1** at scanning rate of $10\text{ }^{\circ}\text{C min}^{-1}$. This compound does not possess liquid crystalline properties, despite containing a lateral fluorine electron-withdrawing group. The results suggest that the length of 2-methylbutoxy terminal chain is too short to induce a mesophase in hydrogen-terminated derivatives. Upon introduction of polar substituent at the opposite terminal (methoxy or butoxy groups), the terminally substituted derivatives (**C2** and **C3**), respectively, are transformed into mesomorphic compounds as shown by DSC thermograms (Figure 4.24). During the second heating, both compounds **C2** and **C3** exhibited only mesophase at 95 and 117°C, respectively which undergo isotropization at 190 and 184°C, respectively. The thermal transitions were enantiotropic, meaning that liquid crystal mesophase was formed upon heating and cooling scans. The peaks at 189°C for compound **C2** and at 182°C for compound **C3** under cooling scan were observed for isotropic-mesophase transition. While for mesophase-crystalline transition were observed at 30 and 73°C, respectively. The melting temperature increases with the increase of the terminal alkoxy-chain length from methoxy to butoxy due to the higher van der Waals interaction between the hydrophobic tails (Naoum et al., 2016; Saad et al., 2019; Thaker et al., 2010). In contrast, the clearing temperature decreases with the increase of the terminal alkoxy chain length due to the dilution of the interactions between the mesogenic units (Imrie & Taylor, 1989; Naoum et al., 2016; Saad et al., 2019).

Comparison between the unsubstituted lateral compounds **S2** and **S3** with laterally fluorinated compounds **C2** and **C3** revealed that the former exhibited higher nematic to

isotropic transition temperatures than the latter. This is attributed to the disruption of the side-to-side intermolecular packing caused by the fluorine lateral unit *ortho* to the azo linkage. This observation has also been reported in similar works with different molecular cores (Ahmed et al., 2018; Ahmed et al., 2020; Ahmed & Saad, 2015; Xu et al., 2014). The fluorine group is an electron-withdrawing group, which have great dipole moment, led to a reduction in the mesophase thermal stability.

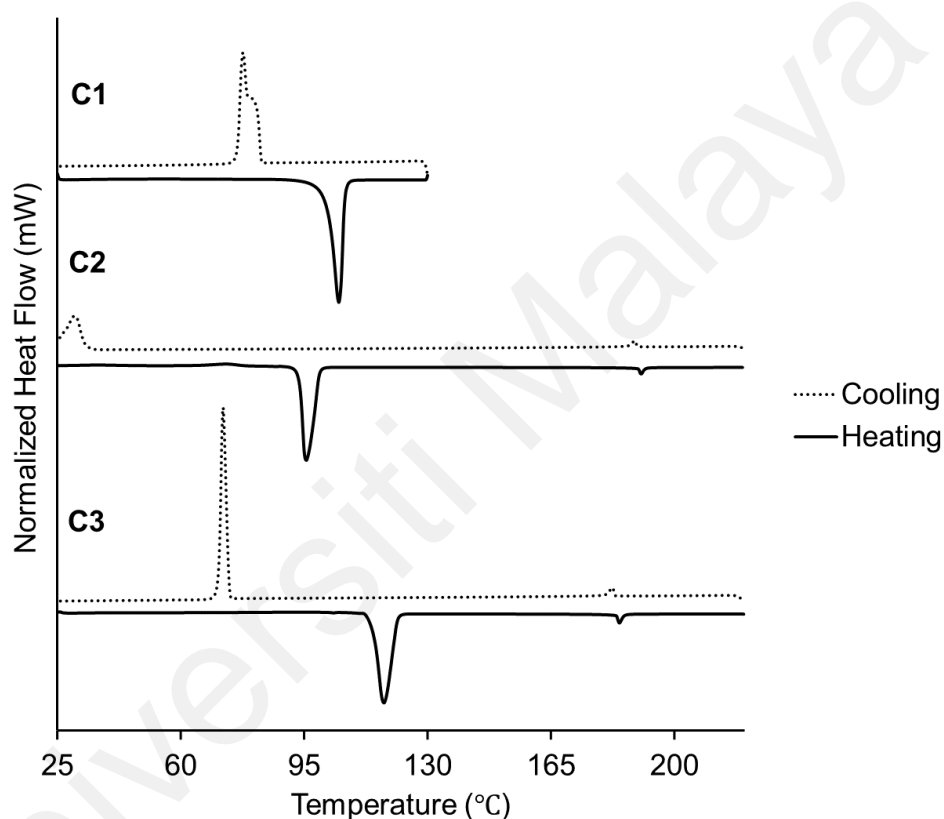


Figure 4.20: DSC thermograms at the scanning rate of $10^{\circ}\text{C min}^{-1}$ of compounds C1, C2 and C3.

Figure 4.21 shows the POM textures of compound C2 at different temperatures. The nematic texture started to appear when the compound was cooled to 185°C as shown in Figure 4.21 (a). Upon cooling to 180°C the grainy nematic texture completely formed (Figure 4.21 (b)). At 41°C , the nematic phase of the compound started to form crystalline phase texture (Figure 4.21 (c), (d)).

Figure 4.22 shows the POM textures of compound **C3** at different temperatures. Upon cooling from isotropic phase, the green droplets appeared at 182°C (Figure 4.22 (a)). The droplets grew to form the Schlieren texture around 181°C as shown in Figure 4.22 (b), (c). When the compound was further cooled from its nematic phase, the crystalline phase appeared at 71°C (Figure 4.22 (d)).

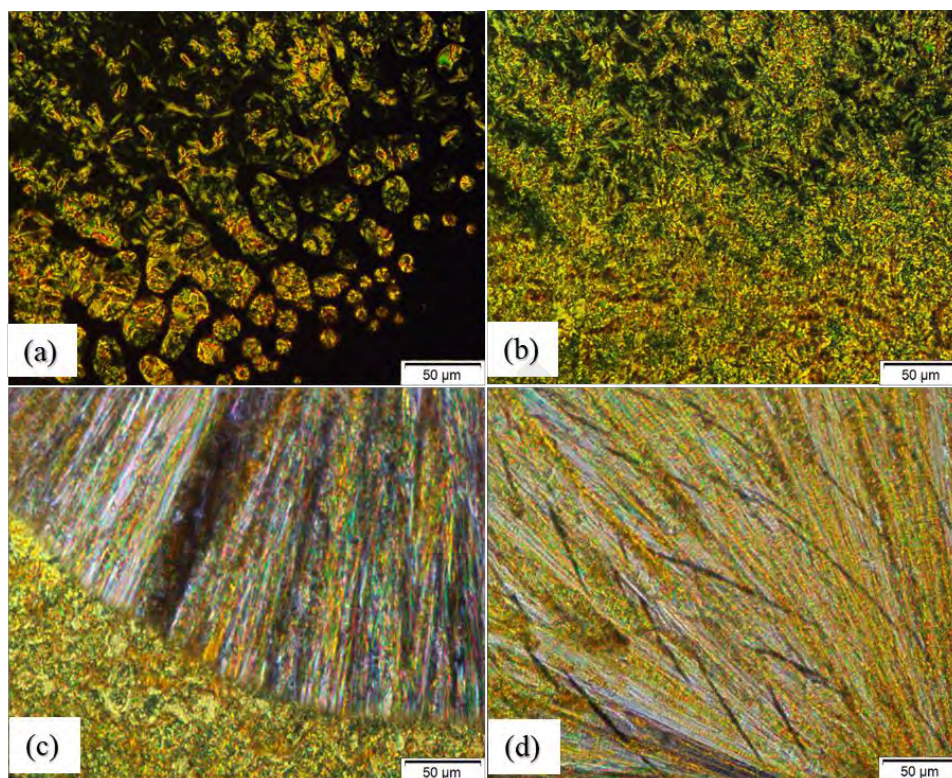


Figure 4.21: POM textures of C2 upon cooling from isotropic liquid at (a) 185°C, (b) 180°C, (c) 41°C and (d) 40°C.

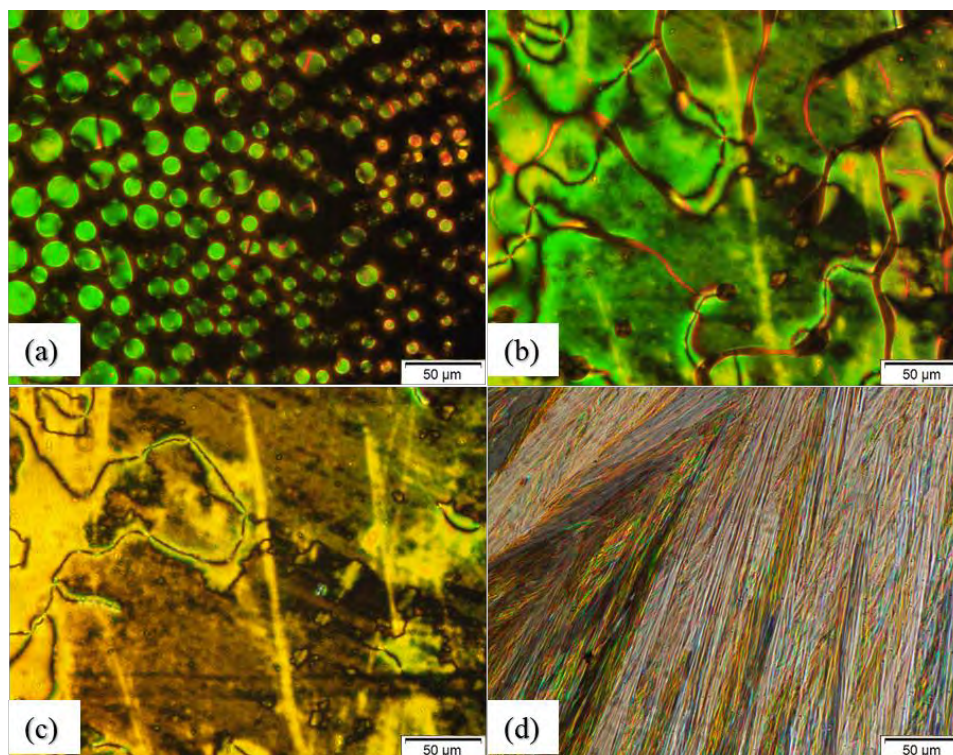


Figure 4.22: POM textures of C3 upon cooling from isotropic liquid at (a) 182°C, (b) 181°C, (c) 180°C and (d) 71°C.

The mesophase behaviors of laterally fluorinated azo-esters containing terminal electron-withdrawing group (C4 and C5) have also been compared with the corresponding laterally-neat analogues (S4 and S5). The presence of inductive electron-withdrawing power of bromo or nitro groups on a substituted aromatic ring increases the polarity of the whole mesogenic core and stabilises the mesophase (Naoum et al., 2014). Figure 4.23 shows the DSC thermograms of compounds S4 and S5 during second heating and cooling cycles at scanning rate of $10^{\circ}\text{C min}^{-1}$. Upon heating, compound S4 exhibited crystal-mesophase and mesophase-mesophase transitions at 148 and 202°C, respectively with the isotropic transition at 211°C. However, compound S5 with terminal electron-withdrawing nitro group only exhibited crystal-mesophase transition at 168°C which undergo isotropization at 238°C. Upon cooling, the transition of compound S4 from isotropic phase gave two mesophases transition peaks at 210 and 200°C which followed

by crystallization at 129°C. Compound **S5** exhibited isotropic-mesophase transition at 236°C and mesophase-crystalline transition at 146°C.

Figure 4.24 shows the DSC thermograms of compounds **C4** and **C5** during the second heating and cooling cycles at scanning rate of 10°C min⁻¹. During the second heating, both compounds **C4** and **C5** exhibited only crystal-mesophase at 115 and 164°C with isotropic transition at 175 and 215°C, respectively. During cooling scan, isotropic-mesophase transition were observed at 174°C for compound **C4** and at 213 °C for compound **C5**. Upon further cooling, compound **C4** gave a mesophase-mesophase transition at 112°C, which undergo crystallization at 83°C, while compound **C5** showed mesophase to crystalline transition at 146°C.

The lateral fluorine substituted analogues **C4** and **C5** with electron-withdrawing groups exhibited lower melting and clearing temperatures compared with their corresponding laterally unsubstituted analogues **S4** and **S5**, as shown in Table 4.4. The finding is similar to those observed in terminal electron-donating substituents which explain that such observation is attributed to the disruption of the side-to-side intermolecular packing caused by the lateral fluoro group. On the other hand, the clearing temperature increases with the incorporation of nitro substituted compounds, **S5** and **C5**, more than the bromo-substituted compounds **S4** and **C4**. This observation is possibly due to the incorporation of the terminal nitro group, which had a larger dipole moment and stronger electron-withdrawing inductive effect, which increases the mesogenic core's polarity and thus the clearing temperature (Naoum et al., 2014).

Generally, the dipole moment of a molecule is greatly influenced by the nature of the terminal substituent, which affects the intermolecular attraction and mesophase stability of the LC compound (Naoum et al., 2014). From Table 4.4, both laterally neat (**S2**, **S3**, **S4**, and **S5**) and laterally monofluorinated (**C2**, **C3**, **C4**, and **C5**) azo-ester

compounds show that their mesophase stability i.e. clearing temperature depends on the polarity of the terminal substituent R that leads to different mesomeric effects and consequently to different dipole-dipole interaction. The clearing temperatures of the laterally neat compounds (**S2**, **S3**, **S4**, and **S5**) were found to decrease according to the terminal substituent in the following order: $\text{NO}_2 > \text{Br} > \text{OCH}_3 \approx \text{OC}_4\text{H}_9$. In this comparison, the nitro and bromo-terminated derivatives have the highest clearing temperatures, which is in accordance with the increase of the mesomeric interactions between the alkoxy oxygen and the ester carbonyl via the phenylazo group (on one side of the molecule) by the inductive electron-withdrawing power of the nitro or bromo groups (on the other side of the molecule). On the contrary, there are opposing electronic effects from both sides of the molecule of the methoxy and butoxy-terminated analogues, resulting in both derivatives having a lower dipolar character and consequently lower clearing temperature values (Naoum et al., 2015b). The following clearing temperatures trends were observed when a lateral fluoro group is added at 2-position to the azo linkage in the laterally fluorinated azo esters (**C2**, **C3**, **C4**, and **C5**): $\text{NO}_2 > \text{OCH}_3 > \text{OC}_4\text{H}_9 > \text{Br}$. All terminal substituents follow the same order as the laterally-neat analogues, except for the bromo group, where the bromo-terminated derivative has the lowest clearing temperature, despite being a polar group. This result suggests that when substitution is made at a lateral position by an electron-withdrawing fluorine group, the resultant dipole moment of the whole molecular structure of bromo-terminated derivative is reduced (Thaker et al., 2010).

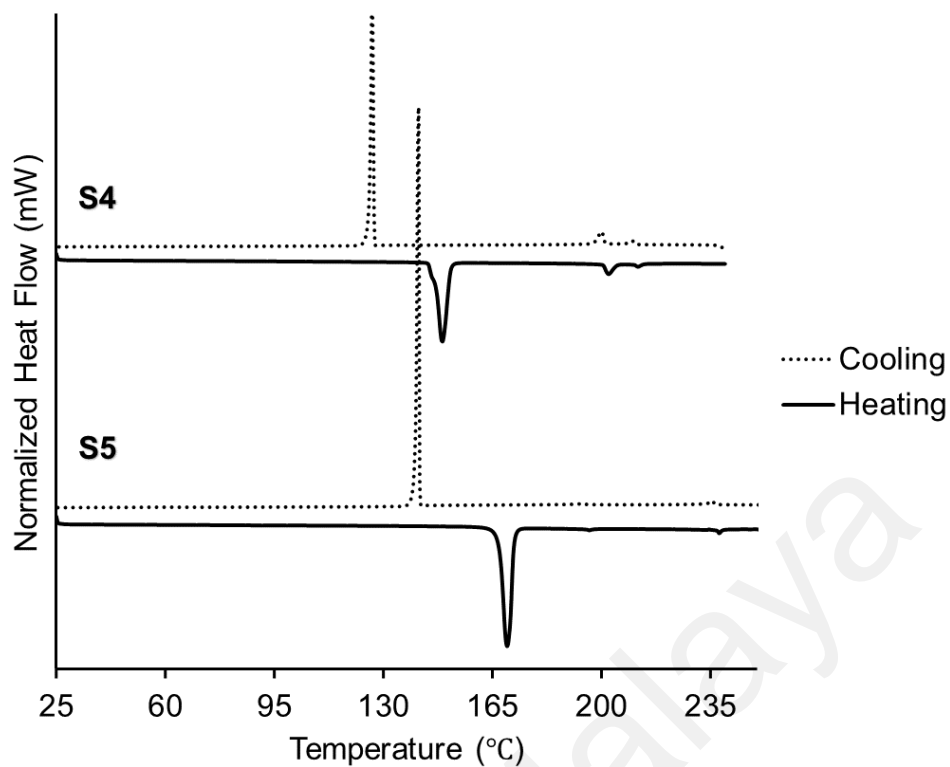


Figure 4.23: DSC thermograms at the scanning rate of $10^{\circ}\text{C min}^{-1}$ of compounds S4 and S5.

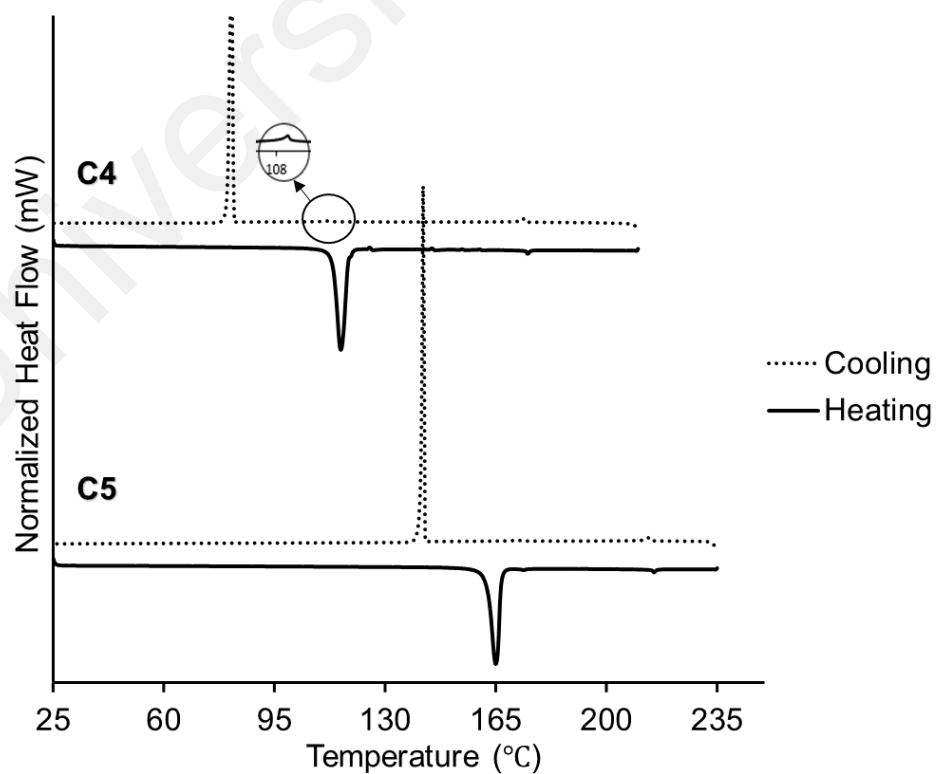


Figure 4.24: DSC thermograms at the scanning rate of $10^{\circ}\text{C min}^{-1}$ of compounds C4 and C5.

Figure 4.25 shows the POM textures of compounds **S4** and **S5** obtained at different temperatures. Upon cooling, compounds **S4** and **S5** exhibited isotropic to nematic transition with Schlieren and grainy textures at 209°C and 236°C, respectively (Figure 4.25 (a, d)). Upon further cooling of compound **S4** to 202°C gave transition from the nematic phase to another nematic phase, which represented here as nematic X (N_X) to differentiate it from the higher temperature nematic phase (N) (Figure 4.25 (b)). Compound **S4** underwent crystallization at 127°C (Figure 4.25 (c)). As for compound **S5**, the nematic texture remains at 183°C with a slight change in birefringence (Figure 4.25 (e)) before it undergoes crystallization at 145°C (Figure 4.25 (f)).

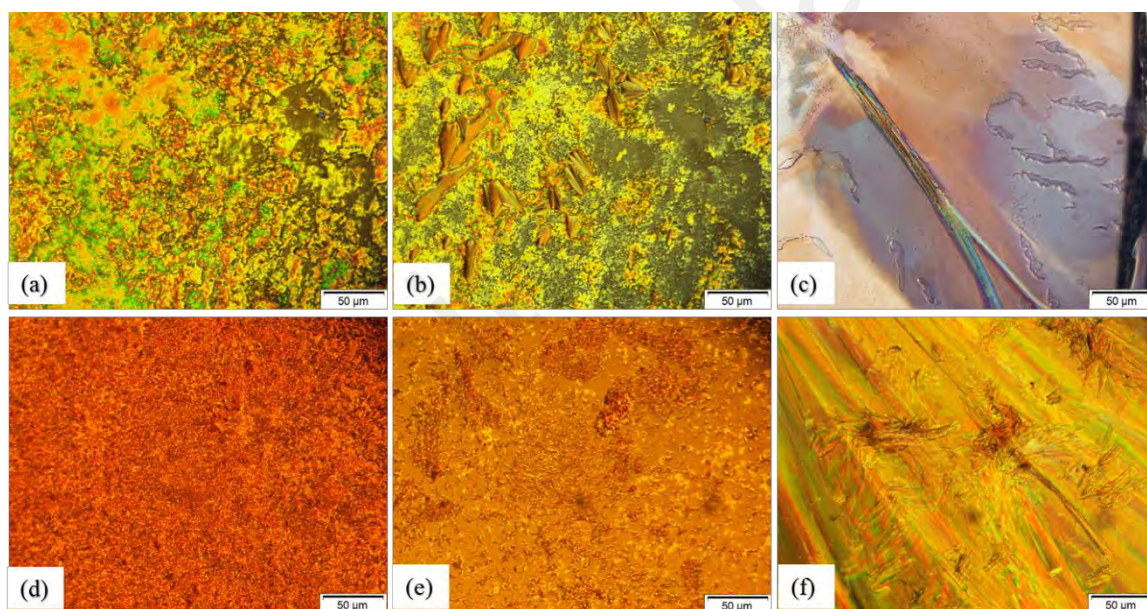


Figure 4.25: POM textures of S4 upon cooling from isotropic liquid at (a) 209°C, (b) 202°C and (c) 127°C and S5 at (d) 236°C, (e) 183°C and (f) 145°C.

Figure 4.26 shows the POM textures of compounds **C4** and **C5** obtained at different temperatures. Upon cooling from an isotropic phase, nematic phase was identified by the appearance of Schlieren texture with fourfold brushes for compound **C4** at 166°C (Figure 4.26 (a)). Different Schlieren texture at 113°C was observed that also displayed high fluidity, signifying a nematic phase (Figure 4.26 (b)). Compound **C5**

exhibited grainy texture with the transition from isotropic liquid to the nematic phase at 181°C (Figure 4.26 (d)). Upon further cooling, a substantial change in birefringence of the nematic phase was exhibited at 172°C (Figure 4.26 (e)). At 83°C and 146°C, the liquid crystalline phase of the compounds **C4** and **C5** changed to form the crystalline phase, respectively (Figure 4.26 (c), (f)).

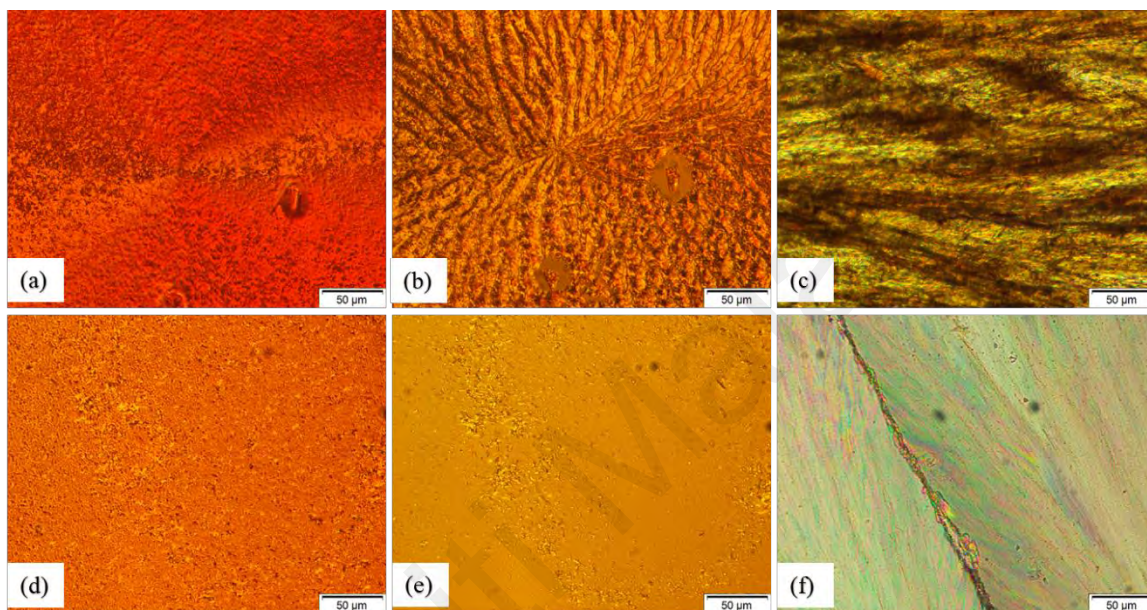


Figure 4.26: POM textures of C4 upon cooling from isotropic liquid at (a) 166°C, (b) 113°C and (c) 83°C and C5 at (d) 181°C, (e) 172°C and (f) 146°C.

The synthesized compounds **C6**, **C7** and **C8** with a lateral methyl group and terminal unsubstituted or electron-donating groups on the mesogen have been also compared with their corresponding laterally-neat compounds **S1**, **S2** and **S3** on the mesomorphic behaviours. Figure 4.27 shows the DSC thermograms during the second heating and cooling cycles of compound **C6**, **C7** and **C8** at a heating rate of 10 °C min⁻¹. Compound **C6** gave similar observation as other hydrogen-terminated compounds **S1** and **C1**, that is the compound did not exhibit liquid crystal properties. The replacement of terminal hydrogen by the electron-donating methoxy and butoxy groups in laterally methyl-substituted derivatives significantly increases the molecular length-to-width ratio to give mesomorphic behavior in **C7** and **C8** (Ha et al., 2009; Ha et al., 2010). Both

compound **C7** and **C8** exhibited a melting phase transition at 105 °C and 107 °C, respectively. Peaks at approximately at 159 °C for both compounds **C7** and **C8** associated with the isotropic-nematic transition were detected during cooling cycle. As can be seen from Table 4.4, independent of the absence or presence of the lateral methyl group, the effect of increasing alkoxy chain length significantly affects the mesomorphic stability. The melting temperature increases with the increase of the terminal alkoxy-chain length from methoxy to butoxy due to the higher van der Waals association between the hydrophobic tails with an increase in the alkyl chain length. Conversely, there is no considerable change in the clearing point with the increase of the terminal alkoxy chain length. This is possibly due to the shorter alkoxy chains used in the present work.

As shown in Table 4.4, higher melting and clearing temperatures were found in compounds **S2** and **S3**. In contrast, compounds **C7** and **C8** with lateral methyl substituent displayed lower melting and clearing temperatures than those without lateral methyl groups. The presence of lateral methyl substituent is anticipated to give combined steric hindrance with a weak positive inductive effect in influencing the mesomorphic behaviour of the laterally substituted azo-ester compounds (Cigl et al., 2016). Similar observations have also been reported by other researchers examining different molecular cores (Karim et al., 2016; Naoum et al., 2015b; Sardon et al., 2021; Thaker et al., 2010). They suggested that the presence of a lateral methyl unit widens the molecular core effectively and subsequently increases intermolecular separation, leading to the reduction in the lateral associations of rod-shape molecules; consequently, the mesophase stability is reduced (Ahmed et al., 2018; Saad et al., 2019).

The lateral group position is another effect that could influence mesomorphic behaviour. Ahmed et al. studied the effect of introducing a lateral polar group *ortho* or *meta* to azo linkage liquid crystalline compounds. They reported that the mesophase

stability of the lateral fluorine group *meta* to azo linkage derivatives are higher than those of the lateral fluorine group *ortho* to azo linkage derivatives. This is attributed to the resultant dipole moment of the whole molecule which varies between the lateral group at an angle of 60° or 120° with the major longitudinal axis of the molecule as well as the polarity of the group. Hence, we anticipate that our azo-esters with lateral substituent at the 2-position of phenylazo ring would result lower clearing temperatures than those with lateral substituent at the 3-position (Ahmed et al., 2018).

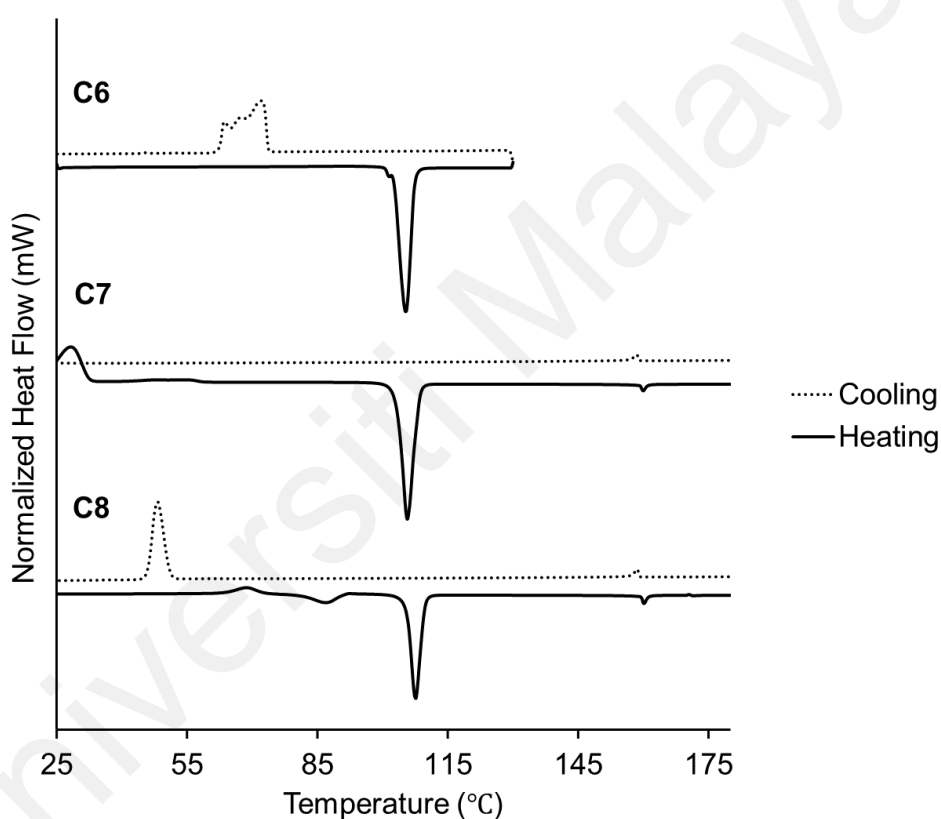


Figure 4.27: DSC thermograms at the scanning rate of $10^\circ\text{C min}^{-1}$ of compounds C6, C7 and C8.

Figure 4.28 shows the POM textures of compound C7 at different temperatures. The Schlieren texture of nematic phase started to appear when the compound was cooled to 158°C from the isotropic temperature and the texture remained at 155°C as shown in

Figure 4.28 (a, b). Upon further cooling to 49°C (Figure 4.28 (c)), the nematic phase started to disappear, and the crystalline texture was observed at 48°C (Figure 4.28 (d)).

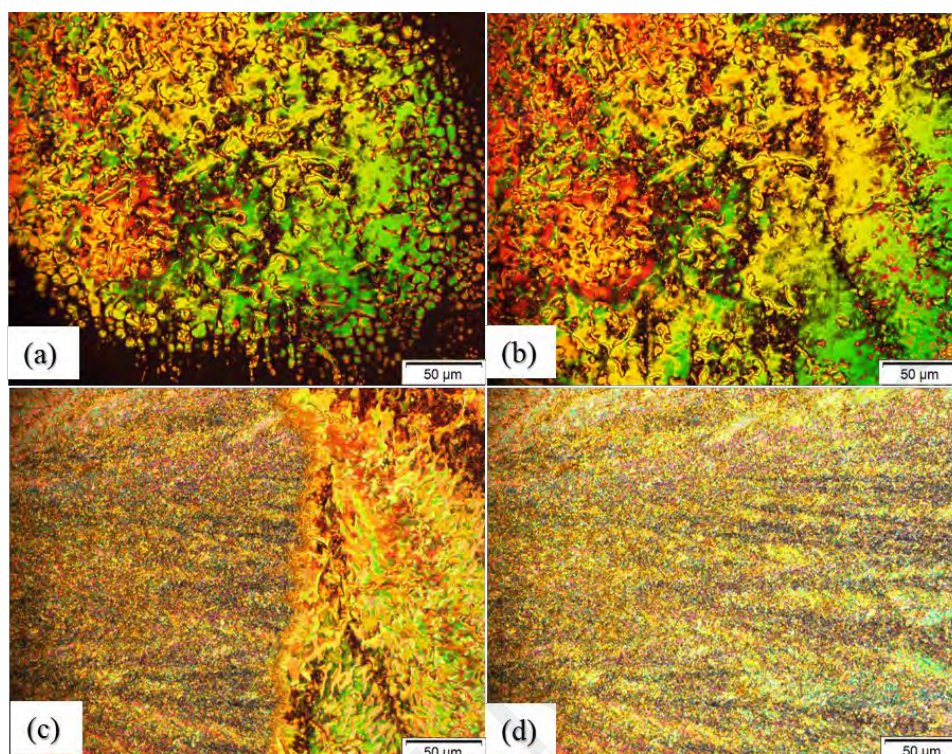


Figure 4.28: POM textures of C7 upon cooling from isotropic liquid at (a) 158°C, (b) 155°C, (c) 49°C and (d) 48°C.

Figure 4.29 shows the POM texture of compound C8 at different temperatures. The Schlieren nematic texture started to appear when the compound was cooled to 158°C from the isotropic temperature (Figure 4.29 (a)) and completed at 157°C (Figure 4.29 (b)). The compound solidified when cooled from its nematic phase to 72°C, at which the crystalline texture displayed a lumber-like mosaic texture (Figure 4.29 (c, d)).

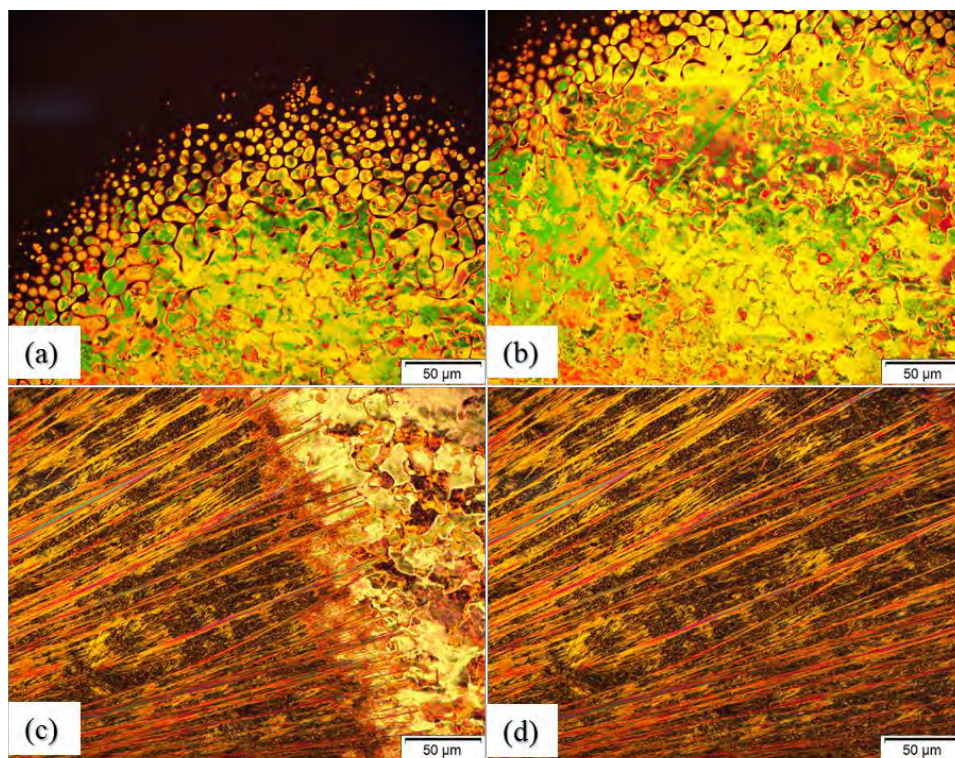


Figure 4.29: POM textures of C8 upon cooling from isotropic liquid at (a) 158°C, (b) 157°C, (c) 72°C and (d) 71°C.

The SWAXS measurements at selected temperatures were applied to confirm the thermotropic behaviour of these azo-esters. Figure 4.30 shows the SWAXS intensity profiles of compound **S2** at 25, 100, 140 and 160 °C upon heating and cooling scan. At 25 °C, the compound showed a few sharp scattering signals in the wide-angle region demonstrating the compound is in crystalline phase (Figure 4.30 (a)). When compound **S2** was heated to 100 °C, sharp signals were observed, indicating that the compound remains as a crystalline powder. After the temperature increased to 140 °C, the sharp peaks disappeared and the broad peak in the small-angle region $2.5\text{-}5.5\text{ nm}^{-1}$ formed, indicating that the compound has entered the nematic phase. The nematic phase remained when the sample was heated to 160 °C. The formation of the nematic phase was also confirmed upon cooling at 160 and 140 °C (Figure 4.30 (b)). A few sharp peaks appeared when the sample was cooled to 80 °C due to supercooling formation.

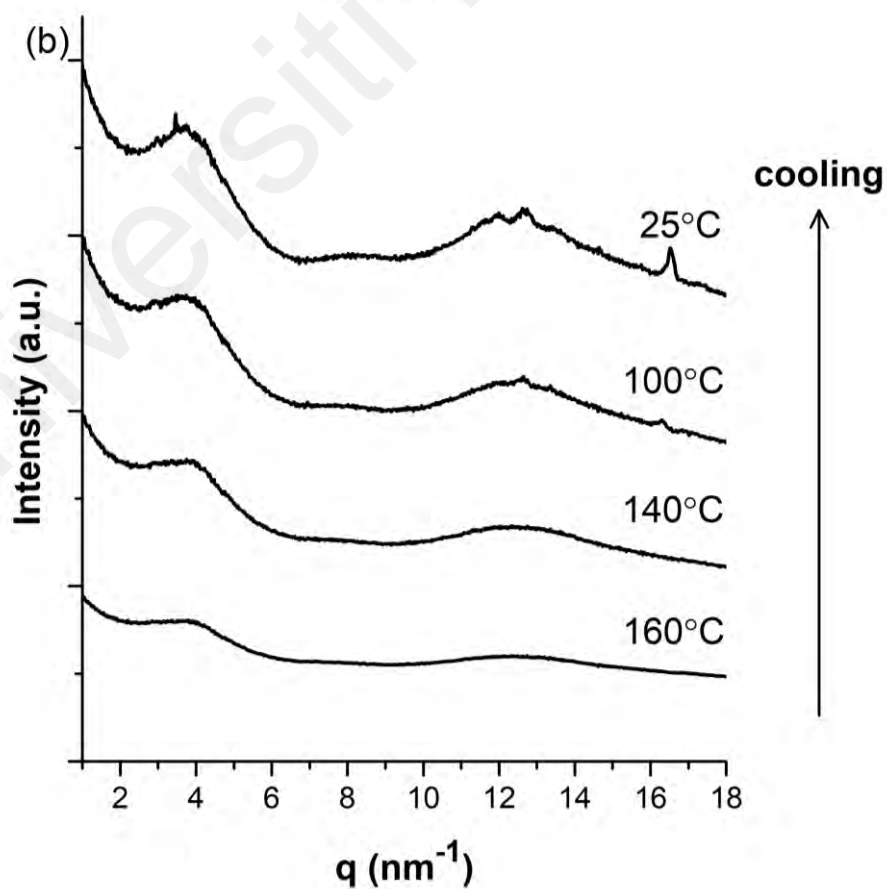
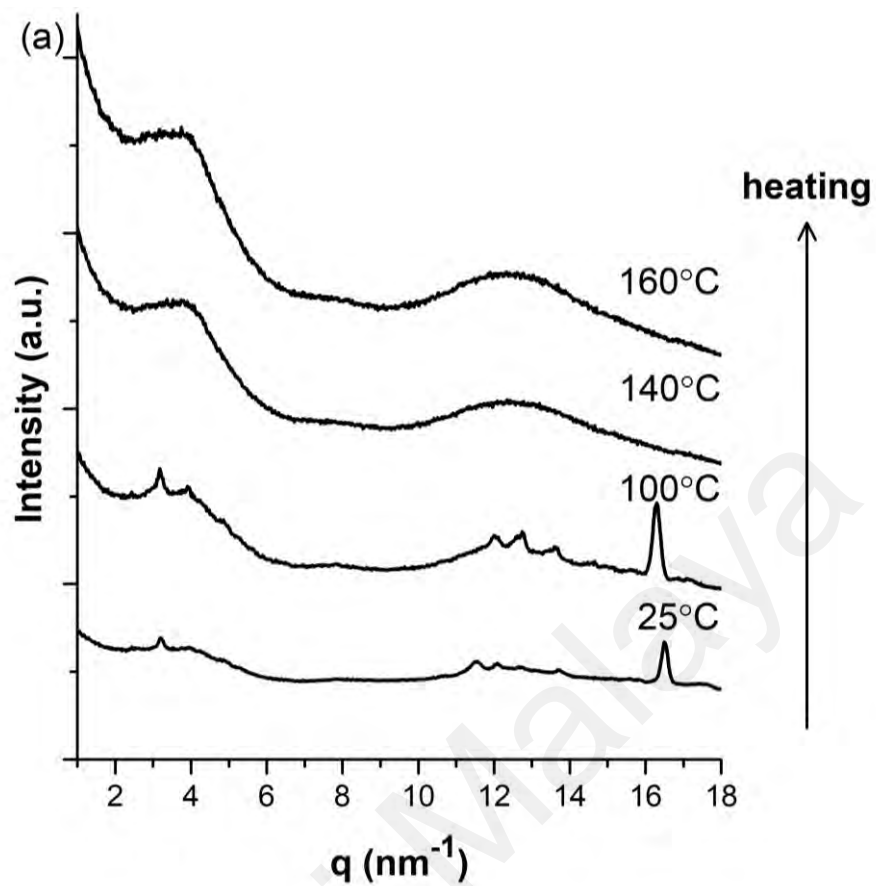
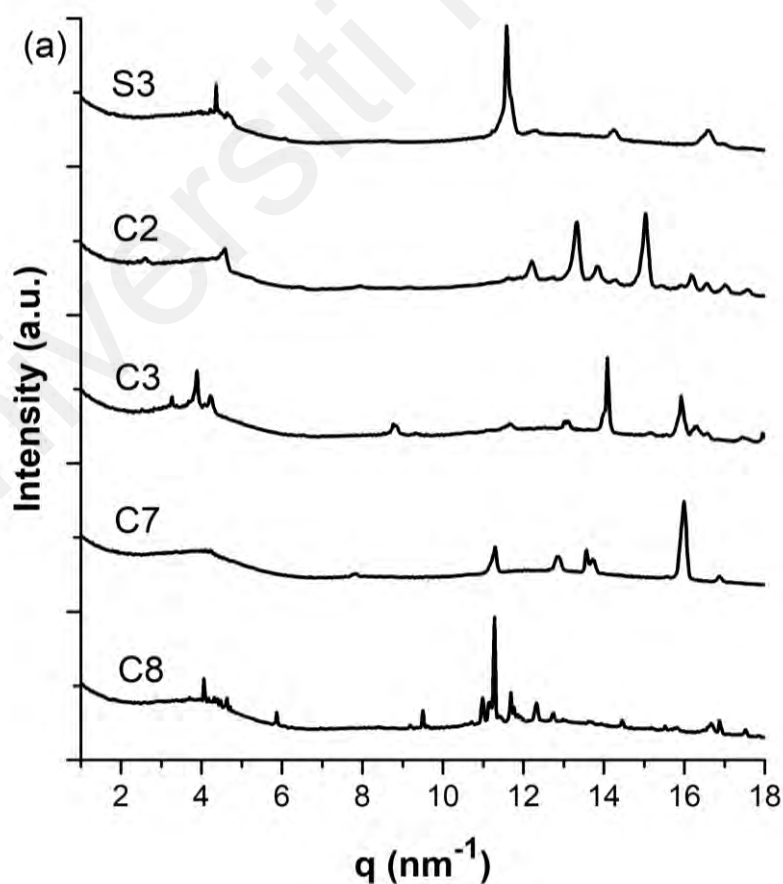


Figure 4.30: SWAXS pattern of S2 at 25, 100, 140 and 160°C (a) upon heating, (b) upon cooling.

Figure 4.31 depicts the SWAXS patterns for the laterally-neat, laterally fluorinated and laterally methyl derivatives with terminal electron-donating groups i.e. **S3**, **C2**, **C3**, **C7** and **C8**. At room temperature, all compounds reflected sharp scattering peaks in the small and wide-angle regions, characteristic of the crystalline phase (Figure 4.31 (a)). After heating to a selected temperature at the liquid crystal phase (as determined from DSC and POM), the sharp peaks disappeared and a broad peak in the small-angle region $2.5\text{-}5.5\text{ nm}^{-1}$ was observed for all compounds, as illustrated in Figure 4.31 (b), a typical pattern that corresponds to the nematic phase. In addition, the diffused peak was observed in the wide-angle region, which identifies as a mesophase of liquid crystal compounds as a result of the liquid-like disorder of the alkyl chain. Based on the DSC, POM and SWAXS results, only the nematic mesophase was observed for all terminal electron-donating substituted compounds under heating and cooling scans.



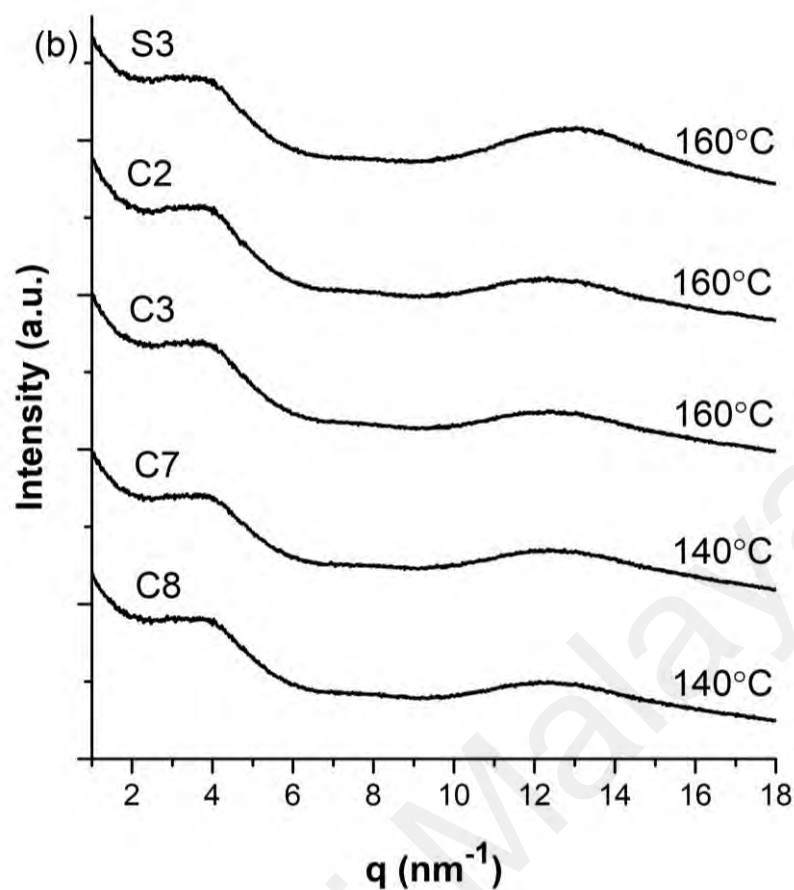


Figure 4.31: SWAXS patterns of S3, C2, C3, C7 and C8 (a) at 25°C, (b) at selected temperatures of nematic phase.

On the other hand, SWAXS patterns for the laterally-neat and laterally fluorinated derivatives with the terminal electron-withdrawing groups i.e. **S4**, **S5**, **C4**, and **C5** at different temperatures (during heating) are shown in Figures 4.32 and 4.33. Sharp scattering peaks in the wide-angle region were observed at room temperature for all samples which is due to the crystalline phase. At 180°C and 100°C (cooling), nematic-to-nematic phase was confirmed for **S4** and **C4**, respectively, via reflection of a similar scattering pattern as the nematic phase at 205°C and 150°C, respectively, as shown in Figure 4.32 (a) and Figure 4.33 (a). A similar transition from nematic-to-nematic phase has been described by Mandle et al. in a highly polar rod-like liquid crystal with short terminal chain. The authors concluded that the lower temperature nematic phase (N_X) is

driven by the formation of antiparallel molecular associations due to the large longitudinal dipole moment (Mandle et al., 2017). The reflections of diffuse scattering patterns at small- and wide-angles of **S5** and **C5** samples at 205°C and 190°C confirm the formation of nematic phase (Figure 4.32 (b), 4.33 (b)).

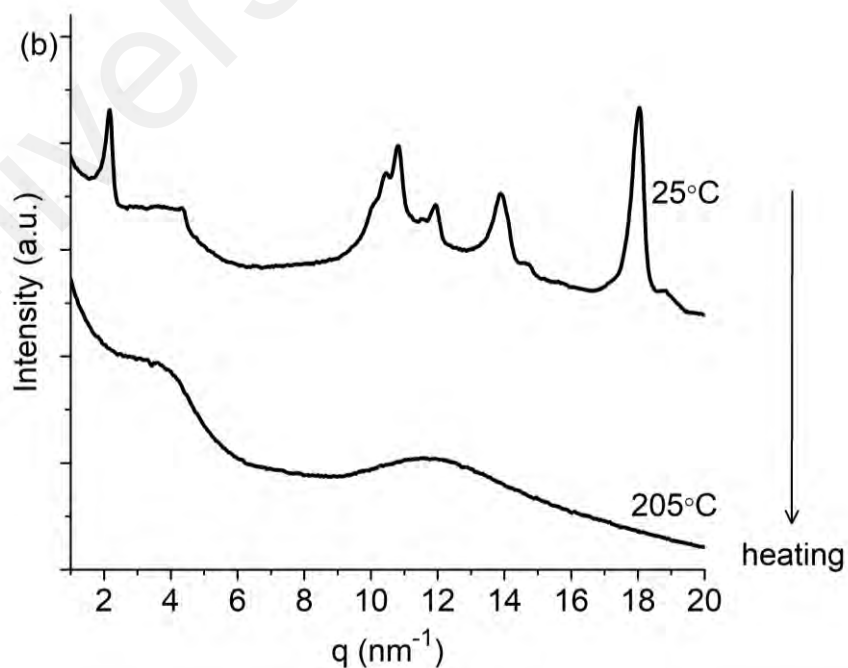
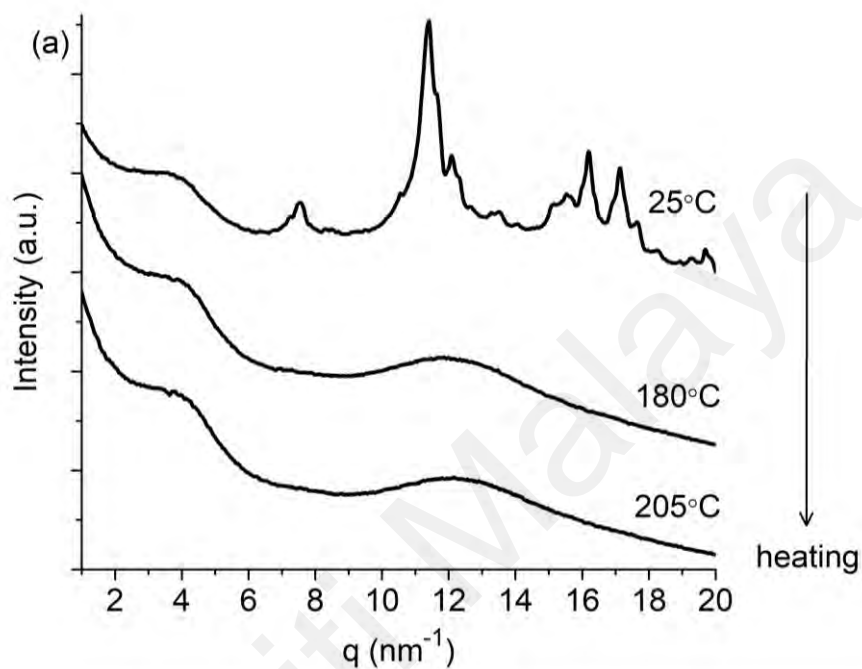


Figure 4.32: SWAXS pattern of (a) S4 at 25, 180 and 205°C; (b) S5 at 25 and 205°C upon heating.

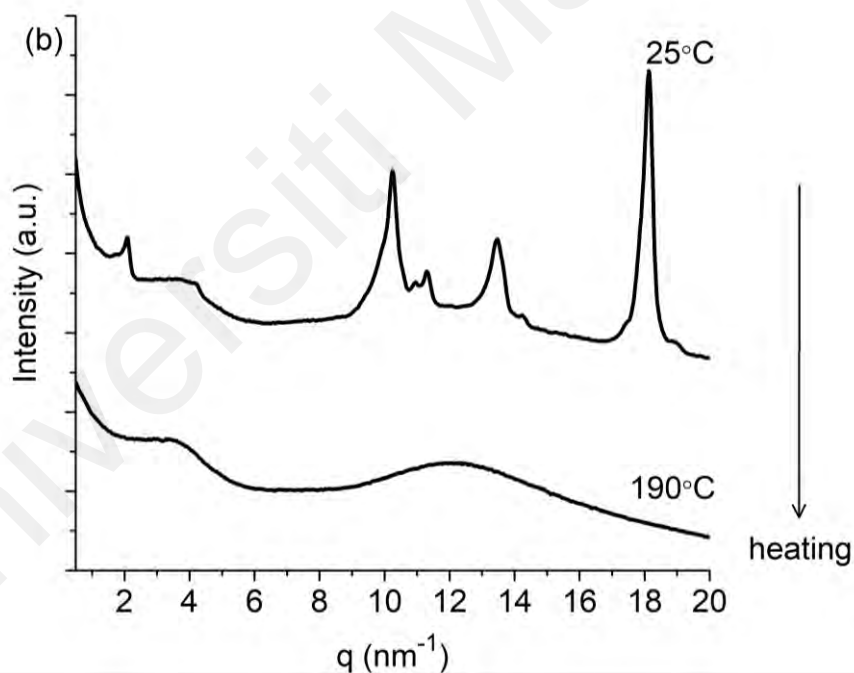
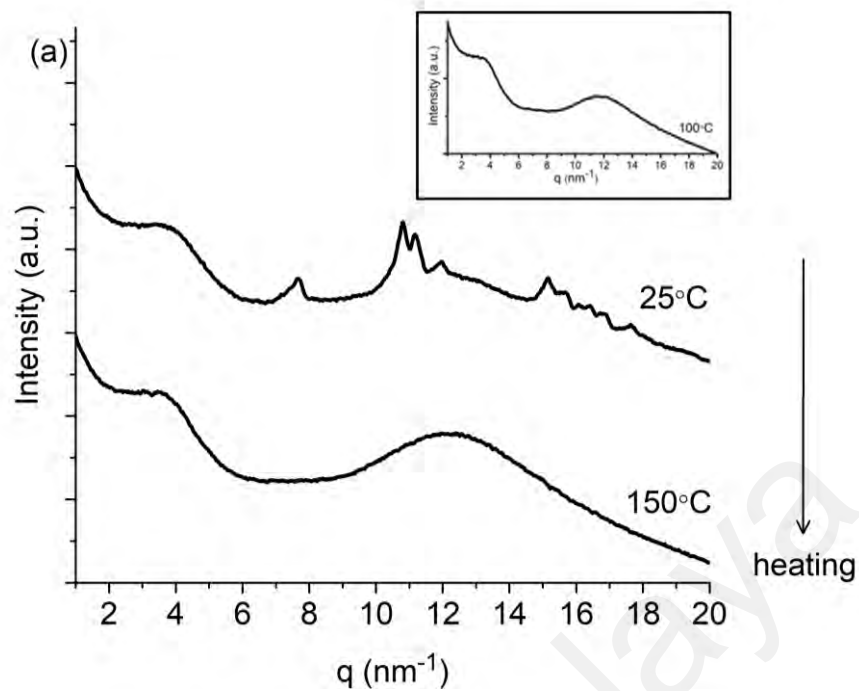


Figure 4.33: SWAXS pattern of (a) C4 at 25 and 150°C upon heating. The inset shows scattering pattern at 100°C recorded on cooling; (b) C5 at 25 and 190°C upon heating.

4.3.3 Optical Properties

The optical properties of LC compounds were characterized by UV-vis absorption and PL spectroscopies. UV-Vis and PL spectra were obtained in dilute CDCl_3 solvent at a concentration of 5×10^{-5} M. The photophysical properties of compounds **S2**, **S3**, **S4**, **S5**, **C2**, **C3**, **C4**, **C5**, **C7** and **C8** are summarized in Table 4.5.

Table 4.5: UV-Vis absorption and PL emission spectral data of LC compounds

Compound	X	R	$\lambda_{\text{max}} \pi-\pi^*$ (nm) ^a	$\lambda_{\text{max}} \pi-\pi^*$ (nm) ^b	$\lambda_{\text{max}} n-\pi^*$ (nm)
S2	H	OCH ₃	225	365	459
S3	H	OC ₄ H ₉	222	365	462
S4	H	Br	259	367	467
S5	H	NO ₂	267	370	467
C2	F	OCH ₃	224	365	459
C3	F	OC ₄ H ₉	222	365	459
C4	F	Br	255	367	464
C5	F	NO ₂	266	368	466
C7	CH ₃	OCH ₃	223	372	470
C8	CH ₃	OC ₄ H ₉	222	372	470

^a For wavelength range from 220–280 nm.

^b For wavelength range from 300–425 nm.

In general, absorption spectra of all LC compounds showed similar characteristics due to the structural similarity of their mesogenic core (see Figure 4.34). Each compound exhibited three absorption bands: (i) a shoulder-like absorption band around 220–280 nm, (ii) an absorption band around 300–425 nm, and (iii) a low-energy absorption band around 450–500 nm. The terminal electron-donating analogues **S2**, **S3**, **C2**, **C3**, **C7** and

C8 displayed a strong absorption band at a short wavelength region, while the terminal electron-withdrawing derivatives **S4**, **S5**, **C4** and **C5** showed a medium-energy absorption band. These absorptions band arise from the HOMO→LUMO transition and may correspond to π - π^* transition of the phenyl rings (Jadeja et al., 2019; Karim et al., 2015; Pal et al., 2018). The absorption band at a higher wavelength range may be regarded as a symmetry-allowed π - π^* transition involving the π -electronic system throughout the whole molecule with a substantial charge transfer character (Ebead et al., 2010; Karim et al., 2016). Lastly, the weak band appeared around 470 nm is due to a symmetry-forbidden n - π^* transition (Sardon et al., 2021). From Table 4.5, the terminal electron-donating group compounds **S2**, **S3**, **C2** and **C3** exhibited intense absorption at 365 nm, while the terminal electron-withdrawing group compounds **S4**, **S5**, **C4** and **C5** exhibited their absorption at a slightly higher wavelengths of 366, 370, 367 and 368 nm, respectively. The lateral methyl compounds with the terminal electron-donating group (**C7** and **C8**) showed the maximum absorption at 372 nm which are red-shifted relative to the laterally unsubstituted and laterally fluorinated analogues.

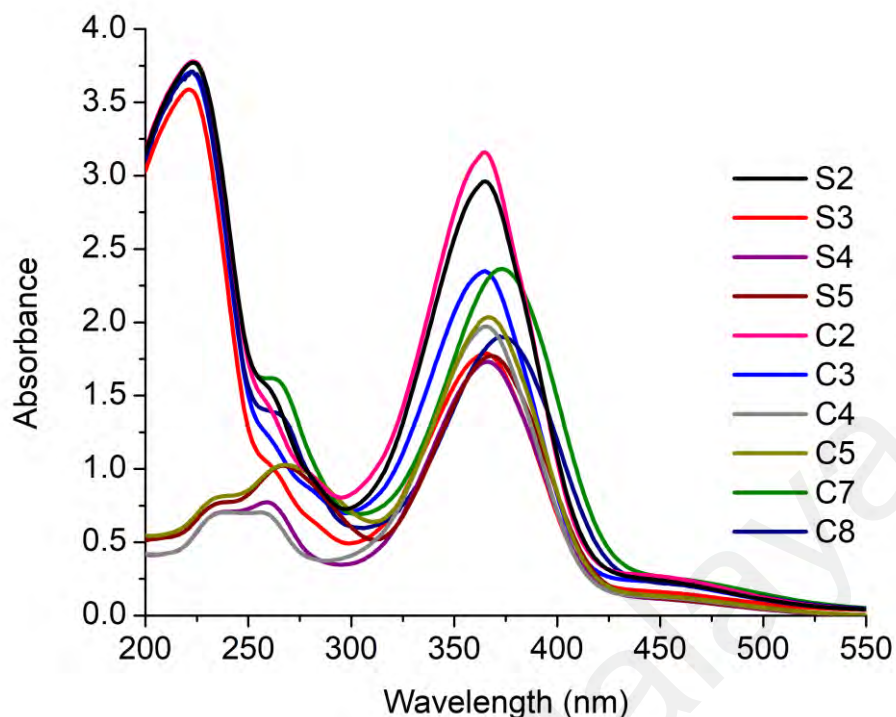


Figure 4.34: UV-Vis absorption spectra of S2, S3, S4, S5, C2, C3, C4, C5, C7 and C8 in CDCl_3 solution of 5×10^{-5} M.

The corresponding fluorescence spectra of LC compounds are depicted in Figure 4.35. Excitation around 365 nm gave a broad unstructured blue emission band centred around 440 nm. As observed in UV-vis spectra, their emission spectra were very similar in shape because of the structural similarities in the mesogenic unit. However, the laterally substituted compounds C7 and C8 have a relatively higher fluorescence intensity compared with that of the laterally-neat and laterally fluorinated analogues. Most of the azo compounds are reported to exhibit a reversible *trans-cis* photoisomerization process upon absorption of a photon within the absorption band (Barrett et al., 2007; Cigl et al., 2016). Nevertheless, suppression of the photoisomerization movement in the azo compounds due to the conformational strain or steric hindrance is considered key to their fluorescent nature (Han et al., 2009; Yoshino et al., 2013). The incorporation of lateral electron-donating groups on phenylazo moiety may affect the HOMO-LUMO energy

gaps that play a key role on the fluorescence intensity of the laterally methyl compounds. Hence, the presence of the lateral methyl donating group *ortho* to the azo linkage in compounds **C7** and **C8** may led to an extension of the conjugation system and higher fluorescence intensity compared with those of the laterally unsubstituted and laterally fluorinated analogues (Karim et al., 2013). The newly lateral methyl derivatives have potential use as fluorescent materials for practical applications such as organic light-emitting diode applications.

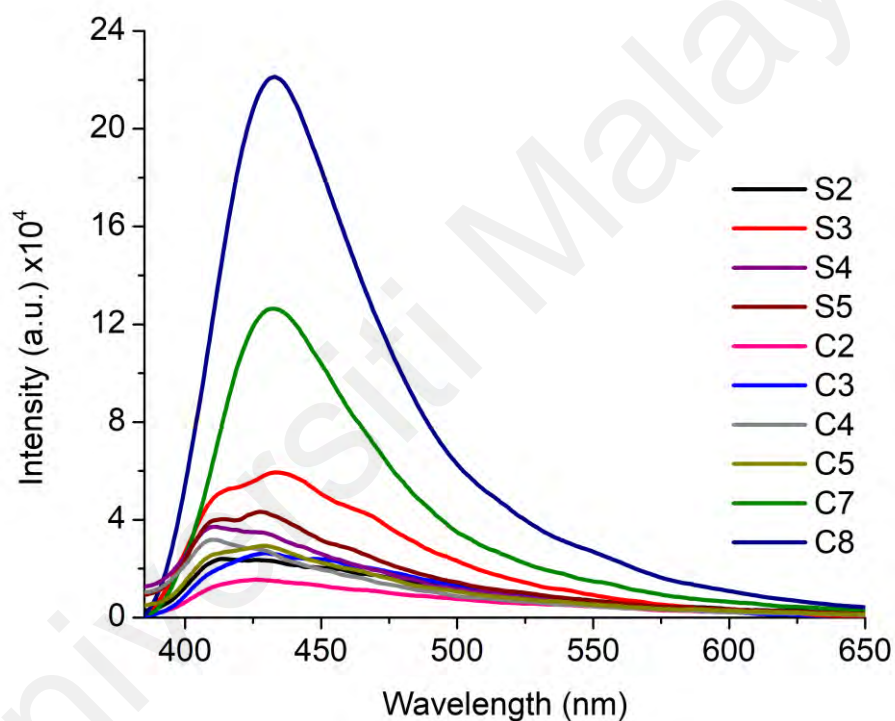


Figure 4.35: PL spectra of S2, S3, S4, S5, C2, C3, C4, C5, C7 and C8 in CDCl₃ solution of 5×10^{-5} M.

CHAPTER 5: CONCLUSION AND FUTURE WORK

5.1 Conclusion

Azo-ester based compounds composed of two and three-benzene-ring molecular core having a 2-methylbutoxy end-group at the phenylazo ring and different terminal groups at the phenyl ester ring (including the terminally unsubstituted analogue) with varied lateral substituent at the 2-position to the azo linkage (including the laterally unsubstituted analogue) were successfully synthesized and characterized. The structures of all compounds have been identified by FT-IR, ^1H and ^{13}C NMR and elemental analyses for final compounds. The TGA analysis showed that the thermal stability of these compounds is relatively high (above 319°C) and their thermal decompositions involved a one-step pathway. The effect of different lateral and terminal substitutions on the mesomorphic properties were investigated to understand the structure property relationship. It has been found that, except for the two-benzene-ring compounds (**T1**, **T2** and **T3**) and the unsubstituted terminal three-benzene-ring derivatives (**S1**, **C1** and **C6**), all the azo-ester compounds are liquid crystalline materials.

The replacement of terminal hydrogen by the terminal electron-donating and electron-withdrawing groups affects the polarization of mesogenic group that facilitated the formation of mesophase in **S2**, **S3**, **S4**, **S5**, **C2**, **C3**, **C4**, **C5**, **C7** and **C8**. Irrespective of the presence or absence of the laterally fluorinated or laterally methyl substituent, the electron-donating substituted derivatives shown to be purely nematogenic. For the electron-withdrawing substituted derivatives, the bromo-terminated analogues induced the nematic-to-nematic phase transition, while the nitro-terminated compounds exhibited nematic phase. Comparison of the melting and clearing temperatures values of laterally fluorinated azo-esters (**C2**, **C3**, **C4**, and **C5**) with their corresponding laterally-neat analogues (**S2**, **S3**, **S4**, and **S5**) revealed that inclusion of the lateral fluoro group at 2-position to the azo linkage caused a decrease in melting and clearing temperatures.

Similarly, comparison of the melting and clearing temperatures values of laterally methyl analogues (**C7** and **C8**) with their corresponding laterally-neat analogues (**S2** and **S3**) revealed that introduction of the lateral methyl group at 2-position to the azo linkage triggered somewhat a decrease in the melting and clearing temperatures.

The mesogenic laterally fluorinated azo-esters exhibited UV-vis absorption bands with λ_{\max} around 300–425 nm for the symmetry allowed π - π^* transition. Comparing the λ_{\max} of these laterally fluorinated azo-esters with that of laterally-neat azo-esters, the lateral ring fluorination resulted in a slight blue-shift in the absorption spectra. The λ_{\max} of the laterally methyl analogues are red-shifted comparing with the laterally unsubstituted analogues. All the mesogenic compounds exhibited blue emission with the laterally methyl substituted compounds having a relatively higher fluorescence intensity compared to that of the laterally unsubstituted and laterally fluorinated analogues.

5.2 Future Work

The research has given us preliminary insight into azo-esters structural properties. In future studies, we will further synthesise three-phenyl-ring azo-esters bearing 2-methylbutoxy unit on the terminal side with fluoro and methyl lateral substituents at middle ring and also three-phenyl-ring azo-esters bearing 2-methylhexoxy group with various lateral groups e.g. -F, -CH₃, -OCH₃ and -Cl groups. It would also be interesting to synthesise similar mesogenic core with Schiff base linking group rather than ester group having different lateral and terminal substituents. Suggested compounds may exhibit lower thermal transition temperatures with good optical properties.

REFERENCES

- Ahmed, S., N. H., Saad, G. R., & Naoum, M. M. (2018). Effect of position of the lateral fluoro substituent on the mesophase behaviour of aryl 4-alkoxyphenylazo benzoates in pure and binary mixtures. *Liquid Crystals*, *45*(10), 1487-1497.
- Ahmed, H., Hagar, M., & Alhaddad, O. (2020). Mesomorphic and geometrical orientation study of the relative position of fluorine atom in some thermotropic liquid crystal systems. *Liquid Crystals*, *47*(3), 404-413.
- Ahmed, H., & Saad, G. (2015). Mesophase behaviour of laterally di-fluoro-substituted four-ring compounds. *Liquid Crystals*, *42*(12), 1765-1772.
- Al-Hamdani, U. J., Abbo, H. S., Al-Jaber, A. A., & Titinchi, S. J. (2020). New azobenzothiazole based liquid crystals: synthesis and study of the effect of lateral substituents on their liquid crystalline behaviour. *Liquid Crystals*, *47*(14), 2257-2267.
- Al-Zahrani, S. A., Ahmed, H. A., El-Atawy, M. A., Abu Al-Ola, K. A., & Omar, A. Z. (2021). Synthetic, mesomorphic, and DFT investigations of new nematogenic polar naphthyl benzoate ester derivatives. *Materials*, *14*(10), 2587-2598.
- Amer, W. A., Wang, L., Amin, A. M., Yu, H., Li, C., & Ma, L. (2013). Study on the electrochemical, thermal, and liquid crystalline properties of poly (diethyleneglycol 1, 1'-ferrocene dicarboxylate). *Designed Monomers and Polymers*, *16*(2), 160-169.
- Anderson, R. J., Bendell, D. J., & Groundwater, P. W. (2004). *Organic spectroscopic analysis* (Vol. 22). United Kingdom: Royal Society of Chemistry.
- Andrienko, D. (2018). Introduction to liquid crystals. *Journal of Molecular Liquids*, *267*, 520-541.
- Aoki, T. (2019). Photoluminescence. In *Optical Properties of Materials and Their Applications* (pp. 157-202). New York: John Wiley & Sons Ltd.
- Arines, J. (2009). Impact of liquid crystals in active and adaptive optics. *Materials*, *2*(2), 549-561.
- Åstrand, P.-O., Ramanujam, P., Hvilsted, S., Bak, K. L., & Sauer, S. P. (2000). Ab initio calculation of the electronic spectrum of azobenzene dyes and its impact on the design of optical data storage materials. *Journal of the American Chemical Society*, *122*(14), 3482-3487.

- Bai, Y., & Abbott, N. L. (2012). Enantiomeric interactions between liquid crystals and organized monolayers of tyrosine-containing dipeptides. *Journal of the American Chemical Society*, 134(1), 548-558.
- Baldock, B. L., & Hutchison, J. E. (2016). UV–Visible spectroscopy-based quantification of unlabeled DNA bound to gold nanoparticles. *Analytical Chemistry*, 88(24), 12072-12080.
- Barrett, C. J., Mamiya, J.-i., Yager, K. G., & Ikeda, T. (2007). Photo-mechanical effects in azobenzene-containing soft materials. *Soft Matter*, 3(10), 1249-1261.
- Bellare, J., Davis, H., Miller, W., & Scriven, L. (1990). Polarized optical microscopy of anisotropic media: imaging theory and simulation. *Journal of Colloid and Interface Science*, 136(2), 305-326.
- Blatch, A. E., Fletcher, I. D., & Luckhurst, G. R. (1997). Symmetric and non-symmetric liquid crystal dimers with branched terminal alkyl chains: racemic and chiral. *Journal of Materials Chemistry*, 7(1), 9-17.
- Brostow, W., & Lobland, H. E. H. (2016). *Materials: introduction and applications*. New Jersey: John Wiley & Sons Inc.
- Carlton, R. J., Hunter, J. T., Miller, D. S., Abbasi, R., Mushenheim, P. C., Tan, L. N., & Abbott, N. L. (2013). Chemical and biological sensing using liquid crystals. *Liquid Crystals Reviews*, 1(1), 29-51.
- Chandrasekhar, S. (1992). *Liquid crystals*. Cambridge: Cambridge University press.
- Chandrasekhar, S., Sadashiva, B., & Suresh, K. (1977). Liquid crystals of disc-like molecules. *Pramana*, 9(5), 471-480.
- Chattopadhyay, A. (2003). Exploring membrane organization and dynamics by the wavelength-selective fluorescence approach. *Chemistry and Physics of Lipids*, 122(1-2), 3-17.
- Cigl, M., Bubnov, A., Kašpar, M., Hampl, F., Hamplová, V., Pacherová, O., & Svoboda, J. (2016). Photosensitive chiral self-assembling materials: significant effects of small lateral substituents. *Journal of Materials Chemistry C*, 4(23), 5326-5333.
- Collings, P., & Hird, M. (1997). *Introduction to liquid crystals : chemistry and physics*. London : Taylor & Francis.

- Collings, P. J. (2002). *Liquid crystals: nature's delicate phase of matter*. New Jersey: Princeton University Press.
- Collyer, A. A. (2012). *Liquid crystal polymers: from structures to applications* (Vol. 1). UK: Springer Science & Business Media.
- Dave, J. S., & Bhatt, H. S. (2012). Synthesis of liquid crystals with lateral methyl group and study of their mesomorphic properties. *Molecular Crystals and Liquid Crystals*, 562(1), 1-9.
- Dave, J. S., Upasani, C., & Patel, P. D. (2010). Effect of lateral substitution on mesogenic properties of fluoro aniline derivatives. *Molecular Crystals and Liquid Crystals*, 533(1), 73-81.
- De Bruyn Ouboter, D., Schuster, T. B., Manton, A., & Meier, W. (2011). Hierarchical organization of purely peptidic amphiphiles into peptide beads. *The Journal of Physical Chemistry C*, 115(30), 14583-14590.
- De Gennes, P. G. (1992). Soft matter. *Reviews of Modern Physics*, 64(3), 645.
- De Gennes, P. G., & Prost, J. (1993). *The physics of liquid crystals* (Vol. 83). UK: Oxford University Press.
- De Sio, L., Ricciardi, L., Serak, S., La Deda, M., Tabiryan, N., & Umeton, C. (2012). Photo-sensitive liquid crystals for optically controlled diffraction gratings. *Journal of Materials Chemistry*, 22(14), 6669-6673.
- Demus, D., Goodby, J., Gray, G., Spiess, H., & Vill, V. (1998). *Handbook of liquid crystals* (Vol. 4): Weinheim: Wiley-VCH.
- Dierking, I. (2003). *Textures of liquid crystals*: Weinheim: John Wiley & Sons.
- Dixit, S., & Intwala, K. (2016). Study of novel thermotropic liquid crystals with lateral nitro substituent. *Molecular Crystals and Liquid Crystals*, 631(1), 1-8.
- Doshi, A. V., & Ganatra, K. J. (1999). Synthesis of new mesogens: 4(4'-n-alkoxy benzoyloxy)-phenyl-azo-4"-methyl benzenes. *Proceedings of the Indian Academy of Sciences - Chemical Sciences*, 111(4), 563-568.
- Dzulkharnien, N. S. F., Salleh, N. M., Yahya, R., & Karim, M. R. (2017). Synthesis of imine-ester-linked benzothiazole mesogen containing liquid crystalline monomers with different terminal substituents. *Soft Materials*, 15(4), 292-301.

- Ebead, Y., Selim, M., & Ibrahim, S. (2010). Solvatochromic, acid–base features and time effect of some azo dyes derived from 1, 3-benzothiazol-2-ylacetonitrile: Experimental and semiempirical investigations. *Spectrochimica Acta Part A: Molecular and Biomolecular Spectroscopy*, 75(2), 760-768.
- Ellis, P. W., Klaneček, S., & Fernandez-Nieves, A. (2020). Polarized epifluorescence microscopy and the imaging of nematic liquid crystals in highly curved geometries. *Physical Review E*, 101(5), 052703.
- Fitas, J., Marzec, M., Tykarska, M., Wróbel, S., & Dąbrowski, R. (2013). Ferroelectric Liquid Crystal for Use in a New Generation of LCDs. *Acta Physica Polonica A*, 124(6), 954-958.
- Fornasieri, G., Guittard, F., & G eribaldi, S. (2003). Influence of the structure of the mesogenic core on the thermotropic properties of ω -unsaturated fluorinated liquid crystals. *Liquid Crystals*, 30(2), 251-257.
- Govindaiah, T. (2016). Electro-optical and thermodynamic studies on induced reentrant smectic-a phase in binary mixture of liquid crystalline materials. *Chemical Technology: An Indian Journal*, 11(6), 106-110.
- Gray, G. W. (1962). *Molecular structure and the properties of liquid crystals*. US: Academic Press.
- Gray, G. W., Harrison, K. J., & Nash, J. (1973). New family of nematic liquid crystals for displays. *Electronics Letters*, 9(6), 130-131.
- G unther, H. (2013). *NMR spectroscopy: basic principles, concepts and applications in chemistry*: Weinheim: John Wiley & Sons.
- Ha, S.-T., Koh, T.-M., Lin, H.-C., Yeap, G.-Y., Win, Y.-F., Ong, S.-T., . . . Ong, L.-K. (2009). Heterocyclic benzothiazole-based liquid crystals: synthesis and mesomorphic properties. *Liquid Crystals*, 36(9), 917-925.
- Ha, S.-T., Koh, T.-M., Yeap, G.-Y., Lin, H.-C., Lee, S.-L., Win, Y.-F., & Ong, S.-T. (2010). Synthesis and mesomorphic properties of 6-methoxy-and 6-ethoxy-2-(2-hydroxy-4-alkanoyloxybenzylidenamino) benzothiazoles. *Molecular Crystals and Liquid Crystals*, 528(1), 10-22.
- Hagar, M., Ahmed, H., & Saad, G. (2020). New calamitic thermotropic liquid crystals of 2-hydroxypyridine ester mesogenic core: Mesophase behaviour and DFT calculations. *Liquid Crystals*, 47(1), 114-124.

- Haines, P. J. (2012). *Thermal methods of analysis: principles, applications and problems*. UK: Springer Science & Business Media.
- Han, M., Ishikawa, D., Muto, E., & Hara, M. (2009). Isomerization and fluorescence characteristics of sterically hindered azobenzene derivatives. *Journal of Luminescence*, 129(10), 1163-1168.
- Hegde, G., Shanker, G., Gan, S. M., Yuvaraj, A. R., Mahmood, S., & Mandal, U. K. (2016). Synthesis and liquid crystalline behaviour of substituted (E)-phenyl-4-(phenyldiazenyl) benzoate derivatives and their photo switching ability. *Liquid Crystals*, 43(11), 1578-1588.
- Heilmeyer, G., Zanoni, L., & Barton, L. (1968). Dynamic scattering in nematic liquid crystals. *Applied Physics Letters*, 13(1), 46-47.
- Heines, S. V. (1958). Peter Griess—Discoverer of diazo compounds. *Journal of Chemical Education*, 35(4), 187.
- Hof, M. (2003). *Basics of optical spectroscopy* (Vol. 1). Weinheim, Germany: Wiley-VCH.
- Höhne, G., McNaughton, J., Hemminger, W., Flammersheim, H.-J., & Flammersheim, H.-J. (2003). *Differential scanning calorimetry*. Germany: Springer Science & Business Media.
- Hrozhyk, U. A., Serak, S. V., Tabiryan, N. V., Hoke, L., Steeves, D. M., & Kimball, B. R. (2010). Azobenzene liquid crystalline materials for efficient optical switching with pulsed and/or continuous wave laser beams. *Optics Express*, 18(8), 8697-8704.
- Imrie, C., & Taylor, L. (1989). The preparation and properties of low molar mass liquid crystals possessing lateral alkyl chains. *Liquid Crystals*, 6(1), 1-10.
- Jacobsen, N. E. (2016). *NMR data interpretation explained: understanding 1D and 2D NMR spectra of organic compounds and natural products*. Hoboken, New Jersey: John Wiley & Sons.
- Jadeja, U. H., Sharma, V. S., Prajapat, V., Shah, A., & Sharma, A. S. (2019). Synthesis and study of azo based liquid crystals: effect of the lateral bromo and terminal alkoxy side chain on thermal, mesomorphic and optical properties. *Molecular Crystals and Liquid Crystals*, 680(1), 46-64.

- Karim, M., Sheikh, M., Islam, M., Salleh, N., & Yahya, R. (2019). Synthesis, crystal structure, mesophase behaviour and optical property of azo-ester bridged compounds. *Journal of Scientific Research*, 11(3), 383-395.
- Karim, M. R., Sheikh, M. R. K., Salleh, N. M., Yahya, R., Hassan, A., & Hoque, M. A. (2013). Synthesis and characterization of azo benzothiazole chromophore based liquid crystal macromers: effects of substituents on benzothiazole ring and terminal group on mesomorphic, thermal and optical properties. *Materials Chemistry and Physics*, 140(2-3), 543-552.
- Karim, M. R., Sheikh, M. R. K., Yahya, R., Mohamad Salleh, N., Lo, K. M., & Mahmud, H. N. M. E. (2016). The effect of terminal substituents on crystal structure, mesophase behaviour and optical property of azo-ester linked materials. *Liquid Crystals*, 43(12), 1862-1874.
- Karim, M. R., Sheikh, M. R. K., Yahya, R., Salleh, N. M., & Azzahari, A. D. (2015). Synthesis of polymerizable liquid crystalline monomers and their side chain liquid crystalline polymers bearing azo-ester linked benzothiazole mesogen. *Colloid and Polymer Science*, 293(7), 1923-1935.
- Karim, M. R., Yahya, R., Sheikh, M. R. K., Salleh, N. M., Hassan, A., & Ekramul Mahmud, H. N. M. (2014). Synthesis, thermal stability, optical and electrochemical properties of halogen terminated azo-benzothiazole mesogen containing smectic side chain liquid crystalline polymers. *Journal of Polymer Research*, 21(6), 487.
- Kašpar, M., Bubnov, A., Hamplová, V., Málková, Z., Pirkl, S., & Glogarová, M. (2007). Effect of lateral substitution by fluorine and bromine atoms in ferroelectric liquid crystalline materials containing a 2-alkoxypropanoate unit. *Liquid Crystals*, 34(10), 1185-1192.
- Kaspar, M., Hamplová, V., Pakhomov, S., Stibor, I., Sverenyák, H., Bubnov, A., . . . Vanek, P. (1997). The effect of a lateral substituent on the mesomorphic properties in a series of ferroelectric liquid crystals with a 2-alkoxypropionate unit. *Liquid Crystals*, 22(5), 557-561.
- Kašpar, M., Sverenyák, H., Hamplová, V., Glogarová, M., Pakhomov, S., Vaněk, P., & Trunda, B. (1995). The effect of a lateral methoxy group on the mesomorphic properties of ferroelectric liquid crystals. *Liquid Crystals*, 19(6), 775-778.
- Kelker, H., & Scheurle, B. (1969). A liquid-crystalline (nematic) phase with a particularly low solidification point. *Angewandte Chemie International Edition in English*, 8(11), 884-885.
- Khoo, I.-C. (2007). *Liquid crystals* (Vol. 64). Hoboken, New Jersey: John Wiley & Sons.

- Kikhney, A. G., & Svergun, D. I. (2015). A practical guide to small angle X-ray scattering (SAXS) of flexible and intrinsically disordered proteins. *Federation of European Biochemical Societies Letters*, 589(19), 2570-2577.
- Kumar, S. (2011). *Chemistry of discotic liquid crystals- From monomers to polymers*. Boca-Raton, USA: Taylor & Francis Group.
- Lakowicz, J. R. (2013). *Principles of fluorescence spectroscopy*. New York, USA: Springer Science & Business Media.
- Lam, J. W., Kong, X., Dong, Y., Cheuk, K. K., Xu, K., & Tang, B. Z. (2000). Synthesis and properties of liquid crystalline polyacetylenes with different spacer lengths and bridge orientations. *Macromolecules*, 33(14), 5027-5040.
- Li, T., Senesi, A. J., & Lee, B. (2016). Small angle X-ray scattering for nanoparticle research. *Chemical Reviews*, 116(18), 11128-11180.
- Li, X., Fang, L., Hou, L., Zhu, L., Zhang, Y., Zhang, B., & Zhang, H. (2012). Photoresponsive side-chain liquid crystalline polymers with amide group-substituted azobenzene mesogens: effects of hydrogen bonding, flexible spacers, and terminal tails. *Soft Matter*, 8(20), 5532-5542.
- Liang, Q., Liu, P., Liu, C., Jian, X., Hong, D., & Li, Y. (2005). Synthesis and properties of lyotropic liquid crystalline copolyamides containing phthalazinone moiety and ether linkages. *Polymer*, 46(16), 6258-6265.
- Liu, J. H., Hsieh, C. D., & Wang, H. Y. (2004). Preparation and characterization of chiral polyacrylates end-capped with bornyl groups in the side chains. *Journal of Polymer Science Part A: Polymer Chemistry*, 42(5), 1075-1092.
- Lutfor, M., Hegde, G., Kumar, S., Tschierske, C., & Chigrinov, V. (2009). Synthesis and characterization of bent-shaped azobenzene monomers: guest–host effects in liquid crystals with azo dyes for optical image storage devices. *Optical Materials*, 32(1), 176-183.
- Madihlagan, E., B N, S., Ngaini, Z., & Hegde, G. (2019). Synthesis, liquid crystalline properties and photo switching properties of coumarin-azo bearing aliphatic chains: Application in optical storage devices. *Journal of Molecular Liquids*, 292, 111328-111337.
- Mandle, R. J., Cowling, S. J., & Goodby, J. W. (2017). A nematic to nematic transformation exhibited by a rod-like liquid crystal. *Physical Chemistry Chemical Physics*, 19(18), 11429-11435.

- Meier, G., Sackmann, E., & Grabmaier, J. G. (2012). *Applications of liquid crystals*. New York: Springer Science & Business Media.
- Mohamed, M. A., Jaafar, J., Ismail, A., Othman, M., & Rahman, M. (2017). Fourier transform infrared (FTIR) spectroscopy. In *Membrane Characterization* (pp. 3-29). Germany: Elsevier.
- Mori, A., Itoh, T., Taya, H., Kubo, K., Ujiie, S., Baumeister, U., . . . Tschierske, C. (2010). Mesomorphic property of 2, 5-dibenzoyloxy-, 5-benzoylamino-2-benzoyloxy-, and 2, 5-dibenzoylamino-tropones with mono-, di-, and tri-alkoxyl groups on the benzoyl groups and their benzenoid derivatives. *Liquid Crystals*, 37(4), 355-368.
- Mosher, M. (1992). Organic Chemistry. Sixth edition (Morrison, Robert Thornton; Boyd, Robert Neilson). *Journal of Chemical Education*, 69(11), A305.
- Muñoz, J., & Alfaro, M. (2000). Rheological and phase behaviour of amphiphilic lipids. *Grasas y Aceites*, 51(1-2), 6-25.
- Naoum, M., Fahmi, A., Alaasar, M., & Ahmed, N. (2011). Effect of exchange of terminal substituents on the mesophase behavior of laterally methyl substituted phenyl azo benzoates in pure and mixed systems. *Thermochimica Acta*, 525(1-2), 78-86.
- Naoum, M. M., Fahmi, A. A., Abaza, A. H., & Saad, G. R. (2014). Effect of exchange of terminal substituents on the mesophase behaviour of some azo/ester compounds. *Liquid Crystals*, 41(11), 1559-1568.
- Naoum, M. M., Fahmi, A. A., Abaza, A. H., & Saad, G. R. (2016). The effect of orientation of the lateral methyl substituent on the mesophase behaviour of 4-alkoxyphenylazo aryl benzoates. *Liquid Crystals*, 43(12), 1831-1845.
- Naoum, M. M., Fahmi, A. A., Ahmed, N. H., & Saad, G. R. (2015b). The effect of lateral methyl substitution on the mesophase behaviour of aryl 4-alkoxyphenylazo benzoates. *Liquid Crystals*, 42(11), 1627-1637.
- Naoum, M. M., Fahmi, A. A., Ahmed, N. H. S., & Saad, G. R. (2015a). The effect of inversion of the ester group on the mesophase behaviour of some azo/ester compounds. *Liquid Crystals*, 42(9), 1298-1308.
- Naoum, M. M., Metwally, N. H., Abd Eltawab, M. M., & Ahmed, H. A. (2015c). Polarity and steric effect of the lateral substituent on the mesophase behaviour of some newly prepared liquid crystals. *Liquid Crystals*, 42(10), 1351-1369.
- Naoum, M. M., Mohammady, S. Z., & Ahmed, H. A. (2010). Lateral protrusion and mesophase behaviour in pure and mixed states of model compounds of the type

4-(4'-substituted phenylazo)-2-(or 3-)methyl phenyl-4'-alkoxy benzoates. *Liquid Crystals*, 37(10), 1245-1257.

Neises, B., & Steglich, W. (1978). Simple method for the esterification of carboxylic acids. *Angewandte Chemie International Edition in English*, 17(7), 522-524.

Nessim, R. I., Naoum, M. M., Mohamed, S. Z., & Nessim, M. I. (2004). Effect of molecular structure on the phase behaviour of some liquid crystalline compounds and their mixtures XIII. 4-(4-Substituted phenylazo) phenyl 4-alkoxybenzoates. *Liquid Crystals*, 31(5), 649-654.

Obodovskiy, I. (2019). Luminescence. In *Radiation* (pp. 207-220). Germany: Elsevier.

Pal, T., Alam, M., Hossen, J., Paul, S., Ahmad, H., & Sheikh, M. (2018). Spectral and biological studies on new mixed ligand complexes. *Journal of Scientific Research*, 10(3), 291-302.

Pavia, D. L., Lampman, G. M., Kriz, G. S., & Vyvyan, J. A. (2014). *Introduction to spectroscopy*. USA: Cengage Learning.

Penner, M. H. (2017). Basic principles of spectroscopy. In *Food analysis* (pp. 79-88). Germany: Springer, Cham.

Podorov, S. G., Faleev, N., Pavlov, K. M., Paganin, D., Stepanov, S., & Förster, E. (2006). A new approach to wide-angle dynamical X-ray diffraction by deformed crystals. *Journal of Applied Crystallography*, 39(5), 652-655.

Prajapati, A. K., & Varia, M. C. (2008). Azomesogens with polar chloro, nitro and phenolic -OH substituents. *Liquid Crystals*, 35(11), 1271-1277.

Prasad, V. (2001). Liquid crystalline compounds with V-shaped molecular structures: synthesis and characterization of new azo compounds. *Liquid Crystals*, 28(1), 145-150.

Prime, R. B., Bair, H. E., Vyazovkin, S., Gallagher, P. K., & Riga, A. (2009). Thermogravimetric analysis (TGA). In *Thermal analysis of polymers: Fundamentals and applications* (pp. 241-317). Hoboken, New Jersey: John Wiley & Sons.

Rameshbabu, K., & Kannan, P. (2004). Synthesis and characterization of thermotropic liquid crystalline polyphosphates containing photoreactive moieties. *Liquid Crystals an International Journal of Science and Technology*, 31(6), 843-851.

- Reinitzer, F. (1888). Beiträge zur Kenntniss des Cholesterins. *Monatshefte für Chemie und verwandte Teile anderer Wissenschaften*, 9(1), 421-441.
- Saad, G. R., Ahmed, N. H., Fahmi, A. A., Kaddah, M. M., & Naoum, M. M. (2019). Influence of lateral methyl and terminal substituents on the mesophase behaviour of four rings azo-ester liquid crystal compounds. *Liquid Crystals*, 46(8), 1285-1297.
- Saha, A., Tanaka, Y., Han, Y., Bastiaansen, C. M., Broer, D. J., & Sijbesma, R. P. (2012). Irreversible visual sensing of humidity using a cholesteric liquid crystal. *Chemical Communications*, 48(38), 4579-4581.
- Salleh, M. N., Sheikh, M. R. K., Yahya, R., Karim, M. R., Azzahari, A. D., & Hassan, A. (2013). Effect of the lateral substituent on the mesomorphic behavior of side-chain liquid-crystalline polymers containing a Schiff base ester. *Journal of Polymer Research*, 20(12), 1-11.
- Sardon, S. N. F., Rahman, N. M. M. A., Karim, M. R., Zahid, N. I., & Salleh, N. M. (2021). Effects of lateral methyl and terminal substituents on thermal, mesomorphic and optical properties of azo-ester mesogens. *Journal of Molecular Structure*, 1225, 129112.
- Scott, W. (2007). *Liquid Crystals: frontiers in biomedical applications*. Singapore: World Scientific.
- Singh, M. S. (2004). *Advanced organic chemistry: reactions and mechanisms*. Varanasi, India: Pearson Education
- Singh, S., & Dunmur, D. A. (2002). *Liquid crystals: fundamentals*. Singapore: World Scientific.
- Sluckin, T. J., Dunmur, D. A., & Stegemeyer, H. (2004). *Crystals that flow: classic papers from the history of liquid crystals*. Boca Raton, USA: CRC Press.
- Stegemeyer, H. (1994). Professor Horst Sackmann, 1921–1993. *Liquid Crystals Today*, 4(1), 1-2.
- Stoker, H. S. (2015). *General, organic, and biological chemistry*. Boston, USA: Cengage Learning.
- Thaker, B. T., Kanojiya, J. B., & Tandel, R. S. (2010). Effects of different terminal substituents on the mesomorphic behavior of some azo-schiff base and azo-ester-based liquid crystals. *Molecular Crystals and Liquid Crystals*, 528(1), 120-137.

- Thieghi, L. T., Bonvent, J., Oliveira, E., Giacometti, J. A., & Balogh, D. T. (2003). Competition between anchoring and reversible photo-induced alignment of a nematic liquid crystal. *Applied Physics A*, 77(7), 911-914.
- Thompson, M. (2008). *CHNS elemental analysers*. UK: The Royal Society of Chemistry.
- Varia, M. C., Kumar, S., & Prajapati, A. K. (2012). H-shaped azoester-oxymethylene containing twin liquid crystalline compounds. *Liquid Crystals*, 39(3), 365-371.
- Wang, X.-J., & Zhou, Q.-F. (2004). *Liquid crystalline polymers*. Singapore: World Scientific Publishing Company.
- Williamson, A. (1850). XLV. Theory of ætherification. *The London, Edinburgh, and Dublin Philosophical Magazine and Journal of Science*, 37(251), 350-356.
- Winterbottom, D. A., Narayanaswamy, R., & Raimundo Jr, I. M. (2003). Cholesteric liquid crystals for detection of organic vapours. *Sensors and Actuators B: Chemical*, 90(1-3), 52-57.
- Xie, J., Zhu, G., Tang, Y., & Wang, Y. (2013). Synthesis and characterisation of reactive liquid crystals containing an azo group. *Liquid Crystals*, 41(1), 36-43.
- Xu, H., Hartono, D., & Yang, K.-L. (2010). Detecting and differentiating Escherichia coli strain TOP10 using optical textures of liquid crystals. *Liquid Crystals*, 37(10), 1269-1274.
- Xu, Y., Hu, K., Chen, P., Gao, A., Du, W., Chen, X., & An, Z. (2014). Synthesis and properties of mesogenic laterally fluorinated compounds containing benzoxazole unit. *Liquid Crystals*, 41(7), 1042-1056.
- Yager, K. G., & Barrett, C. J. (2006). Novel photo-switching using azobenzene functional materials. *Journal of Photochemistry and Photobiology A: Chemistry*, 182(3), 250-261.
- Yao, J., You, Y., Lei, Y., Dong, L., Xiong, C., & Sun, Z. (2009). Main-chain azo polyaramides with high thermal stability and liquid crystal properties. *Journal of Polymer Research*, 16(4), 455-460.
- Yeap, G.-Y., Lee, H.-C., Mahmood, W. A. K., Imrie, C. T., Takeuchi, D., & Osakada, K. (2011). Synthesis, thermal and optical behaviour of non-symmetric liquid crystal dimers α -(4-benzylidene-substituted-aniline-4'-oxy)- ω -[penty-1-4-(4'-phenyl)benzoateoxy]hexane. *Phase Transitions*, 84(1), 29-37.

- Yeap, G.-Y., Osman, F., & Imrie, C. T. (2015). Non-symmetric dimers: effects of varying the mesogenic linking unit and terminal substituent. *Liquid Crystals*, 42(4), 543-554.
- Yoshino, J., Kano, N., & Kawashima, T. (2013). Fluorescent azobenzenes and aromatic aldimines featuring an N–B interaction. *Dalton Transactions*, 42(45), 15826-15834.
- Yuvaraj, A. R., Mashitah, M. Y., & Lutfor, R. (2016). Synthesis of bent-shaped azobenzene liquid crystals derived from resorcinol for optical storage properties. *Molecular Crystals and Liquid Crystals*, 631(1), 21-30.
- Yuvaraj, A. R., Mei, G. S., Kulkarni, A. D., Mashitah, M. Y., & Hegde, G. (2014). Aliphatic/aromatic spacers based azo dye dimers: synthesis and application for optical storage devices. *RSC Advances*, 4(92), 50811-50818.
- Zaki, A. A., Ahmed, H. A., & Hagar, M. (2018). Impact of fluorine orientation on the optical properties of difluorophenylazophenyl benzoates liquid crystal. *Materials Chemistry and Physics*, 216, 316-324.
- Zhang, X., Wang, C., Lu, X., & Zeng, Y. (2012). Nonlinear optical properties of a series of azobenzene liquid-crystalline materials. *Optik*, 123(1), 26-29.
- Zhao, H.-w., He, X.-z., Zheng, J.-J., Song, W.-l., Meng, F.-B., & Hu, J.-s. (2017). Synthesis and properties of chiral azo-liquid crystalline terpolymer containing cyano mesogenic units. *Liquid Crystals*, 44(14-15), 2379-2390.